A Study of Wet Snow Shedding from an Overhead Cable

by

Mathieu Roberge

Department of Civil Engineering and Applied Mechanics

McGill University, Montreal

December 2006

A thesis submitted to McGill University in partial fulfillment of the requirements of the degree of Master of Engineering

Your file Votre référence
ISBN: 978-0-494-32618-3
Our file Notre référence
ISBN: 978-0-494-32618-3

Abstract

Wet snow accumulating and shedding from overhead transmission lines can lead to a number of serviceability, safety and mechanical reliability issues. An innovative and inexpensive method to reproduce wet snow accretions on a cable in a controlled environment is explained. Wet snow sleeves were experimentally reproduced by using this technique to study their shedding mechanism. A numerical modeling technique using nonlinear finite element analysis is proposed to evaluate the dynamic response of an overhead cable subjected to any snow-shedding scenario. A time function is associated to the mass and weight of each snow element, which enables its virtual removal from the model at the time prescribed by the user. The response of a single span of overhead ground wire subjected to total and partial snow shedding scenarios is evaluated.

Résumé

Les accumulations et les déchargements (ou délestages) de neige collante sur les lignes aériennes de transport d'électricité peuvent occasionner plusieurs problèmes de fiabilité et même de sécurité mécanique. Une méthode innovatrice et peu dispendieuse de reproduction d'accrétions collantes en chambre climatique est expliquée. Les manchons de neige reproduits expérimentalement ont été utilisés pour l'étude du mécanisme de délestage. Une technique de modélisation numérique utilisant la méthode non-linéaire des éléments finis est proposée pour évaluer la réponse dynamique d'un câble aérien assujetti à n'importe quel scénario de déchargement. La masse et le poids de chaque élément de neige sont associés à une fonction temporelle, ce qui permet de l'éliminer virtuellement du modèle au moment prescrit par l'utilisateur. La réponse d'un câble de garde de portée simple assujetti à divers scénarios de déchargement total ou partiel est évaluée.

Table of Contents

List of Figures

List of Tables

Acknowledgements

This is the first of a series of wet-snow investigations emerging from a partnership between Électricité de France (EDF) and the CIGELE Industrial Chair on Atmospheric Icing of Power Network Equipment at Université du Québec à Chicoutimi (UQAC), in collaboration with McGill University. Funding for this study was generously supplied by EDF within the framework of this partnership. There are many people without whom this research project would have never been possible, and I would hereby like to acknowledge their contribution in making this 20-month long research a reality.

Many thanks to all of you:
to my supervisor Ghyslaine McClure of McGill University, for assigning me this research project and for all the freedom and guidance provided; to my co-supervisor Masoud Farzaneh of UQAC, Chairholder of CIGELE, for initiating a wet-snow research project, for his precious time and advice and access to quality experimental facilities; to EDF, especially Laure Pellet, Christophe Peyrard and Pierre Pramayon for their hospitality and access to EDF's wet snow archives; to my mentors Ronald Dean and Steve Kacani, for their inspiration and for pushing me towards graduate studies in civil engineering; to Pierre Admirat and Yukichi Sakamoto, world-class specialists on wet snow, for sharing their precious knowledge and fascination for this subject; to Pierre Guilbeault, Hung Huynh, Bernard Dalle and Jean-Louis Lapeyre for their valuable observations; to the CIGELE technicians Pierre Camirand, Marc-André Perron and Xavier Bouchard, for expedient services; to the CIGELE tea club for their good company; to my parents for their support and affection and last but not least, to Stéphanie my muse, my motivation, my love.

1. Introduction

Wet snow typically occurs at air temperatures slightly above the freezing point. Carried by the wind, wet snow particles adhere remarkably well onto any object they encounter: trees, lamp posts, street signs, cables, structures, etc. (Fig.1)

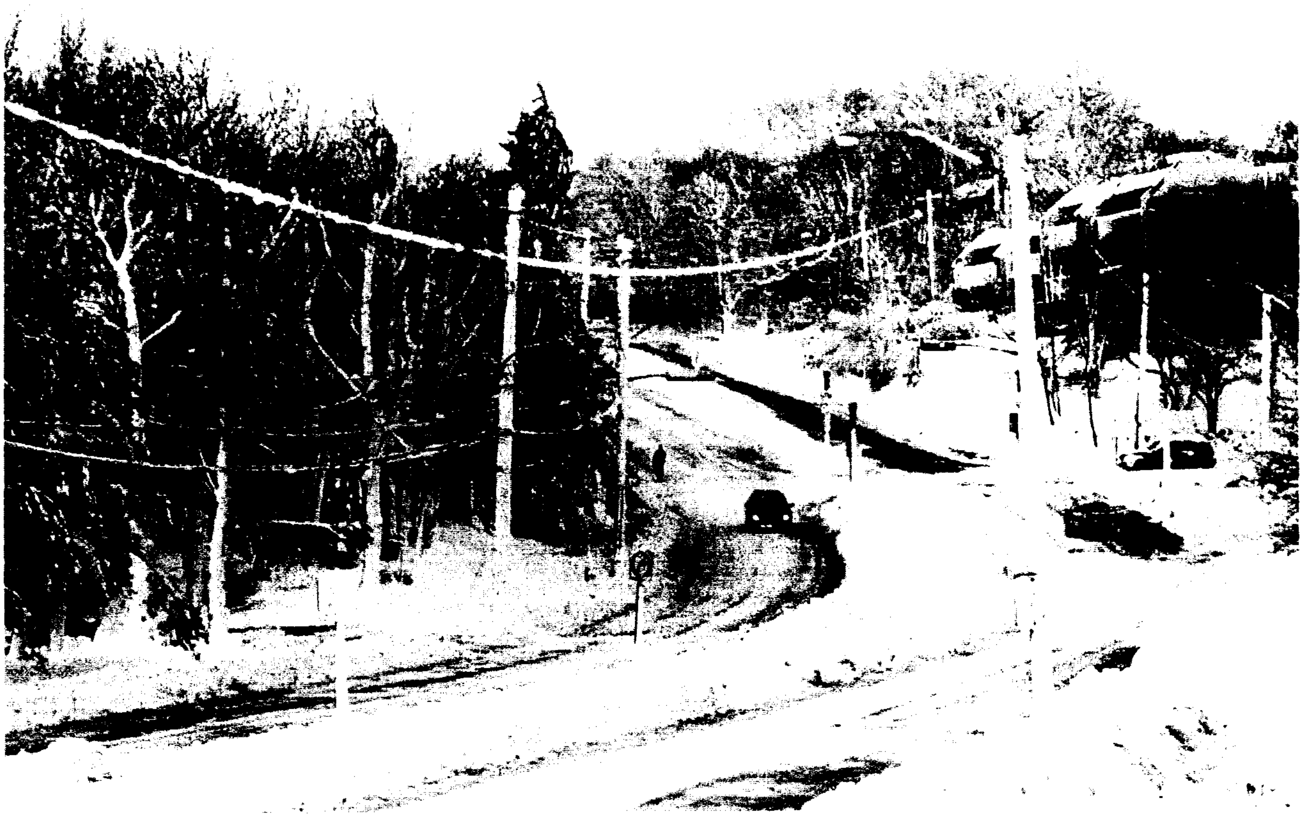

Fig.1 Urban landscape transformed by a wet snow event
Picture taken in Dartmouth, Nova Scotia, December 10th, 2005

Wet snow accretion on overhead transmission line conductors and ground wires can lead to a number of serviceability, safety and mechanical reliability issues. Unequal sags and large cable oscillations due to the shedding of accreted snow can cause flashovers between phases. Dynamic overloads can cause the fatigue and eventual breakage of cables, wear of fittings and members, and the collapse of support structures.

Under the effect of the wind, wet snow tends to accumulate on overhead cables in the form of growing cylindrical sleeves (Wakahama *et al.* 1977, Admirat and Sakamoto 1988). Wet snow accretions, as reported by Colbeck and Ackley (1982), are particularly troublesome because a large mass accumulation can occur in only a few hours.

Wet snow sleeves often shed naturally in the hours following their accumulation. Heating effects such as forced convection, solar radiation and Joule effect contribute to increase the liquid water content of snow accretions: upon reaching high liquid water content values snow sleeves lose their cohesion and shed naturally under the effect of gravity and wind.

Wet snow accretions are difficult to study. They are relatively rare and often limited to specific locations with special topography or microclimate. Field observations are typically made several hours or even days following a storm. Laboratory experiments have been performed in the past using wind tunnels to study the accretion mechanism (Wakahama 1977, Sakamoto 2000). Although the equipment used was often flawed the experiments were nonetheless successful in determining the influence of different environmental factors on some of the properties of snow sleeves.

The subject of this Master of Engineering thesis is the study of wet snow shedding from an overhead cable. Previous researchers have explored the microstructure of wet snow and its accretion mechanisms (including the identification of the heat balance components); others have developed and evaluated devices used to limit its accretion and mapped the risks associated to severe events. To the best knowledge of the author, the subject of wet snow shedding has never been the object of specific studies.

The first objective of this research was to understand the failure mode for snow sleeves and then suggest a mechanical failure criterion that could be included in a finite element model for a snow-covered cable. The latter modeling technique was originally developed by Tamás Kálmán, Ph.D. student at CIGELE, to study the response of an ice-covered cable. Ice accretions subjected to excessive axial and bending stresses tend to fracture and shed: using a mechanical failure criterion for ice, Kálmán has developed a modeling technique that is capable of simulating progressive shedding of ice on a cable subjected to a shock load. Ice elements that meet the failure criterion are automatically removed from the model during the dynamic analysis (Kálmán *et al.* 2005).

However, it is the opinion of the author that such a modeling approach is not applicable to wet snow sleeves because of their inherent visco-plastic behavior and different failure mode. This opinion is shared by many researchers including Tamás Kálmán, Masoud Farzaneh and Pierre Admirat, who is considered as the leading expert in the field of wet snow accretion.

Therefore, a broader set of objectives was established to learn as much as possible about wet snow accretions on cables and to identify future avenues for wet snow research:

A. To understand how wet snow sheds from a cable. This was to be achieved by gathering all of the relevant information found in the literature about wet snow and by combining this knowledge with accounts of researchers who have witnessed the wet snow accretion and shedding mechanisms in the field.
B. To assess the feasibility of reproducing wet snow sleeves in a laboratory environment and to recreate the conditions leading to natural shedding.
C. To develop a finite element modeling technique more adapted to wet snow shedding and to demonstrate some of its capabilities.

All of these objectives were achieved successfully.

Combining the information found in the literature with relevant field observations led to a better understanding of the shedding mechanism of wet snow. The experimental study resulted in an innovative and inexpensive method for creating uniform snow sleeves up to 5 meters in length. In previous wind tunnel experiments, only 1-meter long sleeves of questionable uniformity were produced (Admirat 2006). The rate at which natural shedding occurs along a cable, as well as the holding strength of a freshly accreted snow sleeve, have been measured for the first time.

A modeling technique based on the previous work of McClure *et al.* (Jamaleddine *et al.* 1993, Roshan Fekr and McClure 1995, McClure and Lapointe 2003) was developed to evaluate the response of an overhead cable subjected to any possible snow-shedding scenario. The models generated to illustrate the technique produced a number of pertinent results.

This thesis is divided in three parts, each corresponding to the objectives stated above. Part A comprises chapters 2 to 6 and Parts B and C correspond respectively to chapters 7 and 8.

Note on terminology: throughout this text the term "overhead cable" is used to designate a stranded phase conductor or ground wire (regular or optical) used in overhead electric transmission lines.

2. Snow accretions on overhead cables

Most of the useful literature on the physics of wet snow accretions comes from authors who have studied and observed the accretion mechanism in the field or in a wind tunnel (Wakahama *et al.* 1977, Admirat *et al.* 1988, Sakamoto 2000). Numerical accretion models were developed and calibrated based on wind tunnel and field observations, in an attempt to predict the amount of snow overload on cables during a wet snow event (Poots 1996, Grenier *et al.* 1986).

2.1 Types of snow accretions

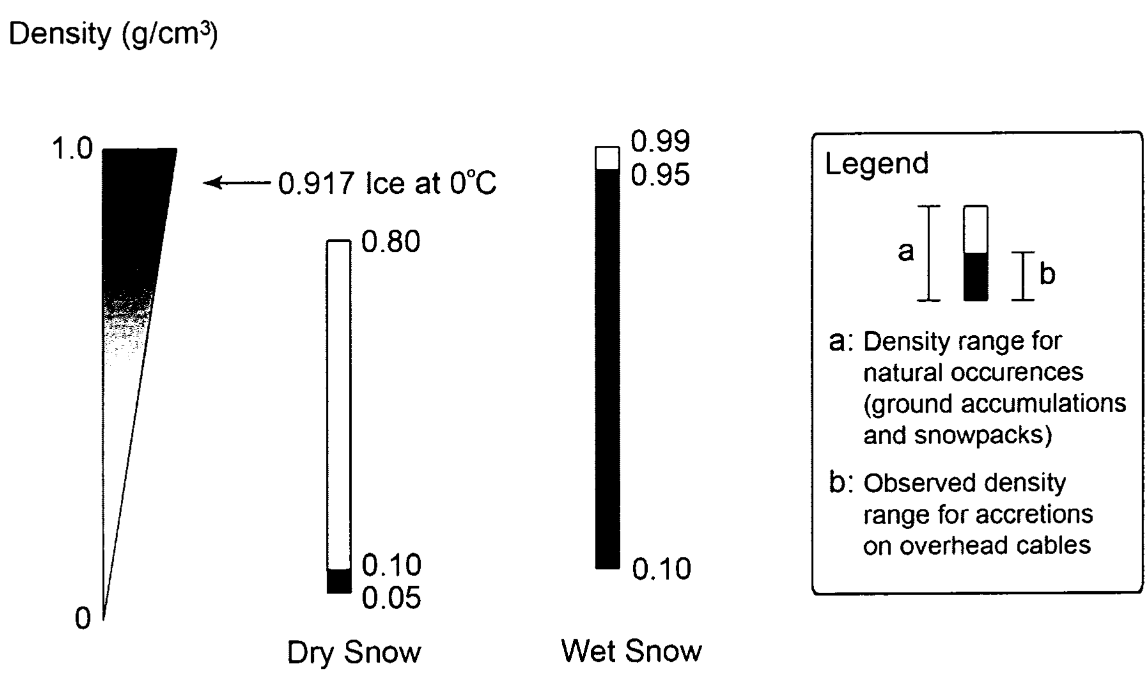

Fig.2 Density comparison for wet and dry snow accretions

2.1.1 Dry snow accretions

In practice, two types of snow accretions can be distinguished: wet and dry. Dry snow accretions occur at sub-zero air temperatures, and are limited to very low wind speeds (typically less than 2 m/s); their densities are low and rarely exceed 0.1 g/cm^3; their adhesive force is also very low and they rarely give rise to extreme loads. However, a complete cylindrical sleeve may form and shed spontaneously along an entire cable span, leading to a pronounced dynamic rebound (Sakamoto 2000).

2.1.2 Wet snow accretions

Wet snow accretions typically occur at air temperatures slightly above the freezing point. They are heavier than dry snow accretions and their density (see Fig.2) spans a much wider range (0.10 g/cm³ to 0.95 g/cm³). On cables, they may also form into complete cylindrical sleeves, but their greater adhesive strength makes them unlikely to shed from wind loads alone, causing significant gravity and wind-on-accretion overloads.

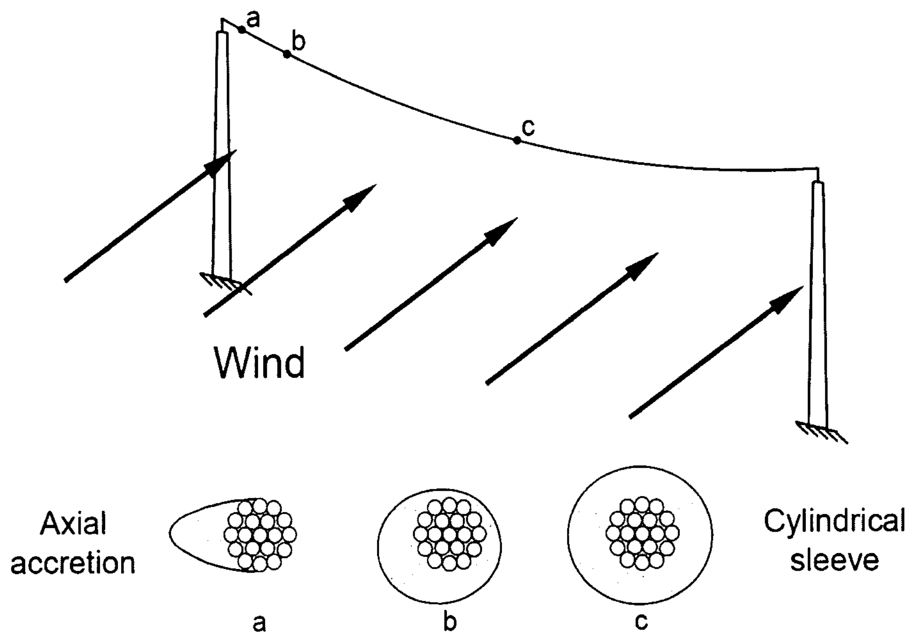

Fig.3 Variation of snow accretion profile along the span of an overhead cable

Wet snow accretions are commonly described in terms of their radial thickness (added to the cable) and their weight per cable length. Typical values found in the literature range from 0 cm to 5 cm for radial accretions and 0 kg/m to 10 kg/m for snow overloads. Severe wet snow storms generating radial accretions up to 15 cm and snow overloads up to 20 kg/m have been reported, but they appear to be extremely rare.

2.2 Growth of wet snow accretions

As in the case of rime ice accretions, wind-borne wet snow particles adhere to the windward side of overhead cables. The accreted mass grows into the wind, causing an eccentric load on the cable (Poots 1996). Two modes of accretion have been observed along spans of overhead cables: axial growth and cylindrical sleeve growth (Fig.3).

2.2.1 Axial growth (Fig.4)

Axial growth occurs on the windward surface of a cable when its rotation is prevented (e.g. at the towers where the cable is attached, or on bundled conductors). In this case, the snow accretion simply grows outwards into the wind.

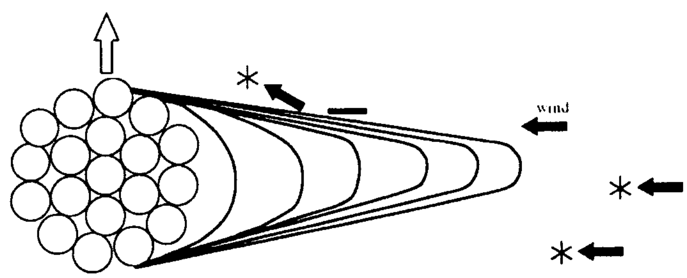

Fig.4 Axial growth on a stranded cable
(from Sakamoto 2000)

2.2.2 Cylindrical sleeve growth (Fig.5)

Using wind tunnel experiments, Wakahama *et al.* (1977) were the first to demonstrate how the wind causes an accretion to rotate and build uniformly around a cable. Since an overhead cable has finite torsional stiffness, it rotates about its axis under the effect of the eccentric snow loading. At its mid span the cable can undergo more than one revolution and the accretion becomes a cylindrical sleeve. As the cable goes through several revolutions its diameter is further increased. This accretion mode is known as "cylindrical sleeve growth". In the case of a cable having low torsional stiffness (such as an overhead ground wire or a single phase conductor – as opposed to a bundle of two or more conductors) a cylindrical sleeve may cover almost the entire span (Poots 1996).

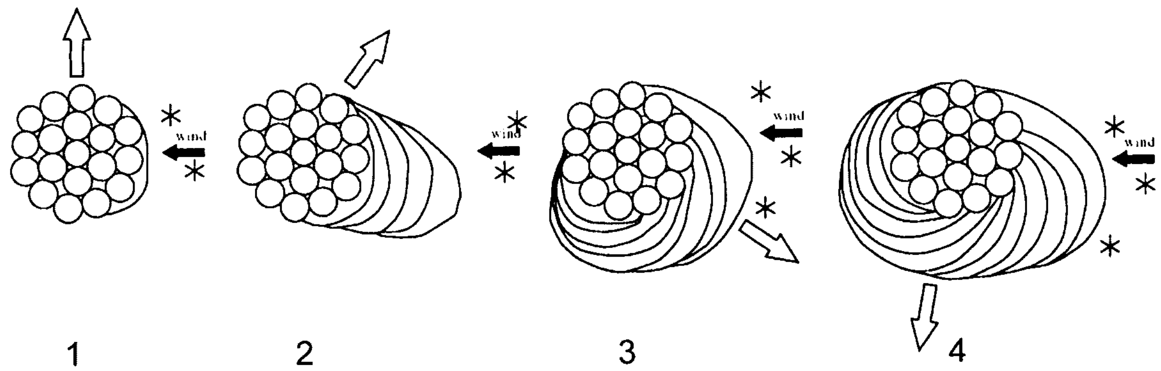

Fig.5 Cylindrical sleeve formation
The white arrows indicate cable rotation (from Sakamoto 2000)

2.3 Effects of the wind

The wind is responsible for packing the accreting snow grains to a high density. The impacting forces of snow particles and the wind drag contribute to densify the accretion. Snow densities on cables are normally much higher than those found on the ground during the same event. After the snowfall the accretion is further compacted by wind drag and gravity; both effects are balanced by the increased tension in the cable. Wet snowflakes are easily compressible: wind has a considerable effect on their compaction as they impact snow sleeves, especially at higher liquid water content values (Colbeck and Ackley 1982).

The apparent diameter of an overhead cable increases as a snow sleeve grows. This increased weight bears on the support structure and may lead to its collapse if the load exceeds its capacity. Wind-on-cable loads are also amplified by the increase in exposed area. Sustained quasi-steady winds and/or dynamic gusts can cause significant transverse loads on cables and on the supporting towers.

Apart from mechanical loads, the wind plays an important role in the heat exchanges between a wet snow sleeve and its environment. The wind can have a heating or cooling effect by bringing forced convection to the accretion.

3. Wet snow metamorphism and its saturation regimes

Colbeck and Denoth are the most important contributors to the understanding of the physics of wet snow. Their research efforts dealt with the evolution of the microstructure of wet snow (Colbeck 1973, 1979, 1982, 1997) and the study of its liquid water content (Denoth 1982).

3.1 The physics of wet snow

"During wet snow accretion on an overhead wire, occurring at positive air temperatures, the liquid water content (LWC) of the snow matrix controls the strength of the capillary forces and promotes contact between ice granules leading to ice bonding." (Poots 1996)

The previous quote is a very elegant and concise summary of the origin of wet snow's cohesive strength when it is accumulating on an overhead cable. In order to appreciate it fully one needs to have a better understanding of what wet snow is, how it evolves under environmental factors and how it is described and quantified.

Wet snow particles are an agglomeration of snowflakes and a mixture of ice, liquid water and air. The physical properties of wet snow are extremely variable. Different ratios of ice, water and air produce microstructures with different densities and liquid water content. This, in turn, leads to a wide range of adhesive properties and strengths (Poots 1996). Moreover, the microstructure is continuously evolving and it undergoes metamorphism with changes in liquid water content, temperature and/or temperature gradient (Colbeck 1982, 1997).

3.2 The liquid water content (LWC) of wet snow

The key variables used to describe wet snow accretions are: radial thickness, density, overload (mass or weight per meter of cable length) and liquid water content (LWC).

Most of the documentation on snow metamorphism and snow accretion on overhead cables is consistent; however, the LWC parameter is expressed differently from one author to the next, which may be confusing. There is no standard definition for the LWC of wet snow accreted on an overhead cable, but there is a trend that goes against the convention established to describe the LWC of snow accumulated on the ground.

In 1985, the International Commission on Snow and Ice established the Working Group on Snow Classification to update the classification system for snow on the ground. The group, chaired by S.C. Colbeck, defined the LWC of snow as the percentage of liquid water per volume of snow. This definition became an international standard to describe the LWC of snow layers on the ground, and it is currently used by researchers studying mountain snowpacks and avalanches (Colbeck *et al.* 1990).

Liquid water content **General symbol: θ**

Measurements of liquid water content or wetness are expressed as a percentage by volume, which usually requires a separate measurement of density. Several methods are in use today for field measurements to determine liquid water content: hot (melting) and cold (freezing) calorimetry, dilution and dielectric measurements. ~~A general classification of liquid water content is given in Table 4~~.

Liquid water is only mobile if the irreducible water content is exceeded. The irreducible water content is about 3% by volume and depends significantly on snow texture, grain size and grain shape. This is the water that can be held by surface forces against the pull of gravity.

(from Colbeck *et al.* 1990)

The above description is referred to in this review as "%LWC by volume". It does not give a complete representation of the level of water saturation of snow. Denoth (1982) has a better way to express the extent to which snow is saturated with liquid water: he defines saturation as the ratio of the LWC of snow (% volume) to its porosity. In other words, Denoth defines the amount of *water saturation* as the extent (%) to which liquid water fills the available pore space in the snow matrix.

Wakahama (1977, 1979), Poots (1996), Admirat (1986, 1988, 1990) and Sakamoto (2000, 2005) all express the LWC as the mass of liquid water divided by the total mass of wet snow, as a percentage (%LWC by mass). LWC can also be defined as the mass of water per unit volume of solid (g/m^3). In the literature the last definition is rarely used to describe the LWC of wet snow.

3.3 The regimes of liquid water saturation

Wet snow has two basic modes, or regimes, of liquid water saturation: the *pendular* and the *funicular*. At low LWC values (Fig.6a), snow is said to be in the pendular regime and air is continuous throughout the pore space. The funicular regime (Fig.6b) occurs at higher LWC values, when water becomes continuous throughout the pore space.

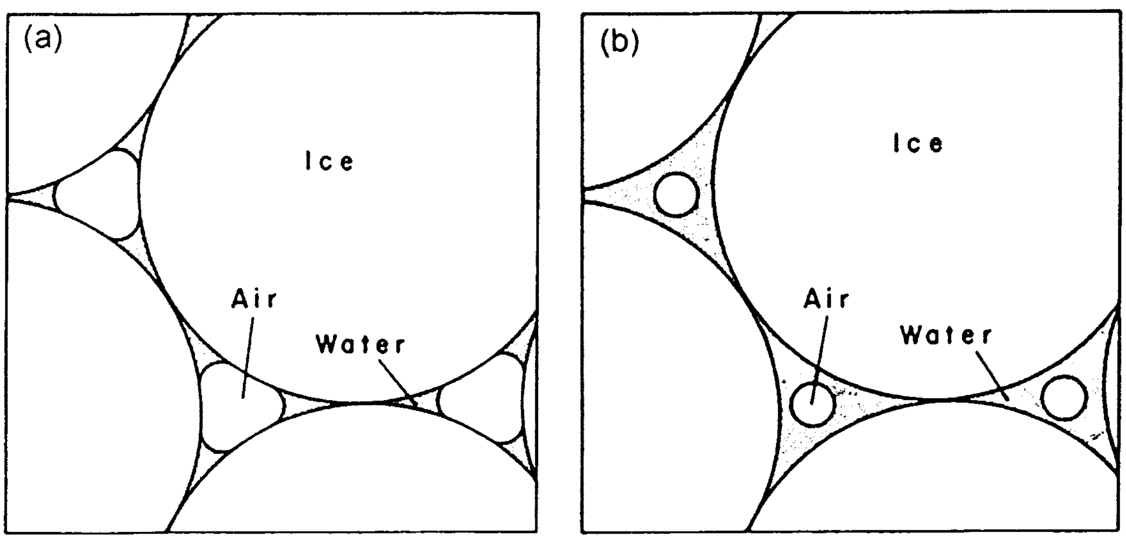

Fig.6 Wet snow in the pendular (a) and funicular (b) regimes
(from Colbeck 1973)

Using an ideal model of uniform spherical grains, Colbeck (1973) estimated the transition between the pendular and funicular regimes at a liquid saturation of about 14%. Denoth (1980) observed experimentally that the transition between the two regimes occurs over a range of liquid saturation that varies for different types of snow. For new, fine grained snow, it was observed between 13% and 18% which roughly corresponds to a LWC of 7% by volume, or 27% by mass (for a density of 0.20 g/cm^3).

It should be stressed that the amount of liquid saturation and the LWC are two different measures. Although the LWC may be used to calculate the amount of liquid saturation, the two measures are not mutually proportional. The LWC is used to evaluate the amount of liquid water in wet snow mainly because it is readily measured using simple tools. However, it does not truly represent the amount of liquid saturation of the snow matrix.

The LWC of wet snow increases upon melting and decreases upon freezing. Since wet snow is often accompanied by rain and/or freezing rain, liquid precipitations may also increase the LWC of wet snow sleeves.

3.3.1 Wet snow metamorphism in the pendular regime

At low LWC (less than 7% by volume), wet snow is said to be in the pendular regime. Liquid water is contained in menisci held between individual particles and air is continuous throughout the pore space (Fig.6a). Typical field measurements for the LWC in this "unsaturated" regime range between 3% and 5% by volume (Colbeck 1979).

As wet snow adheres to an overhead cable, the large packing forces exerted by the wind bring the ice particles into close contact. By capillarity, the liquid water contained in the snow matrix facilitates contact between individual ice grains and promotes heat transfer (Colbeck and Ackley 1982).

In wet snow, ice grains attempt to reach a state of minimum surface free energy: this means that individual grains tend to cluster, get rounder and fewer (larger ones grow at the expense of smaller ones) (Colbeck 1982, 1995). This metamorphism is driven by the conduction heat flow resulting from small temperature differences between individual grains. In the case of accretion on an overhead cable, the metamorphism begins in the atmosphere where wet snow flakes fall through air at a slightly positive temperature. The dendritic snowflake shapes are lost upon impact with the cable, and grain rounding takes place as the accretion is subjected to wind loads and thermal exchanges with the environment and with the cable. In such conditions, Admirat and Sakamoto (1988) suggested that the complete rounding and clustering process occurs within a few seconds of the impact.

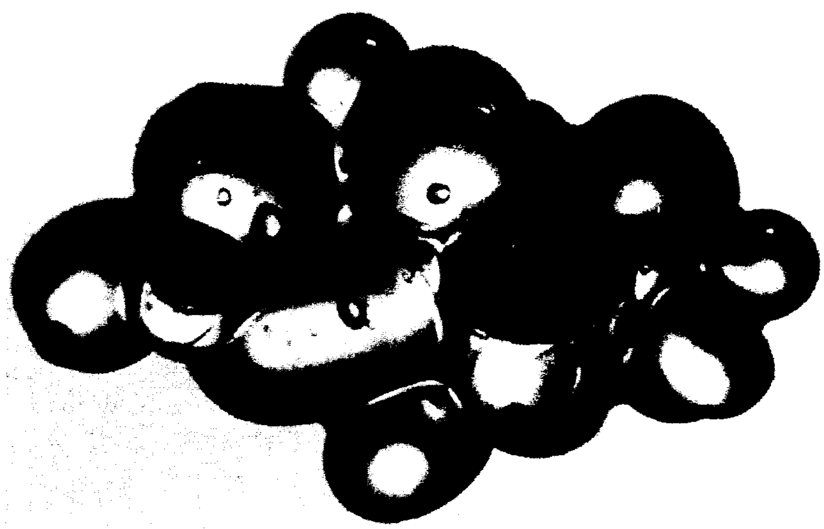

Fig.7 Grain cluster in the pendular regime
(from Colbeck 1997)

Grain clusters (Fig.7) develop naturally because they minimize the surface free energy. Large grain boundaries are more stable thermodynamically but they tend to melt if subjected to large normal compressive loads. The density of each grain cluster averages between 0.5 g/cm^3 and 0.6 g/cm^3, but this does not reflect the density on the macroscopic scale as the bulk density of snow depends on how closely packed grain clusters are with respect to one another. In fact, the density is much lower if there are large air-filled voids among the grain clusters. On the other hand, the overall snow strength depends on the number of grain boundaries found in a given volume of snow: a higher number of grain boundaries means that there are more interconnecting links between grain clusters, and hence greater overall strength. As the density of wet snow increases above approximately 0.6 g/cm^3 the grain clusters are replaced by a continuous network of interconnected grains and, as a result, snow strength is further increased (Colbeck 1982).

"In the snow cover on the ground these higher densities take months to achieve unless many meters of wet snow accumulation occur. On power lines, in the presence of high winds, the forces are sufficient to cause high accretion densities and the large specific grain boundary areas. Thus only a few hours is required to develop high strength, simultaneously with grain growth and grain rounding, in wet snow on power lines." (Colbeck and Ackley 1982)

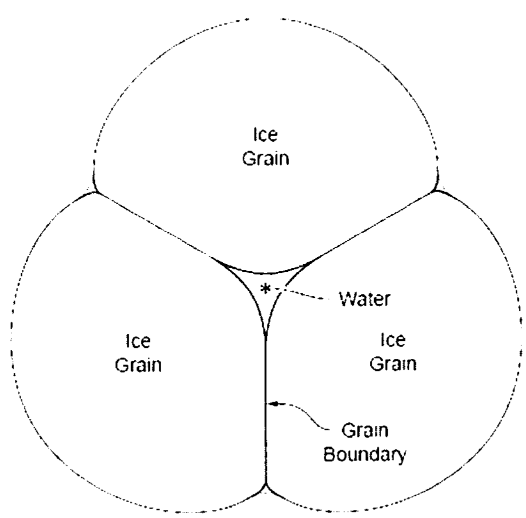

Fig.8 Three-grain cluster
(from Colbeck 1997)

As mentioned at the beginning of this sub-section, liquid water is contained in the menisci held by individual particles, in internal veins and external fillets (Fig.8). Veins occur at triple grain junctions and liquid fillets are found along grain boundaries (Colbeck 1997). Veins and fillets are quickly frozen if the temperature of the snow matrix drops below 0°C and they are not necessarily reformed upon melting (Fig.9). This explains the significant increase in the strength of wet snow sleeves that are subjected to overnight freezing, as reported by Sakamoto (2000).

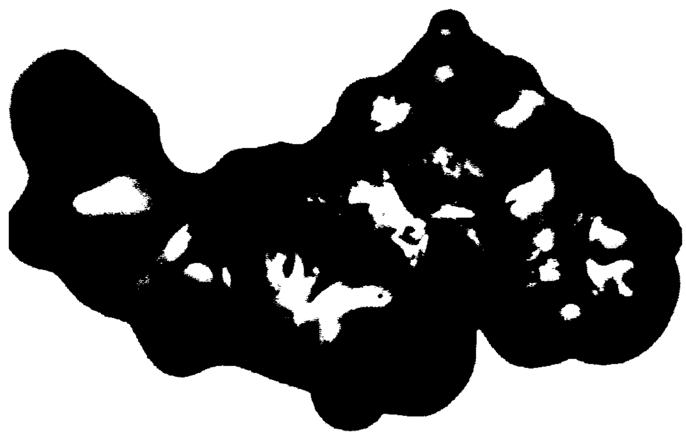

Fig.9 Amorphous grain cluster produced by melt-freeze cycles
(from Colbeck 1997)

Wet snow is well bonded in the pendular regime and its cohesive strength increases with increasing LWC. Individual ice grains joined in groups of two or more and are tightly held by ice-to-ice and capillary bonds (through water films). Capillary forces are strong in tension but weak in shear. However, snow sleeves exhibit considerable shear strength by resisting both gravity and wind forces against an overhead cable: solid-to-solid particle bonding must occur, even in the absence of subfreezing external conditions. Colbeck and Ackley (1982) demonstrated that capillary forces alone cannot explain the strong cohesive forces found in wet snow sleeves and that ice bonding through metamorphosis is necessary.

3.3.2 Wet snow metamorphism in the funicular regime

At high LWC (20% to 50% by volume), liquid water is continuous throughout the pore space, and air is trapped in the form of bubbles. This "slushy" regime can only occur if the water contained in the snow is prevented from draining. In this regime, the ice crystals are relatively large and the snow matrix acts almost like a fluid (Fig.10). Slushy snow has a low bonding strength because the crystals are fewer, rounded and weakly held together (Colbeck 1982, 1997).

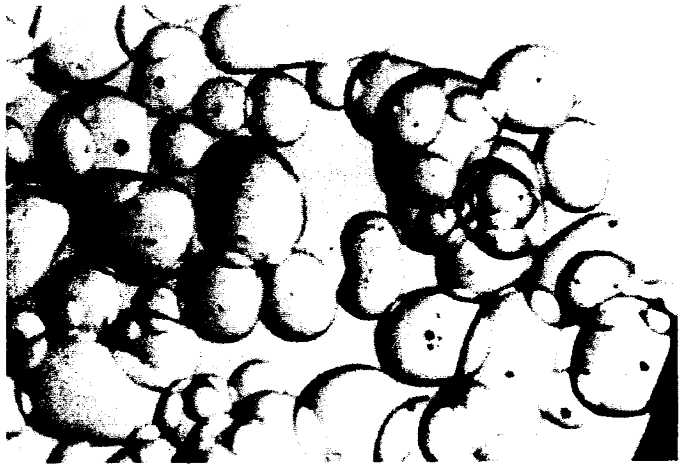

Fig.10 Wet snow grains in the funicular regime
(from Colbeck 1997)

In the funicular regime, ice bonds disappear as the LWC increases. As the number of ice bonds decreases, coherent forces are reduced to capillary bonds which are strong in tension and weak in shear. Natural shedding of wet snow sleeves from overhead cables occurs in the funicular regime when the gravitational and aerodynamic loads exceed the internal forces holding the sleeves together and on the cable (Grenier *et al.* 1986, Poots 1996).

A close parallel can be made between wet snow shedding from an overhead cable and wet snow avalanches: it is believed that water-saturated snow layers (in the funicular regime) are responsible for causing this specific type of avalanche (Colbeck 1986).

3.4 Heat balance of a wet snow sleeve

Grenier and Admirat studied the heat balance of a wet snow sleeve during the 1980's, as part of the French wet snow program initiated by Électricité de France. A model of the cylindrical accretion process was established that included precipitation rate, surface collection efficiency and the influence of various environmental parameters such as the wind speed and air temperature. This model was calibrated using both wind tunnel experiments and *in situ* observations and has been used to predict the density, diameter and LWC of wet snow sleeves.

A summary of this model can be found in Grenier *et al.* (1986) and Poots (1986). A more detailed explanation should soon be available in a chapter, authored by Pierre Admirat, in a book on atmospheric icing to be published in 2007. It is a very good attempt at modeling the complicated interactions of a number of factors during the accretion stage.

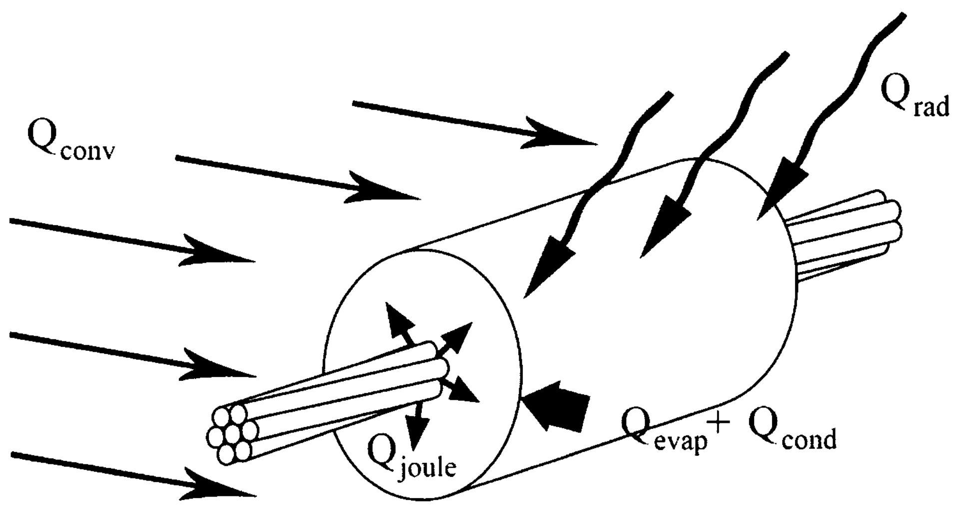

Fig.11 Heating and cooling effects on a wet snow sleeve

The model is based on the thermal equilibrium of a cylindrical sleeve. The heating and cooling effects are balanced by the melting or freezing of water inside the snow mass, i.e. by a variation of the LWC. Fig.11 illustrates the components of the thermal balance equation.

The heating and cooling effects are identified as:

- Q_{conv} : Heat supplied or removed by forced convection. During the accretion stage, the air temperature is slightly above the freezing point and heat is supplied to the snow sleeve. After the accretion stage, the air temperature may drop below the freezing point: in that case heat is removed by convection.

- Q_{evap}: Heat removed by evaporation/sublimation at the surface of the accretion. This effect should be neglected during the accretion stage since wet snow falls usually occur at a relative humidity close to 100%, which prevents evaporation.

- Q_{cond}: Heat supplied by condensation on the surface of the accretion. Condensation also increases the amount of liquid water in the snow sleeve.

- Q_{rad}: Heat supplied by ambient radiation and solar radiation. The amount of heat from ambient (air-snow) radiation is negligible and the model established by Grenier *et al.* (1986) neglects these radiation effects. It is fair to disregard solar radiation effects during the accretion stage when precipitations are heavy. However, they should be included when modeling a snow sleeve during the persistence and shedding stages.

- Q_{joule}: Heat supplied by Joule effect if the cable carries an electrical current. Rare meteorological conditions can maintain the LWC of a wet snow sleeve in the pendular regime. During such exceptional events, unrestricted growth of snow sleeves may occur, possibly leading to severe overloads and damages to overhead cables and structures (Poots 1996). In such circumstances, Grenier *et al.* (1986) suggest that Joule heating of the conductor be used to increase the LWC of the snow matrix and promote snow melting and shedding.

4. Field and laboratory observations

Wet snow accretions are difficult to study. They are rare and often limited to specific locations with special topography or microclimate. Field observations are typically done during the hours or days following a storm.

Compared to other types of icing accretion, it is more difficult to observe natural wet snow accumulated on an overhead cable since it might shed in a relatively short time or undergo rapid changes in LWC and strength (Sakamoto 2000).

4.1 Field observations in France, Japan and Iceland

Wakahama *et al.* (1977) state that it was Shōda who first studied in detail, in the early 1950's, the growth process and mechanisms of snow accretion on cables. Shōda observed wet snow accreting at temperatures between -1°C and +1.5°C, and wind speeds less than 3 m/s. Wind speeds exceeding 3 m/s blew the accreted snow off the cable; the snow accretions observed had low densities (0.2 g/cm^3). Those findings were published in 1953 in a Japanese article, unavailable in English, but have been reported by Wakahama *et al.* (1977).

Sakamoto (2000) reports that dry snow accretions are easily blown off from cables at wind speeds exceeding 2 m/s, and that they rarely exceed a density of 0.1 g/cm^3. Considering the range of temperatures and the low wind speeds, it would appear that Shōda was describing a mix of dry and wet snow sleeves similar to the kind of accretions sometimes found in France. Admirat *et al.* (1990), in their summary of the observations and measurements of the French wet snow program of 1983-1990, reported that a succession of dry and wet snowflakes was often observed at temperatures close to 0°C. Under low wind speeds (between 0 m/s and 5 m/s) the densities of those mixed accretions were observed between 0.10 g/cm^3 and 0.22 g/cm^3.

A comparison of wet snow data reported by monitoring programs in France, Japan and Iceland over the past 30 years is presented in Fig.12 and Table 1. Most northern countries such as Canada, USA, UK, Germany, Norway and Slovenia have also reported wet snow falls that have affected their overhead transmission network. However, wet snow accretion occurrences in these countries are not as common or as catastrophic as they are in France, Japan or Iceland.

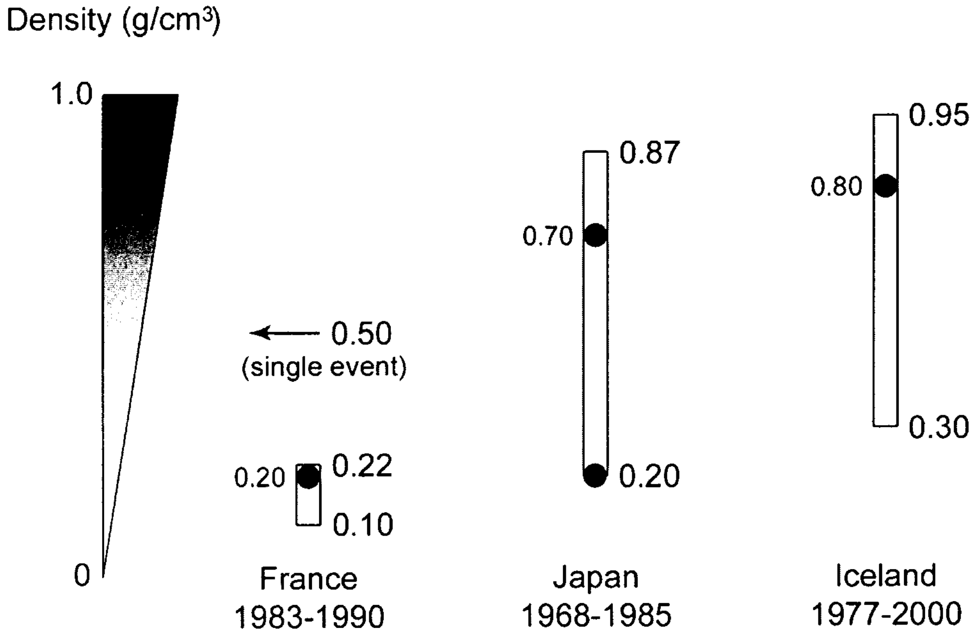

Fig.12 Density of wet snow accretions on overhead cables reported in three studies (data from Admirat *et al.* 1990, Wakahama *et al.* 1977, Sakamoto 2000, Elíasson and Thorsteins 1996)

The black dots in Fig.12 mark peaks in the wet snow density distributions. Two peaks are found in the data from Japan, corresponding to two distinct synoptic weather conditions. "Monsoon-induced snow accretions", as observed by Shōda (reported by Wakahama *et al.* 1977), occur at low wind speeds and produce low density accretions (0.2 g/cm³). However, "cyclone-induced snow accretions" are more severe, occur at high wind speeds and produce high density accretions (typically 0.7 g/cm³).

	France (1983-1990)	**Japan** (1965-1985) "monsoon"	"cyclone"	**Iceland** (1977-2000)
Wind Speed (m/s)	0 ~ 5	0 ~ 3	> 10	10 ~ 25
Density (g/cm^3)	0.1 ~ 0.22 0.50 (single event)	0.2	0.2 ~ 0.87	0.3 ~ 0.95
Snow Overload (kg/m)	0 ~ 10	0 ~ 5	0 ~ 15	0 ~ 20

Table 1: Density, wind speed and snow overload comparison for the studies carried out in France, Japan and Iceland (data from Admirat *et al.* 1990, Wakahama *et al.* 1977, Sakamoto 2000 and Elíasson and Thorsteins 1996)

The research efforts displayed by Japan and France reflect the fact that these countries are vulnerable to wet snow accumulation on overhead cables and structures. Their historical records show that they are at risk of being subjected to severe wet snow storms.

Sakamoto (2000) reports only 14 noticeable wet snow incidents in Japan, from 1962 to 1985. Wet snow falls do not occur often in Japan: on average, only once or twice a year, with noticeable storms approximately once every three years (Sakamoto 2005). For the last 50 years, the Japanese records do not show recurrence of severe wet snow incidents locally. Therefore, installing an instrumented test line in Japan has little chance of providing useful data on wet snow accretions (Sakamoto *et al.* 2005).

In France, wet snow falls occur on average two to three times a year. There have been several winters without such events, and some with up to seven wet snow episodes (based on 30 years of data given in Strauss (1986)). The numbers reported for France in Fig.12 and Table 1 only represent the data collected during a 7-year monitoring program, from 1983 to 1990. It should not be used to draw conclusions as to the typical densities of accretion that can be found in France.

Iceland records on average 8 to 10 wet snow episodes each year (Elíasson and Thorsteins 1996). In many cases the events are localized but in other cases they cover half of the country. Test spans of overhead cables are currently being monitored in Iceland.

4.2 Wet snow wind tunnel experiments

Wet snow accretion on a stranded conductor has been studied in wind tunnel laboratories in Japan since the 1970's. Wind tunnels were originally used to study the growth of wet snow accretions as well as their adhesive properties, their textures and the trajectories of individual snow flakes as they impact or pass by a cable (Wakahama *et al.* 1977). The artificial wet snow used in wind tunnels was obtained either by heating natural dry snow or by injecting a water spray along with crushed ice or dry snow.

Wind tunnel experiments were used in the 1980's during the France-Japan wet snow research collaboration to develop and validate accretion models. The latter studies, led by Sakamoto and Admirat, were successful in determining the effects of varying key meteorological parameters on the wet snow accretion process (Sakamoto *et al.* 2005). In order to perform a large number of experiments within the allowable time, parameters such as precipitation intensity and ambient air temperature were increased. Unfortunately, these modifications impaired the equivalence between the experimental and natural conditions (Sakamoto *et al.* 2005). In the opinion of the French wet snow specialists, the equivalence was difficult to achieve due to the poor design of the wind tunnel itself, which could not provide flow uniformity at the test section. Furthermore, suggested corrections were never implemented (Admirat 2006, Lapeyre and Dalle 2006).

In Japan, wet snow wind tunnels were occasionally used in the 1990's and in 2000 to study accretion shapes and the effect of conductor diameter on the size of wet snow sleeves (Yukino *et al.* 1998, Shugo *et al.* 2002).

5. Wet snow shedding

Observations of natural wet snow shedding from a cable are rare and not well documented. Very few people have actually witnessed the phenomenon and observations are varied and scattered. Shedding occurs following an increase of the LWC of a snow sleeve, governed by its thermal equilibrium. The exact LWC at which shedding occurs is difficult to predict: it depends on the density of snow and external factors (for example, snow shedding on a conductor may be triggered at a lower LWC if it is subjected to a sudden transverse acceleration). The range of LWC values reported at the time of shedding varies between 20% and 40% by mass (Admirat and Sakamoto 1988, Admirat 2006).

5.1 Observation of wet snow shedding in wind tunnels

Wind tunnel experiments seem to indicate that wet snow shedding on a conductor is a random process. On short cable sections (1 m to 2 m in length) wet snow was observed to shed suddenly along the entire length or in partial, random segments (Sakamoto *et al.* 2005).

The following trends have been observed during wind tunnel testing:

a) Low density snow tends to shed more easily than higher density snow.
b) At high wind speeds, accretions tend to hold well onto a cable, even if the eccentric weight and cable twist are large. Accretions formed under high wind speeds do not drop off easily.
c) The likelihood of shedding does not depend significantly on the air temperature.
d) Accretions tend to shed more easily from torsionally stiff cables.
e) Once a complete snow sleeve has formed it is very unlikely to shed by wind and gravity loads alone.

It should be emphasized that observations a) to d) apply to accretions that have not yet formed into a complete cylindrical sleeve (Sakamoto *et al.* 2005). To be more precise, observation e) should state that a snow sleeve is unlikely to shed in a relatively short period of time after its accretion: as the sleeve warms up and its LWC increases it becomes more likely to shed. It has been described in section 3.3.2 how the natural shedding of a wet snow sleeve occurs in the funicular regime, once gravitational and aerodynamic loads exceed the reduced internal cohesive forces.

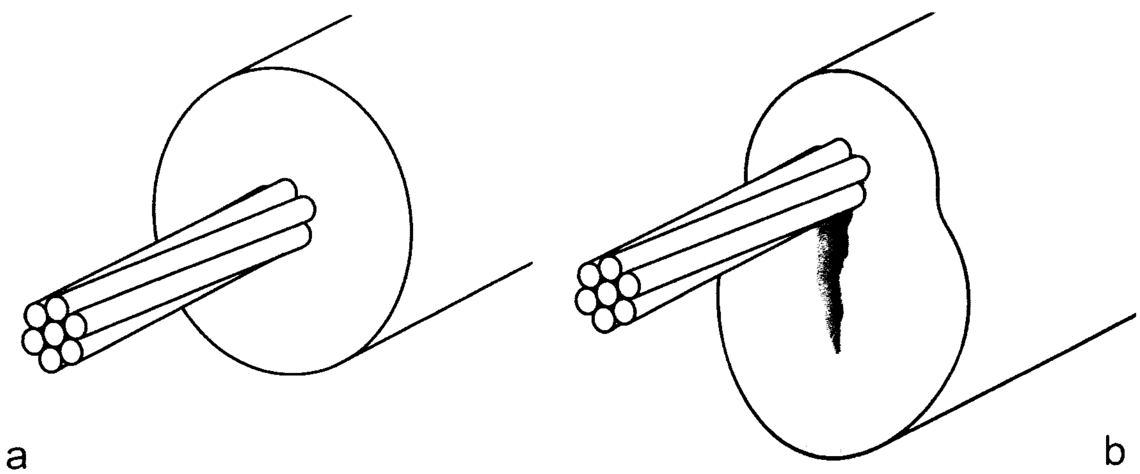

Fig.13 Wet snow creep at high LWC
Density 0.4 ~ 0.7 g/cm³, LWC ~ 40% by mass (re-drawn from EDF 1986)

At high LWC values snow creep was observed prior to shedding. As illustrated schematically in Fig.13, the initial cross-sectional profile (Fig.13a) became elongated and a cavity formed below the cable as the snow migrated slowly due to gravity (Fig.13b). The snapshots were taken 20 minutes apart.

Wet snow sleeves were observed to melt when subjected to air temperatures above 0°C or when the cable was heated (Sakamoto *et al.* 2005). The liquid water produced by melting migrated to the bottom of the accretion, which became saturated with water and appeared translucent. Water droplets dripped from the bottom of the snow sleeve, but the LWC of the top of the accretion remained more or less the same (Sakamoto *et al.* 2005). Sakamoto has even witnessed cases where the bottom half of the accretion had shed but the top part remained on the cable. The melting phenomenon described above was also observed when liquid water was sprayed onto the snow sleeve to simulate rain.

5.2 *In situ* observation of wet snow shedding

5.2.1 Natural shedding

Field observations show that shedding of wet snow sleeves first occurs on axial growths close to the towers, where cable rotation is prevented or reduced. Fig.14 illustrates where axial growths have shed: the conductor is bare on the first 20 to 30 meters from the tower, and the remaining accretion is cylindrical (with the maximum sleeve diameter at the center of the span).

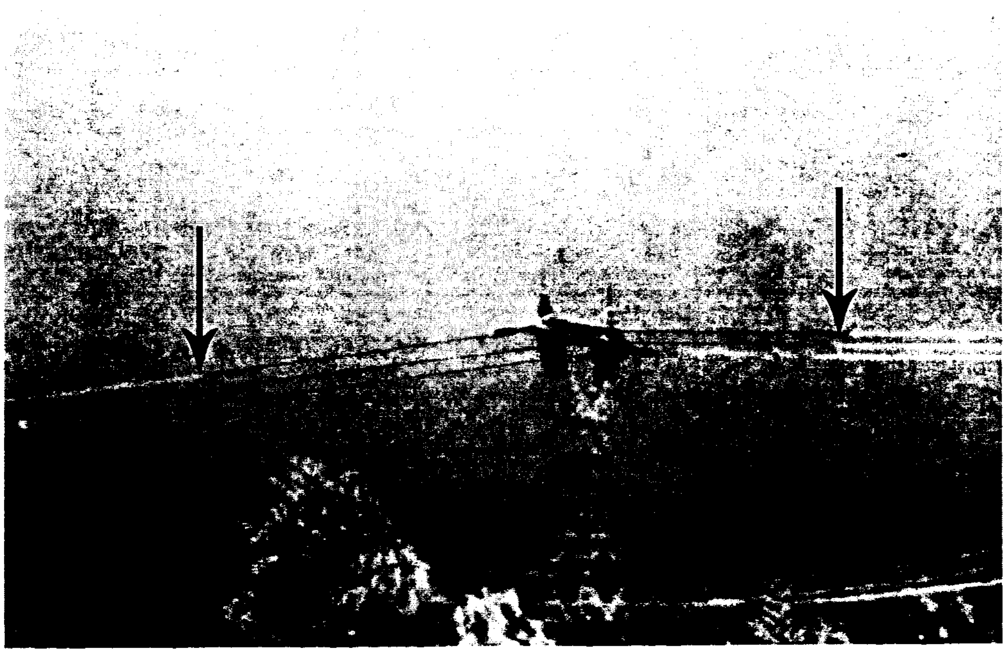

Fig.14 Axial accretion shedding
(from Admirat and Lapeyre 1986)

In general, cylindrical sleeves shed partially and randomly over the span, in segment lengths up to 30 meters (rough approximation). Total unloading by partial shedding may take place in 5 to 10 minutes (Admirat 2006).

During wet snow events, successive cycles of accumulation and shedding (saw-tooth loading cycles) have been observed on overhead cables. It is possible to increase the frequency of these cycles by using Joule heating, since increasing the LWC of wet snow sleeves promotes shedding. Joule heating may be used to limit the maximum snow overload and to delay the onset of the accretion phase during a storm (Grenier *et al.* 1986).

Poots (1996) suggested that a wet snow sleeve may also shed suddenly along the entire length of the span. At first, this may seem like a reasonable hypothesis. However, it has never been observed in the field and it is very unlikely that all of the snow would shed at the same instant.

Poots has developed mathematical models of snow and ice accretion based on thermodynamic, heat transfer and fluid flow equations. These accretion models rely on basic physical mechanisms and have been summarized by Poots (1996). A continuation of his work could lead to a 3-dimensional, time-dependent model of the growth, persistence and shedding of snow accretion on an overhead cable that would be valid for a full range of precipitation rates, temperatures and wind speeds. Such a model would be very useful to predict the amount of accumulated snow on cables. Saw-tooth loading cycles could also be predicted, as well as the amount of Joule heating necessary to limit overloads (or even to ensure shedding before overnight freezing).

Pierre Guilbeault, a test engineer at Hydro Quebec's Research Institute (IREQ), made some observations on the wet snow that accumulated on the Hydro Quebec experimental line in Varennes, Quebec, on March 22nd 2001 (Guilbeault 2005). He observed snow shedding in a random and partial manner on phase conductors (non-energized). Some overhead ground wires shed in an "unzipping" fashion along their entire span, which caused large cable oscillations with mid span displacements of the order of a few meters. Some of the fallen accretions were weighted and the snow overload was roughly estimated at 5 kg/m (Guilbeault 2005). Observations were made on the day of the event, when snowfalls were moderate. Weather conditions reported for this 30-hour long snow event were as follows: 40 to 60 cm of snow accumulation on the ground, some periods with large precipitation rates, air temperature between 0°C and 1°C, wind speeds between 10 m/s and 15 m/s (Environment Canada's Climatic Database web reference, data for Montreal, Quebec).

It is unlikely that the unzipping shedding witnessed came from wet snow falling naturally from the ground wire from one tower to the next. A more realistic scenario would be that partial shedding (or a succession of partial shedding events) on an adjacent span generated a transverse wave that traveled along the entire span of the ground wire. The LWC of the snow sleeve must have been high enough to reduce significantly its cohesive strength, and the vertical acceleration caused by the wave, sufficiently large to trigger snow shedding as it progressed along the span. Hence shedding traveled along the ground wire at the speed of the transverse wave.

The speed c at which a wave progresses along a taut cable can be estimated by the following wave mechanics equation:

$$c = \sqrt{\frac{T}{\mu}} \qquad (5.1)$$

where T is the tension in the cable and μ is the mass of the cable per unit length.

It is interesting to note that the unzipping shedding phenomenon described by Guilbeault (2005) was only observed on ground wires. It could be that unzipping shedding is more likely to occur on an overhead cable with a smaller diameter.

There may also be other modes of wet snow shedding. For example, it is likely that a snow sleeve may not be uniform in density and LWC along the length of an overhead cable and that unzipping may be limited to fractions of a span (e.g. 25% or 40%). The remaining accretion could shed in random segments if there is no means of generating another transverse wave on the cable. Such a case would be a mixed mode of shedding. It is unfortunate that the available literature lacks descriptions of *in situ* wet snow shedding.

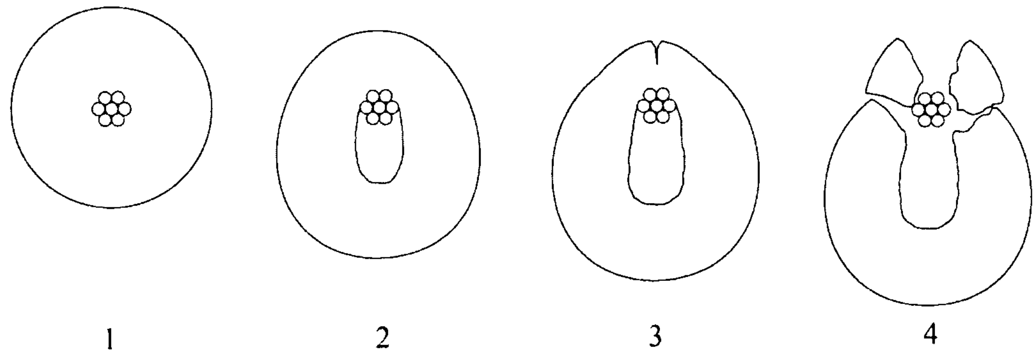

Fig.15 Creep progression up to shedding

Hung Huynh, a professional engineer at Nova Scotia Power, has also witnessed the effects of a few wet snow storms on overhead lines. He confirms the observation of wet snow creep prior to shedding, under the influence of gravity and environmental factors such as temperature, wind, liquid precipitations and solar radiation (Huynh 2006). Fig.15 illustrates the creep of a snow sleeve as he describes it.

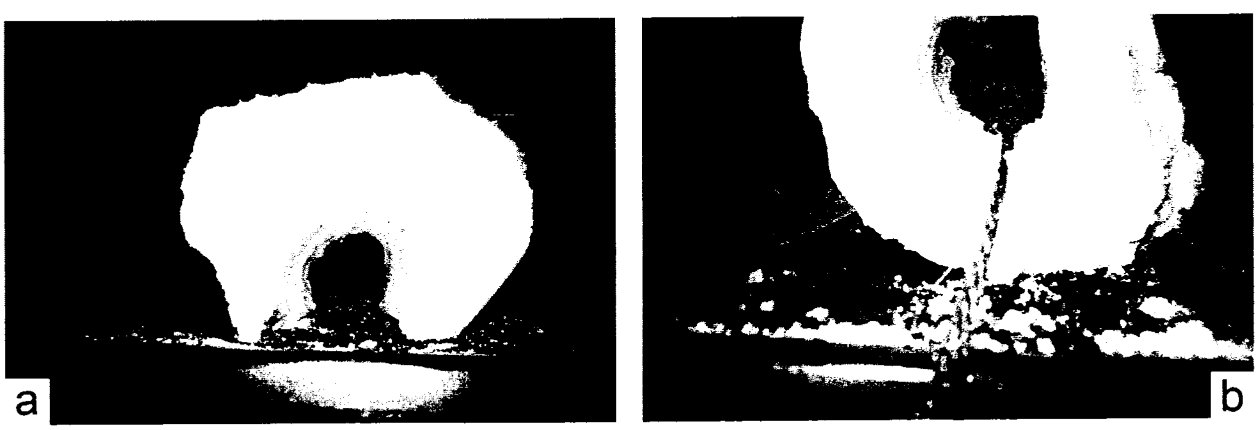

Fig.16 Large circular cavity in a wet snow sleeve due to the action of gusty winds
Density ~ 0.40 g/cm³ (from Huynh 2006)

If the air temperature is close to the freezing point and creep takes place under the action of gusty winds, the cavity carved by the cable inside the snow sleeve may become almost circular (Fig.16) instead of being narrow and elongated.

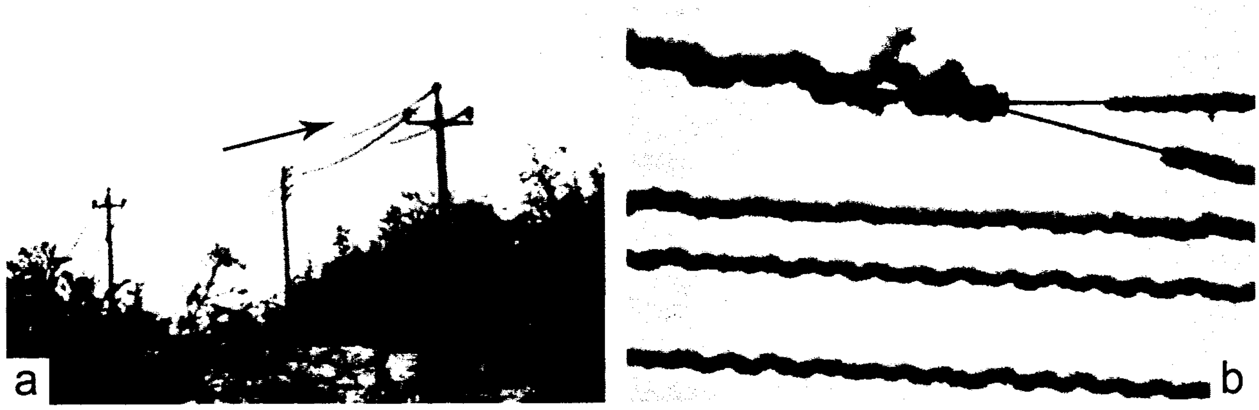

Fig.17 Creep of a wet snow sleeve on a steep cable
Density 0.2 g/cm³ to 0.3 g/cm³ (from Admirat and MacCagnan 1985)

Another type of creep has been observed on wet snow sleeves, one that occurs along the length of an overhead cable. Wet snow tends to flow down along steep cables (over 30 to 40 degrees of inclination), especially if the accretion is not a completely formed sleeve. This type of creep (Fig.17) has been observed in France in mountainous terrain (Admirat and MacCagnan 1985).

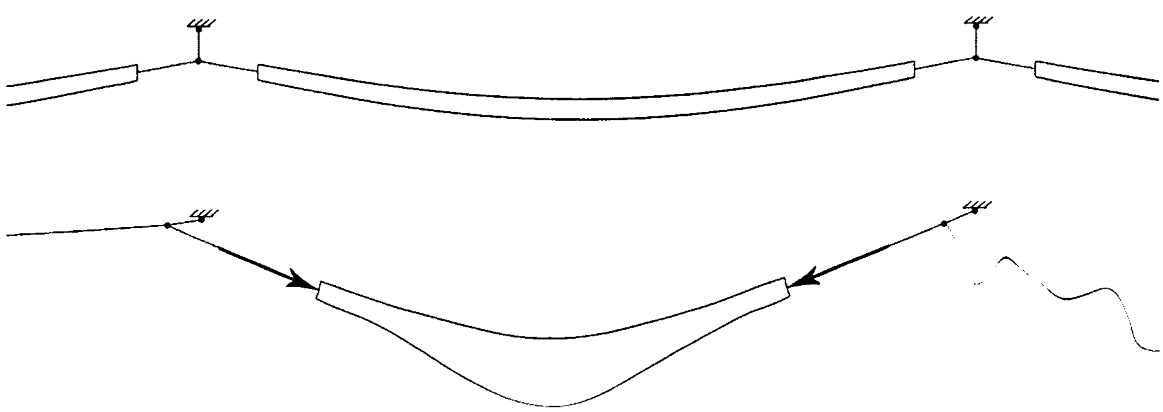

Fig.18 Wet snow creep along a sagging cable

Observations of snow creep along a cable have also been reported in Nova Scotia on cables adjacent to collapsed spans (Fig.18). The radial dimension of the initial, fully formed sleeve was estimated at 7.5 cm. As shown in Fig.19, the radial dimension was over 50 cm at mid span, following creep (Huynh 2006).

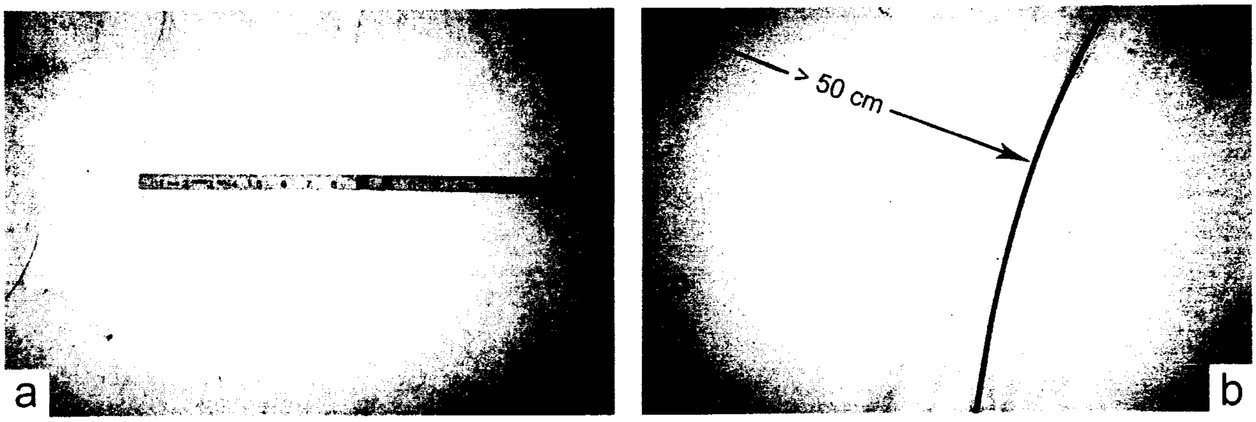

Fig.19 Wet snow creep along a sagging cable, at the mid span
(from Huynh 2006)

5.2.2 Natural shedding after overnight freezing

Natural shedding strongly depends on the weather conditions during and following the accretion. During the wet snow event described by Guilbeault (2005), the air temperature was more or less steady and always above or equal to 0°C; on top of that the event took place at the end of March when solar radiation is significant at the site, even through a cloudy sky.

If a wet snow sleeve is subjected to overnight freezing it is unlikely to shed naturally by the mechanisms described above. Instead, it will remain on the cable and shed later in a similar manner as rime ice and glaze ice, i.e. by slow sublimation and/or melting (if the temperature gets above the freezing point). In Iceland, such hardened snow accretions have been reported to persist for many weeks (Elíasson and Thorsteins 2000).

The photograph in Fig.20 was taken from a report issued on January 18th, 2005, by the Nova Scotia Utility and Review Board. On November 13th and 14th, 2004, a severe storm struck the province of Nova Scotia. The event was characterized by strong winds, temperatures close to the melting point and a large amount of precipitation in the form of wet snow, sometimes accompanied by ice pellets and rain (Environment Canada's Climatic Database web reference, data for Halifax, Nova Scotia).

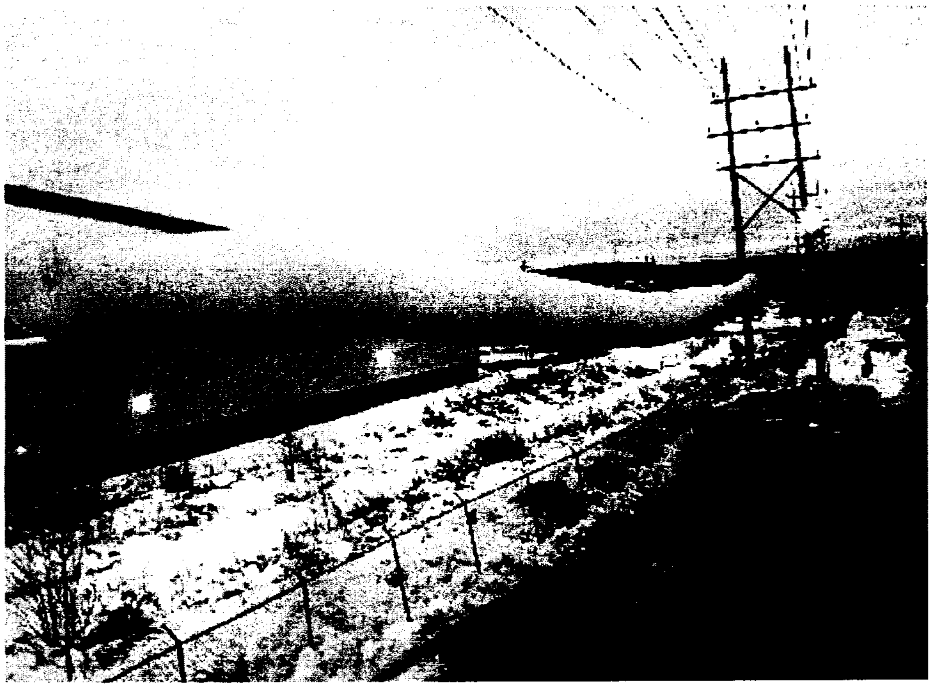

Fig.20 Wet snow sleeve still holding to a cable, November 17th, 2004
(from Nova Scotia Utility and Review Board 2005 report reference)

The photograph in Fig.20 was taken three days after the storm and shows an accretion that is still holding to about half of the span of a cable. A particular feature in this picture is the cable showing out of the top of the snow sleeve on the left-hand side. This may be giving a hint as to how snow sleeves shed after being subjected to freezing.

5.2.3 Forced shedding

Poots (1996) suggests that wet snow accretions may also shed by some of the mechanisms observed with glaze and rime ice. A sudden twist given to a rime ice accretion, or a significant axial traction or bending moment on a glaze ice accretion (e.g. from a propagating axial or transverse wave on the cable) can lead to the fracture and shedding of the accretion. However, there is no field observation to confirm that these could be applicable to wet snow.

Since wet snow is a highly plastic material it is uncertain that an applied static deformation could trigger its shedding. However, it is reasonable to assume that any accretion can be removed from a cable by subjecting it to a sufficiently large transverse acceleration caused by a combination of gravity, wind and inertia effects. In such a scenario the resultant load may exceed the cohesive strength of the snow sleeve, causing the cable to punch trough the accretion.

6. Mechanical properties of snow

In the literature surveyed, there is no mention of any material testing ever performed on wet snow sleeves, either from field samples or wind tunnel experiments. One of the biggest difficulties to expect when attempting to measure the strength of a snow sleeve comes from the fact that the material structure of these accretions evolves rapidly: field samples are typically collected hours or even days after their accretion (or shedding). So far, artificial snow with physical properties and microstructure approaching that of natural wet snow has not yet been generated for material testing.

The subject of wet snow mechanics is practically inexistent. However, some work has been done in dry snow mechanics. Intuitively, wet snow in the pendular regime (i.e. at low LWC) and dry snow should exhibit similar behavior under given loading conditions, since they are made of the same constituents and their internal structure is somewhat similar.

6.1 Current state of knowledge of the mechanical properties of dry snow

To the best knowledge of the author, Shapiro *et al.* (1997) published the most recent review on the state of knowledge of snow mechanics in relation to practical engineering applications. Unfortunately, their review was limited to dry snow. This is not surprising since most of the work done so far in snow mechanics dealt with dry snow at sub-freezing temperatures, with the exception of a few scattered cases where snow properties were measured close to the melting point.

The mechanical behavior of dry snow has been studied to some extent, but not thoroughly. Pertinent data on the mechanical behavior of snow has been gathered since the 1930's. Mechanical properties of snow were first measured during avalanche studies in Switzerland, and were compiled by Bader *et al.* (1939). In the 1950's and 1960's numerous experimental observations were made at the U.S. Army Corps of Engineers'

Cold Regions Research and Engineering Laboratory (CRREL) in Hanover, New Hampshire. During the same period, Canada, Switzerland and Japan also conducted a considerable number of laboratory and *in situ* experiments on snow mechanics (Shapiro *et al.* 1997).

Up to the late1960's, most of the experimental work was devoted to developing constitutive models of linear elasticity, viscosity and visco-elasticity. In the 1970's, emphasis was shifted on developing nonlinear deformation and fracture theories. Work was also done to develop new constitutive relationships based on the study of the microstructure of snow during its deformation.

Most of these studies on snow mechanics were motivated by research on snow roads and runways, avalanches and vehicle mobility. Compressive, tensile and shear experiments have been performed on dry snow samples, both in controlled laboratory environment and *in situ.*

The data on the mechanical properties of snow are usually organized and presented as a function of its density. However, snow density alone is not a reliable parameter to describe these properties. In reality, for a given temperature and loading condition, the response to a load depends primarily on the microstructure of the snow deposit (grain shape, size, bond density, etc.), which is not directly correlated to its density.

At present, there is no workable method to relate the observable physical characteristics of snow (i.e. snow type, grain size and shape, density, liquid water content, temperature) to its mechanical response to a given load or imposed deformation. The mechanical properties of snow have been determined experimentally for a few load cases only, and the constitutive relationships developed so far are unable to describe the behavior of snow over its full range of deformation (Shapiro *et al.* 1997).

6.2 Qualitative deformation properties of dry snow

In this section, it is interesting to outline some of the properties of dry snow when it is subjected to different loading conditions as these may, to a certain extent, also apply to wet snow in the pendular regime (low LWC).

Langham (1981) gives a good explanation of the mechanical behavior of snow:

"Snow may be deformed elastically when subjected to a small load applied for a short period of time. Under these conditions the strains are small enough not to disrupt the grain structure and are recoverable once the stress is removed. Snow also deforms continuously and permanently if a sustained load is applied; this is referred to as creep or viscous plastic flow. Strictly speaking, plastic flow requires a threshold stress to be reached before flow can start. However, for snow this stress is so small that it cannot be measured and so snow is referred to as a visco-plastic material."

The deformation of dry snow is rather complex and is characterized as follows (Fukue 1977, St. Lawrence and Tang 1980):

- loading rate dependent
- loading history dependent
- temperature dependent
- undergoes large deformation before fracture
- stiffening behavior under compressive load
- softening behavior under tensile loading

Some of those aspects are shown in Fig.21. The loading rate affects the failure mode in such a way that it is ductile at low deformation rates, and brittle at high deformation rates. Grain metamorphism, from dendritic snowflakes to spherical grain shapes, is also found in dry snow, along with an increase in cohesive strength. The rate of metamorphism is slower in dry snow than in wet snow, taking place over a period of time measured in days, weeks or even months. Fig. 21 indicates that snow samples that are six days old exhibit 10 times the compressive strength of fresh snow (30 minutes old).

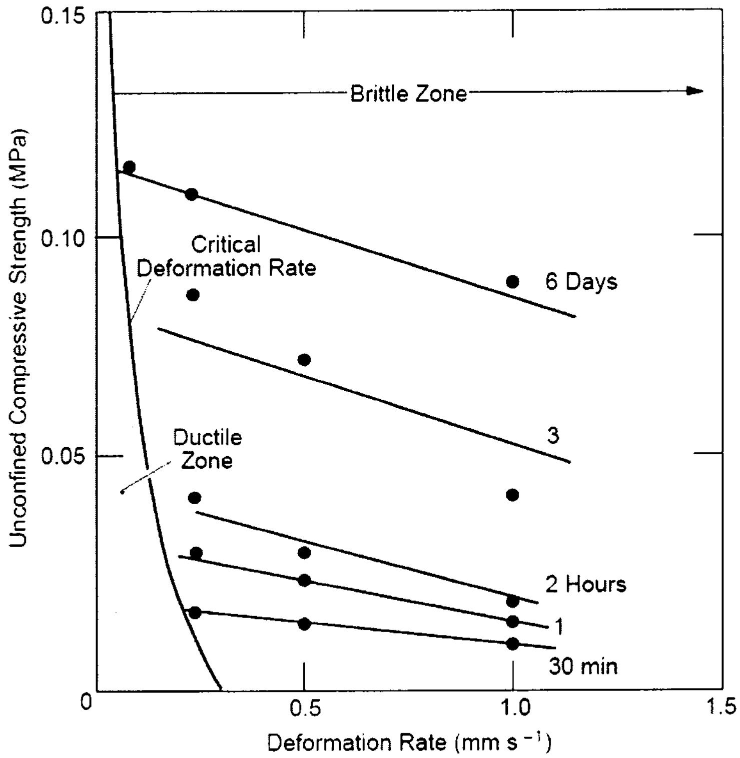

Fig.21 Unconfined compressive strength vs. deformation rate for snow samples of various age, 15-cm long
(from Fukue (1977), reproduced in Shapiro *et al.* (1997))

The difficulties encountered when attempting to describe the mechanical properties of snow in a general way are well illustrated by Fukue (1977) when he compares them to the difficulties of characterizing sand and clay. The variation in the nature of snow, from fresh powder to something close to ice may in fact be similar to the variations found between sand and sandstone, or clay to shale.

7. Experimental Study

Experiments were performed by the author in March 2006, at the CIGELE Pavillon de recherche sur le givrage at UQAC, Chicoutimi, Quebec, in order to assess the feasibility of reproducing wet snow sleeves.

Wet snow sleeves were successfully reproduced from fresh dry snow collected on the UQAC campus grounds, in view of understanding the phenomenon of wet snow shedding. The large climate rooms of the CIGELE facilities were ideal to perform such a study (Fig.22). The raw material required (i.e. fresh dry snow of good quality) is not in short supply at UQAC during the winter season since the Chicoutimi area receives over 3 meters of natural snowfall every year (The Weather Network web reference, data for Bagotville, Quebec).

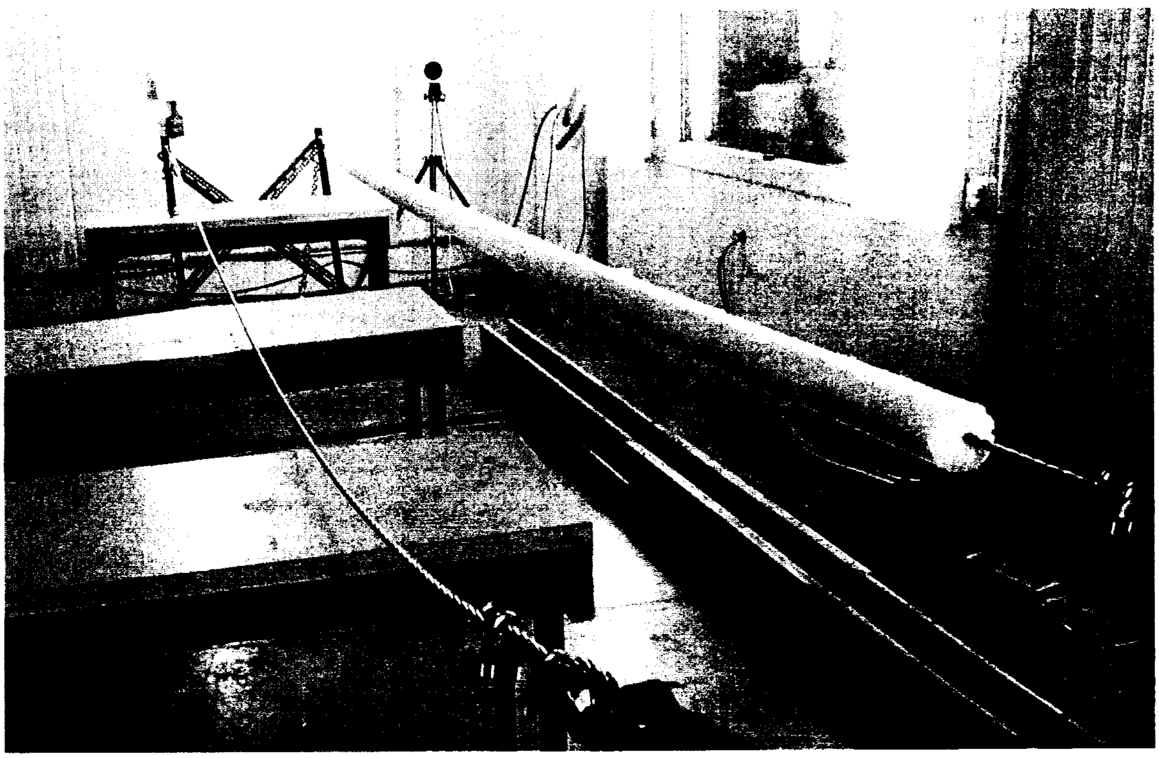

Fig.22 Inside view of one of the CIGELE climate rooms

This chapter contains a description of the experimental setup, details about the technique developed to make wet snow sleeves and a full explanation of the fusion calorimeter method used to measure the LWC of snow (LWC values are all given as a percentage of the total mass). Experiments were carried out using the wet snow sleeves thus made: for the different wet snow sleeves fabricated, they generally consisted of letting the snow melt slowly and observing the difference in shedding behavior.

7.1 Experimental setup

The experimental setup used to simulate wet snow accretion shedding is shown schematically in Fig.23. Two 5-meter-long stranded conductor (ALCAN Pigeon 6/1 ACSR, 12.75 mm diameter) were installed approximately 1 meter above the floor. The cables were tensioned using cable-hoists to remove most of the sag due to the snow load.

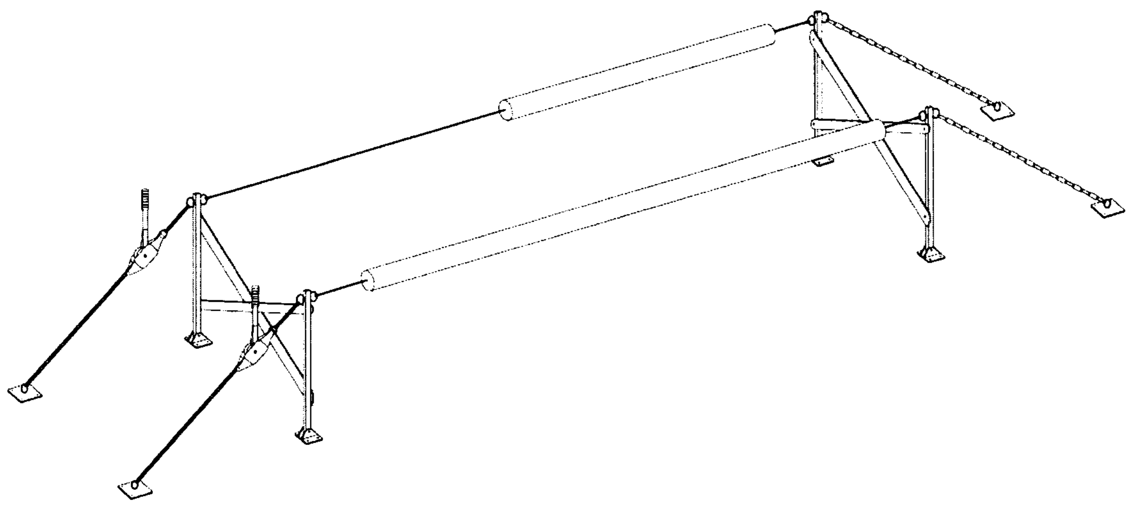

Fig.23 Experimental setup used in one of the CIGELE climate rooms

This setup was installed in a climate room. For most experiments the room temperature control was set at 3°C. Actual room temperature measurements varied between 2.3°C and 3.1°C. The relative humidity was measured between 80% and 95%, and could not be controlled.

7.2 Wet snow sleeve molding

The wet snow used for all the experiments was obtained by bringing fresh dry snow into the climate room and spreading it evenly, 1 cm to 2 cm thick, on sheets of polystyrene insulation board. The dry snow was collected from the top layer of snow banks that had accumulated less than 12 hours earlier. The LWC of the snow approached that of precipitating wet snow after being exposed to warmer air at 3°C for a period of one hour. This method produced an adequate wet snow material with good LWC uniformity and was based on the recommendations of Sakamoto (2000, 2005).

An inexpensive technique was developed using simple tools to produce wet snow sleeves around a cable. Fig.24 illustrates how the sleeves were molded.

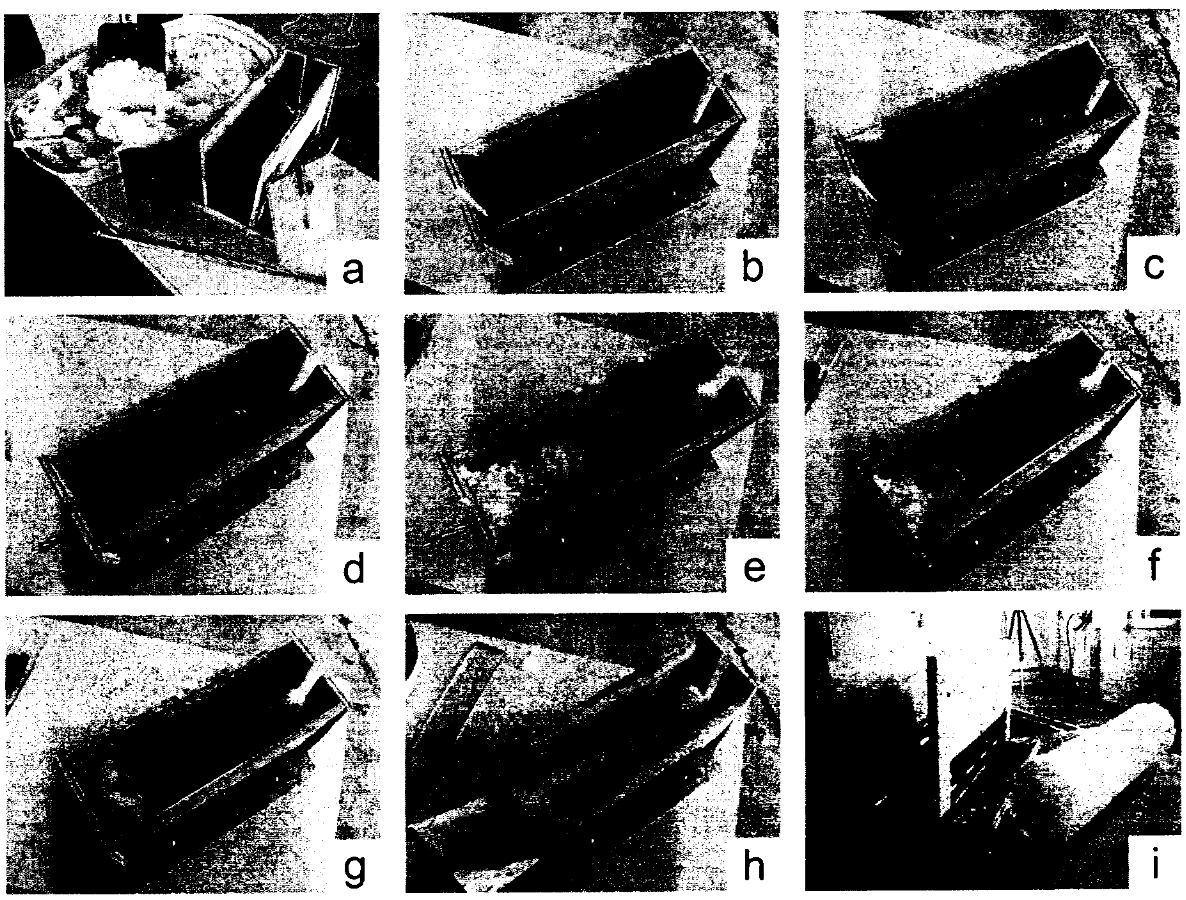

Fig.24 Molding a snow sleeve around a conductor

Wet snow was laid in a semi-cylindrical mold and compacted evenly in a succession of layers (Fig.24a, b, and c). Once the bottom half of the sleeve was formed the mold was placed under the cable and raised until the snow touched the cable (Fig.24d). The top half of the sleeve was formed using a semi-cylindrical hand tool and was also made of compacted layers of wet snow (Fig.24e, f, and g). Upon mold removal the fabricated snow sleeve had a uniform diameter of 10 centimeters.

A short mold was designed for the purpose of developing and fine tuning the molding process illustrated in Fig.24. A longer mold was fabricated once a reliable and repeatable molding technique was acquired, in order to make snow sleeves up to 5 meters in length (Fig.25a).

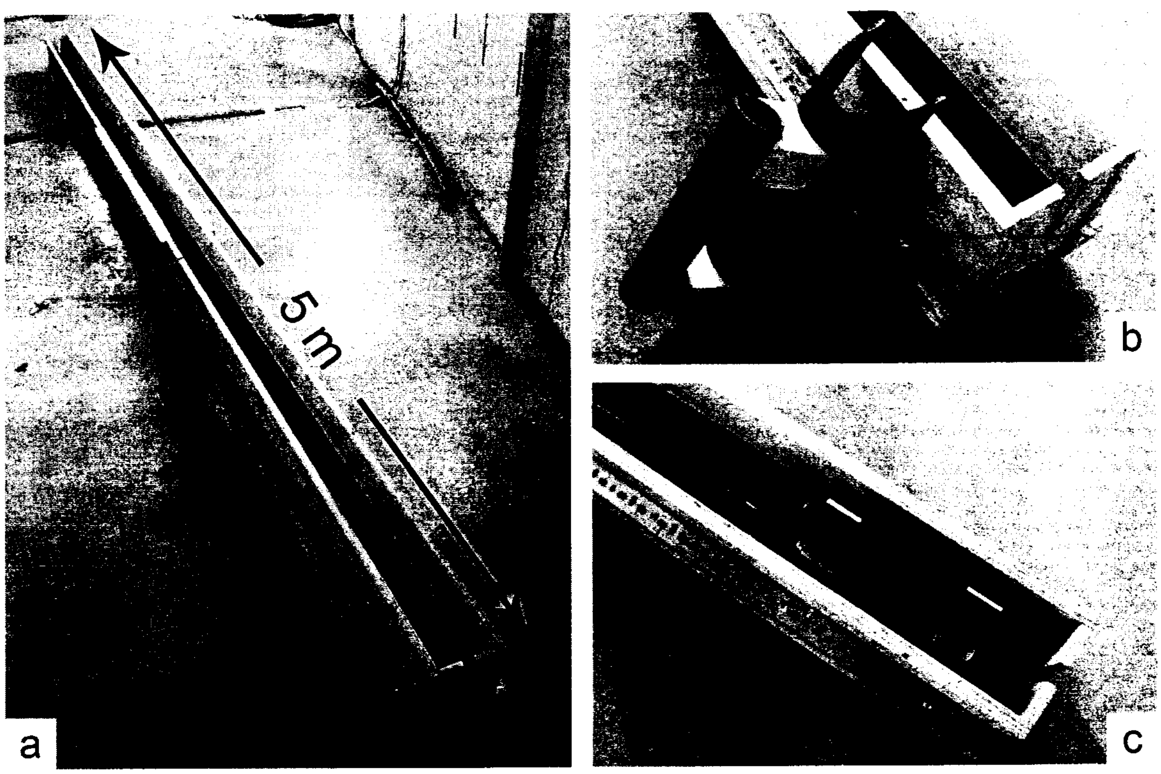

Fig.25 Tools used for full-size snow sleeve fabrication

7.3 LWC measurement using a fusion calorimeter

The amount of liquid water contained in a snow sample can be estimated by using a hot calorimeter (Colbeck *et al.* 1990). It is a simple thermodynamics exercise but it should be explained in detail since it is the most important tool used to characterize snow.

Material required (Fig.26):

Adiabatic container (750ml stainless steel thermos with cover)

Digital thermometer (ideally with 2 probes)

Digital scale(s)

Fig.26 Equipment used in calorimetric experiments

7.3.1 Calorimeter calibration

The first task at hand is to find the heat capacity of the calorimeter's container. If this step is neglected the amount of heat absorbed by the container during a LWC measurement will alter the results. The heat capacity of the container can be evaluated by mixing warm and cold water together in the calorimeter. It is calculated using the heat balance equation of the system.

Let

$m_1 = 250\text{g}$ of warm water

$T_1 =$ temperature of m_1

$m_2 = 250\text{g}$ of cold water

$T_2 =$ temperature of m_2

$m_3 = m_1 + m_2 =$ total mass

$T_3 =$ final temperature of the mix

$c_{water} =$ specific heat capacity of water $= 4.187\, \text{kJ}/\text{kg} \times \text{K}$

$C_{container} =$ heat capacity of the calorimeter's container

Procedure (as illustrated schematically in Fig.27):

- Flush the calorimeter with warm water, empty and dry
- Weight m_1
- Put in m_1, close lid, stir and let sit for one minute
- Measure T_1
- Weight m_2 and measure T_2
- Put in m_2, close lid and stir for one minute
- Measure T_3

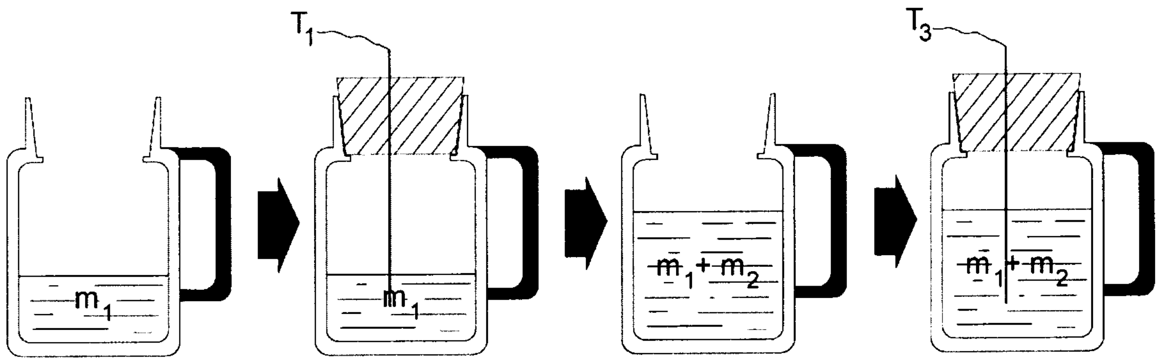

Fig.27 Calibration of the fusion calorimeter

Assuming that the total system (water mix + calorimeter) is perfectly adiabatic (no heat exchange with the environment) all of the extra heat gained by the water during the mixing comes from the calorimeter. It is reasonable to assume that the system is adiabatic since during a 30-minute preliminary test with warm tap water (50°C ~ 55°C) the temperature drop was less than 1.0°C. Considering that the entire LWC measurement can be performed in less than 3 minutes, the maximum temperature drop expected during a typical LWC measurement due to losses to the environment is therefore less than 0.1°C.

The heat balance equation of the system (water mix + container) is:

$$m_1\, c_{water}\, T_1 + C_{container}\, T_1 + m_2\, c_{water}\, T_2 = m_3\, c_{water}\, T_3 + C_{container}\, T_3 \qquad (7.1)$$

Solving for $C_{container}$ (the calorimeter's heat capacity) we get

$$C_{container} = \left(\frac{m_3\, T_3 - m_1\, T_1 - m_2\, T_2}{T_1 - T_3} \right) \times c_{water} \qquad (7.2)$$

Substituting $m_3 = m_1 + m_2$, and letting $\lambda = C_{container} / c_{water}$

$$\Rightarrow \quad \lambda = \frac{m_1 (T_3 - T_1) + m_2 (T_3 - T_2)}{(T_1 - T_3)} \qquad (7.3)$$

The thermos container used for this study was found to have the following heat capacity:

$C_{container} = 45.51\ {}^{J}\!/_{K}$

This value was obtained by taking the average of five calibration runs and it was repeatable within 2%. Dividing by c_{water} yields the value of $\lambda = 10.88$ grams of warm water.

7.3.2 Evaluating the LWC of a snow sample

An experiment similar to the above calibration step is performed to obtain the LWC of a snow sample.

Let

$m_1 = 500\text{g}$ of warm water

$T_1 =$ temperature of m_1

$m_2 = m_{2L} + m_{2S} =$ mass of the snow sample (liquid + solid parts)

$T_2 =$ temperature of the snow sample (0°C if it is a wet snow sample)

$m_3 = m_1 + m_2 =$ total mass

$T_3 =$ final temperature of the mix

$c_{ice} =$ specific heat capacity of ice $= 1.84\ {}^{kJ}\!/_{kg \times K}$

$c_{water} =$ specific heat capacity of water $= 4.187\ {}^{kJ}\!/_{kg \times K}$

$C_{container} =$ heat capacity of the calorimeter's container

$L =$ specific latent heat of fusion of water (ice) $= 333.51\ {}^{kJ}\!/_{kg}$

Procedure (as illustrated schematically in Fig.28)

- Flush the calorimeter with warm water, empty and dry
- Weight m_l
- Put in m_l, close lid, stir and let sit for one minute
- Measure T_l
- Weight m_2 and measure T_2 (if this is a dry snow sample it may be less than 0°C)
- Put in m_2, close lid and stir for one minute
- Measure T_3

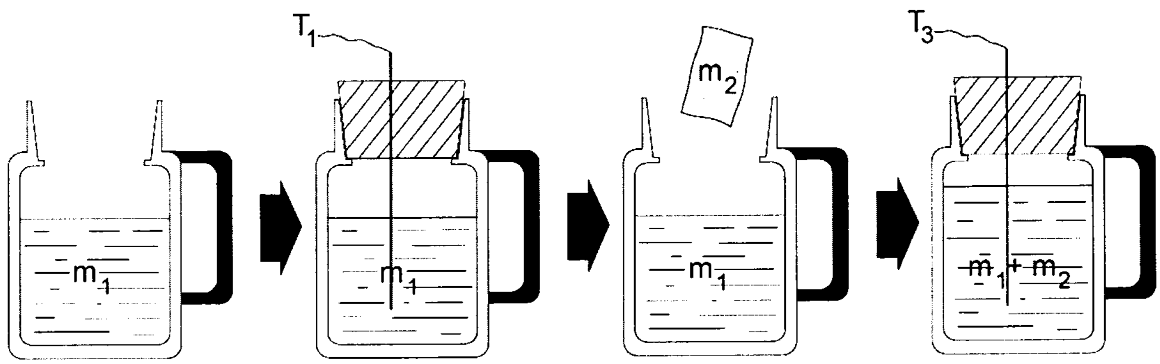

Fig.28 LWC measurement using a fusion calorimeter

The heat balance equation of the system (water + wet snow + container) is:

$$m_l\, c_{water}\, T_l + C_{container}\, T_l + m_{2L}\, c_{water}\, T_2 + m_{2S}\, c_{ice}\, T_2 - m_{2S}L = m_3\, c_{water}\, T_3 + C_{container}\, T_3 \qquad (7.4)$$

Substituting $m_3 = m_l + m_{2L} + m_{2S}$ and dividing by c_{water}

$$m_l\, T_l + \lambda\, T_l + m_{2L}\, T_2 + \frac{m_{2S}\, c_{ice}\, T_2 - m_{2S}L}{c_{water}} = (m_l + m_{2L} + m_{2S})T_3 + \lambda\, T_3$$

Re-arranging

$$(m_l + \lambda)(T_l - T_3) + m_{2S}\left(\frac{c_{ice}\, T_2 - L}{c_{water}} - T_3\right) = m_{2L}(T_3 - T_2)$$

Solving for m_{2S}

$$m_{2S} = \frac{m_{2L}(T_3 - T_2) + (m_l + \lambda)(T_3 - T_l)}{\left(\frac{c_{ice} T_2 - L}{c_{water}} - T_3\right)} \equiv m_2 - m_{2L} \tag{7.5}$$

Solving (7.5) for m_{2L}

$$m_{2L} = \frac{m_2\left(\frac{c_{ice} T_2 - L}{c_{water}} - T_3\right) - (m_l + \lambda)(T_3 - T_l)}{\left(\frac{c_{ice} T_2 - L}{c_{water}} - T_2\right)} \tag{7.6}$$

Finally, the LWC of the snow sample is obtained:

$$\rightarrow \ LWC = \frac{m_{2L}}{m_2} \times 100\% \tag{7.7}$$

7.3.3 Precision of the LWC measurement

The precision of the LWC value obtained from the calorimetric experiment depends on handling factors and on the precision of the digital equipment used.

The precision of the equipment used was rated as follows:

Small scale (used to weight m_2): $\pm$ 0.001g

Large scale (used to weight m_l): $\pm$ 0.01g

Thermometer: $\pm$ 0.05°C

Upon removing the lid of the thermos container there is a risk that a droplet of condensed water may fall outside of the container. The effect of one droplet on m_l was estimated at 0.10g (this corresponds to the weight of a water droplet of average size).

To measure each mass necessitated two weightings: one for the liquid/snow with its container and another one for the empty container. To account for some heat loss T_3 can was offset by 0.1°C.

Therefore, the following precision ranges applied:

→ Max effect on m_1 = + 0.02g, - 0.12g

→ Max effect on m_2 = ± 0.002g

→ Thermometer readings T_1 and T_2 = ± 0.05°C

→ Thermometer reading T_3 = +0.05°C, -0.15°C

Considering only the precision of the digital instruments and the risk of losing a drop of warm water when opening the lid, the precision of the LWC measurements performed ranged from +1.7% to -2.5%LWC (by mass). These values were obtained by numerical simulations, setting up a spreadsheet with formulas (7.3), (7.6) and (7.7) and using the worst effects on m_1, m_2, T_1, T_2 and T_3.

It is difficult to estimate the amount of uncertainty introduced by other aspects of the calorimetric experiments. The most important source of error certainly occurred when handling the snow sample and introducing it into the thermos container: a lot of care had to be taken to ensure that all of the snow went into the container without touching its top lip.

It is reasonable to assume that most LWC values obtained were accurate within ± 3% LWC (by mass). Many practice runs were necessary to acquire a good handling routine, which led to repeatable LWC readings. Also, over a dozen LWC readings were performed with various types of snow (e.g. dry snow at sub freezing temperature, cohesive wet snow, very slushy snow, etc.) to test the method.

7.4 Observations for centered snow sleeves

Three tests were performed with snow sleeves that were centered with respect to the cable (Fig.29).

The objective of these experiments (including the ones reported in sections 7.5 and 7.6) was to understand how snow sheds naturally from a cable if it is left undisturbed at an air temperature above the freezing point (Fig. 30).

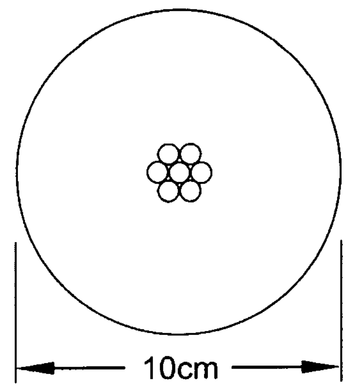

Fig.29 Centered sleeve cross section

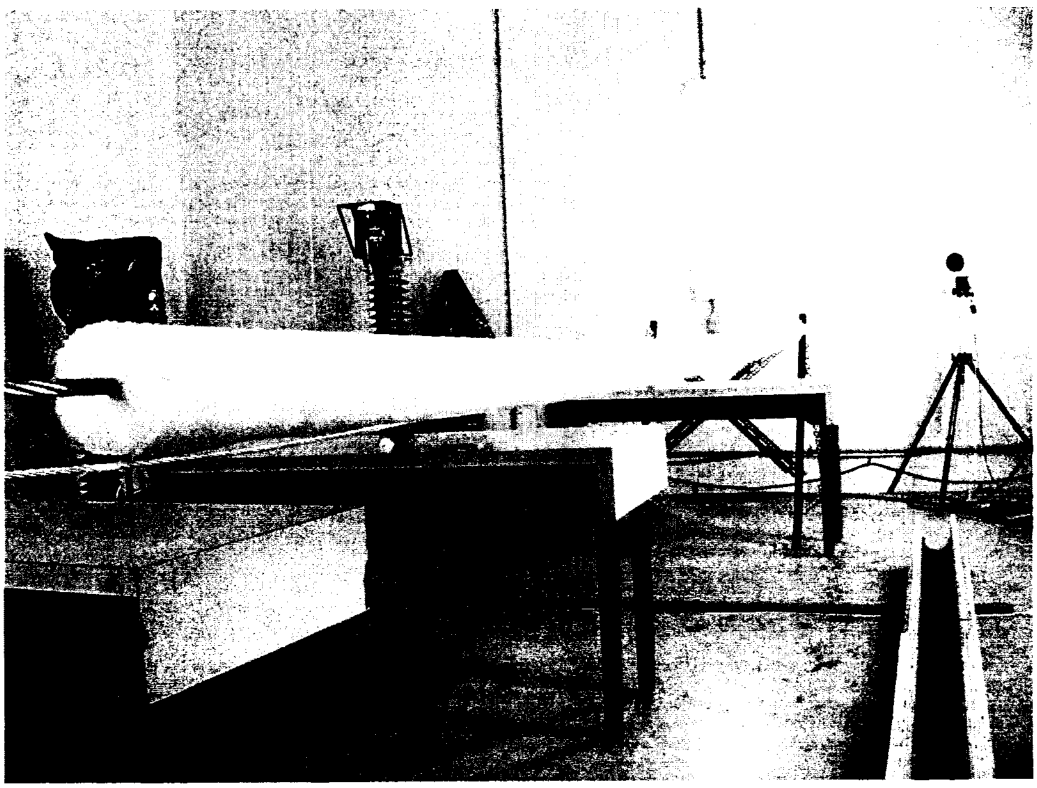

Fig.30 Centered snow sleeve after mold removal
Density ~ 0.4 g/cm³, 19% LWC

Melting was observed in each centered sleeve test. As snow grains melted, the diameter of the accretion reduced and the liquid water migrated to the bottom of the snow sleeve. The LWC and the density increased as the liquid fraction increased (e.g. density from 0.4 to 0.7g/cm³ over 11 hours).

The bottom of the accretion became saturated with water after a few hours: it became translucent and liquid water dripped to the floor (Fig.31a). Measurements showed that the bottom part of the snow sleeve had LWC values almost twice as high as the top part.

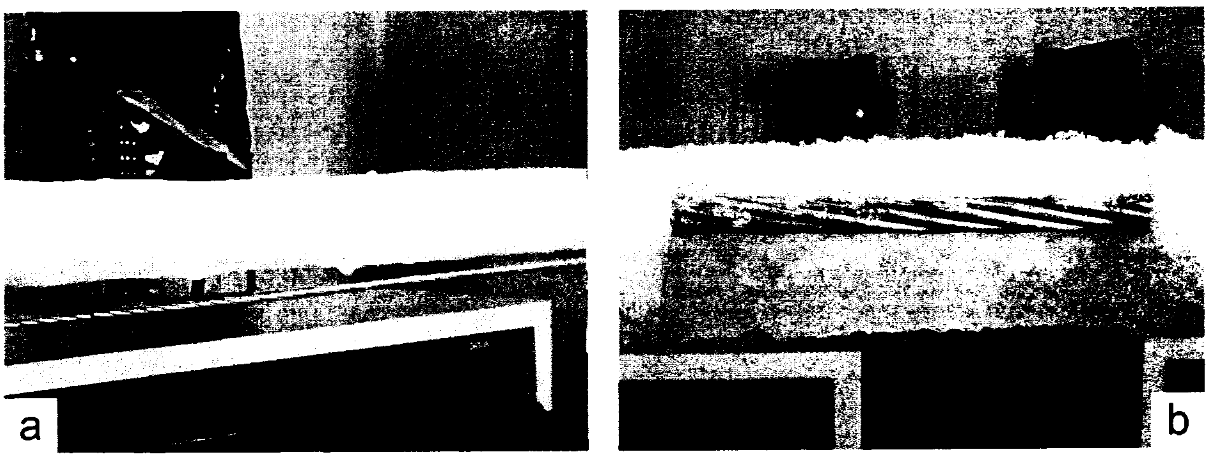

Fig.31 Liquid water migration
a: Water droplets (+8 hours)
b: Cut (+11 hours, 25% LWC top, 44% LWC bottom)

The wet snow sleeve also became slightly eccentric with respect to the cable due to the migration of melt-water from the top to the bottom (Fig.31b). Snow grains in the top part of the accretion had good cohesion, even when the LWC reached 25%. Some of the top grains were found to be frozen onto the cable.

Snow shedding was observed. It progressed very slowly from each end of the sleeve, in sections 15 cm to 20 cm long. The sections drooped and ruptured in bending under their self weight as the cable melted its way through. Fig.32 illustrates the rate of the slow melting and shedding process. One section was observed to shed from each end approximately every 3 hours.

A sample table of results used to record data and calculate key parameters is given in Appendix A. Similar tables were used for all the tests reported in sections 7.5 to 7.8.

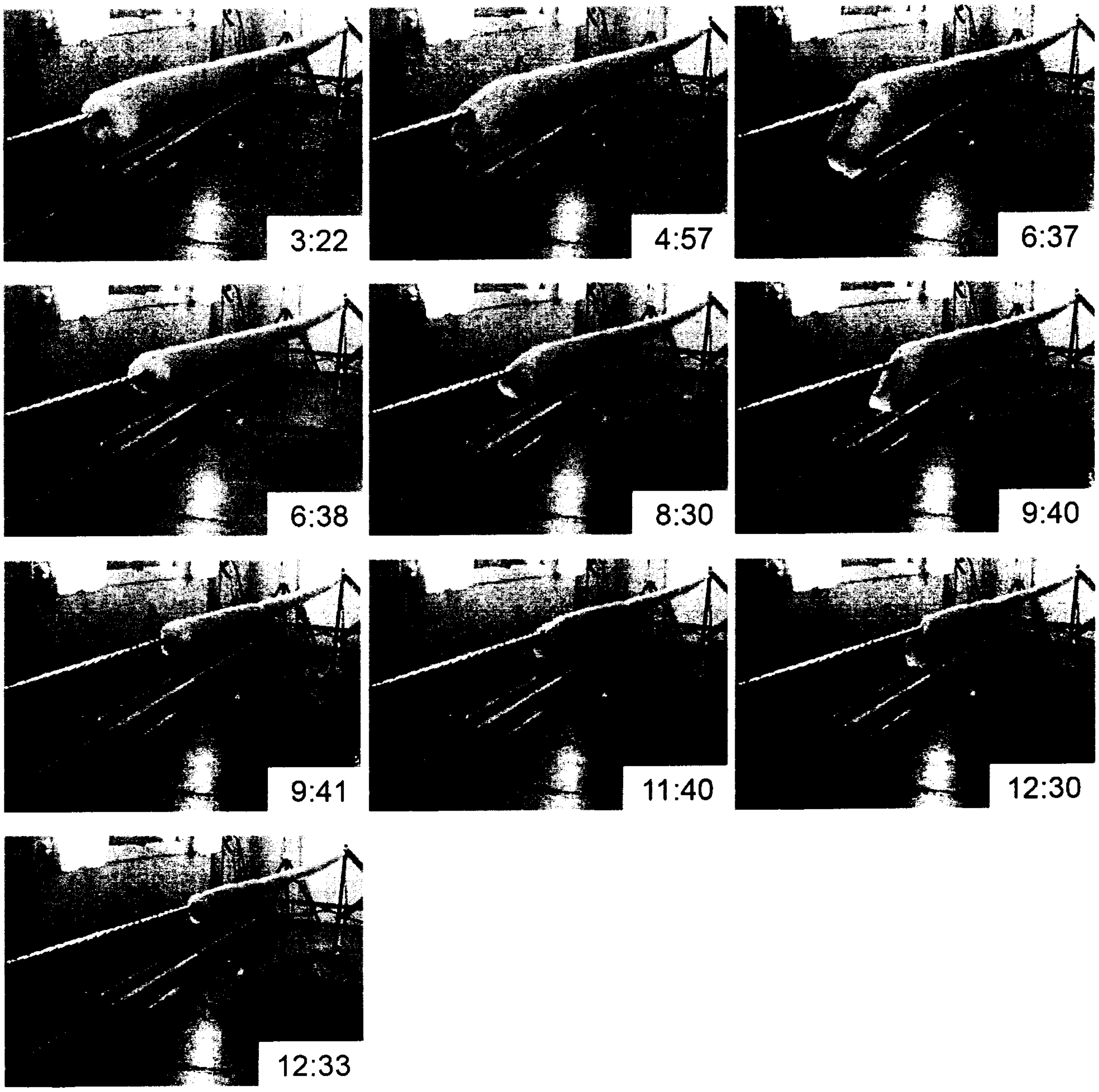

Fig.32 Slow shedding snapshots

Table 2: Summary of measurements for the centered sleeve tests

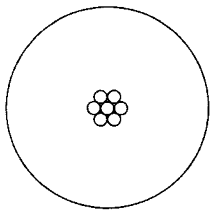

time	0h	+11h	
density	0.3 ~ 0.5 g/cm³	0.5 ~ 0.7 g/cm³	
LWC	19.4%	25.3% (top)	
		43.7% (bottom)	

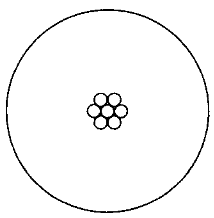

time	0h	+9h	
density	0.44 g/cm³	0.66 g/cm³	
LWC	16.9%	27.9% (top)	
		48.4% (bottom)	

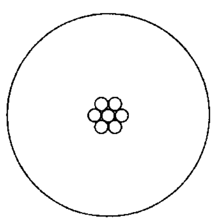

time	0h	+3h	+6h
density	0.36 g/cm³	0.57 g/cm³	0.67 g/cm³
LWC	8.3%	16.5% (top)	26.9% (top)
		31.8% (bottom)	50.5% (bottom)

7.5 Observations for eccentric snow sleeves

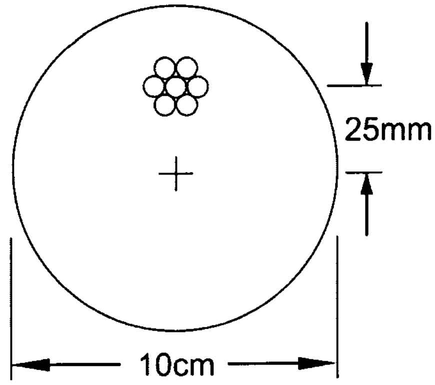

Fig.33 Eccentric sleeve cross section

Two tests were performed with snow sleeves that were not centered with respect to the cable. The location of the center of the sleeve's cross section was offset by 25 mm (Figs.33 and 34).

The observations for eccentric snow sleeves were similar to those for centered snow sleeves:

- Slow snow melting, water migration, translucent bottom portion, water droplets
- Reduction in sleeve diameter, increase in density and LWC
- Sections drooping and breaking off slowly from the ends (Fig.35). The time interval between shedding events varied between 4 and 6 hours.

Measurements were only performed during the first test. The second test was performed to confirm the slow drooping and shedding mechanism.

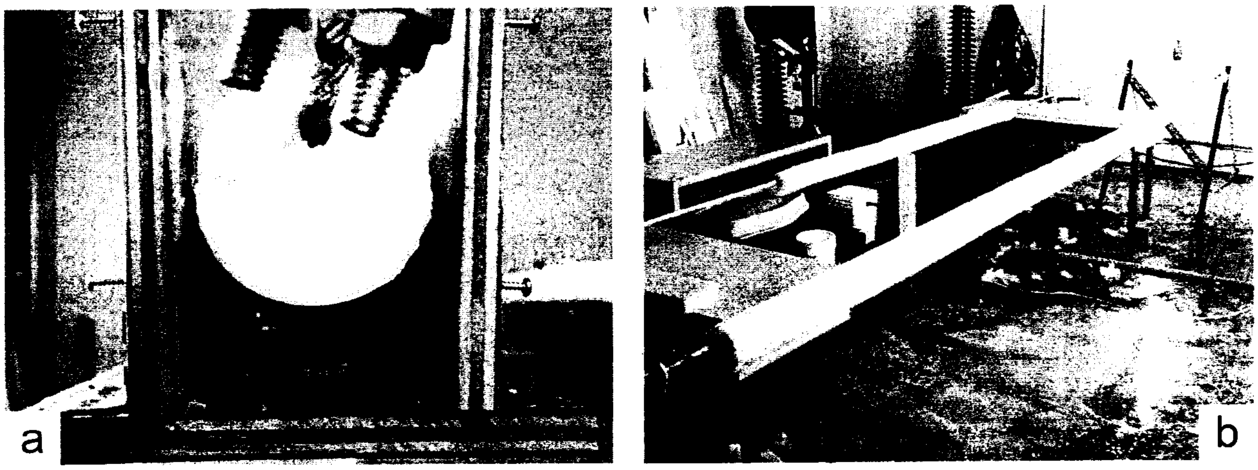

Fig.34 Eccentric wet snow sleeve
a: Removing the mold, b: Full size, after mold removal

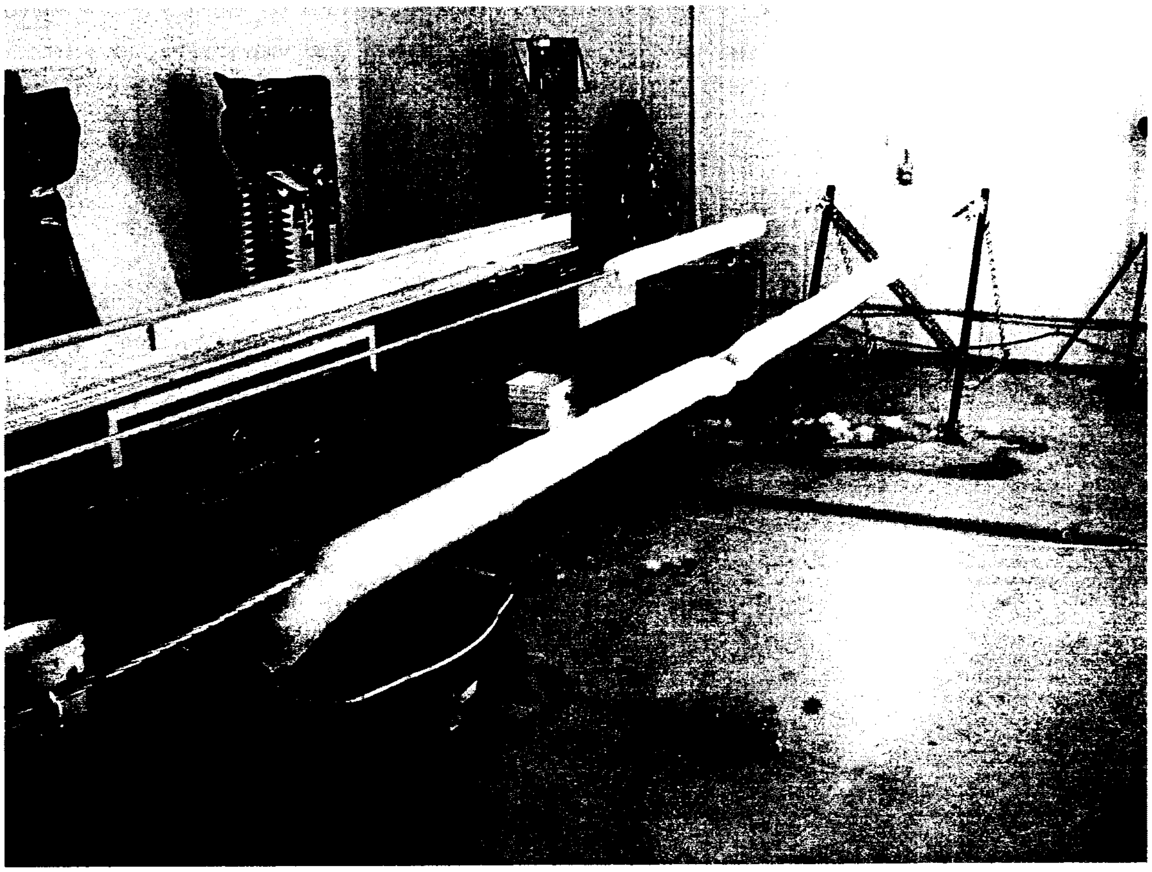

Fig.35 Drooping end sections (+5 hours)

Table 3: Summary of measurements for the first eccentric sleeve test

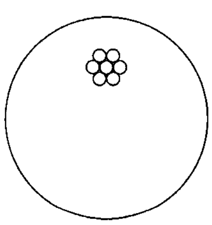

time	0h	+13h
density	0.44 g/cm^3	0.78 g/cm^3
LWC	17.0%	21.6% (top)
		41.5% (bottom)

7.6 Observations for hollow snow sleeves

Two tests were performed with hollow snow sleeves (Fig.36) reproduced with the hope of generating a different shedding behavior. The hollow sleeve simulated the shape of an accretion that exhibits a significant amount of creep and wind-induced carving.

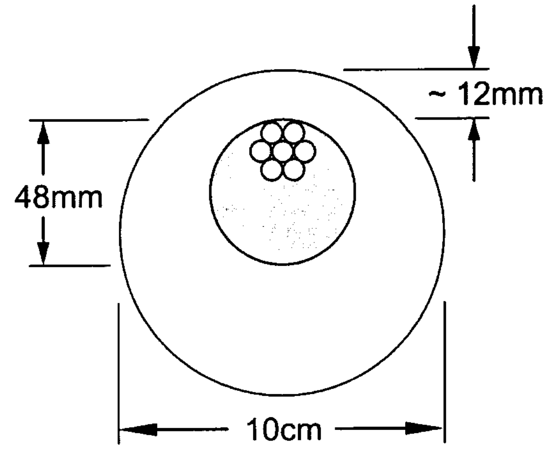

Fig.36 Hollow sleeve cross section

As shown in Fig.37a, a plastic pipe was included in the sleeve during the molding process to make the hollow profile. The diameter of the cavity in each sleeve (48 mm) was governed by the dimension of the nearest pipe available. A minimum thickness of 12 mm was kept between the top of the cable and the top of the snow sleeve. After extracting the plastic pipe (Fig.37b) the mold had to be lowered very carefully to prevent the premature rupture of the hollow sleeve in its thinner top section.

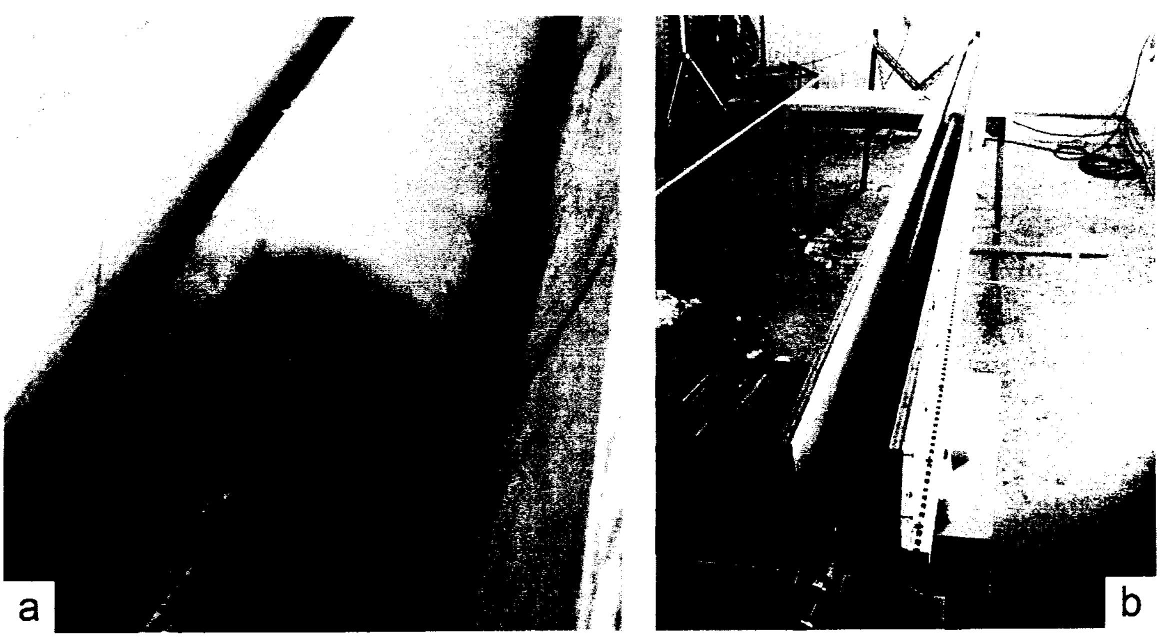

Fig.37 Hollow sleeve fabrication
a: Tube included during molding, b: Tube extracted prior to removing the mold

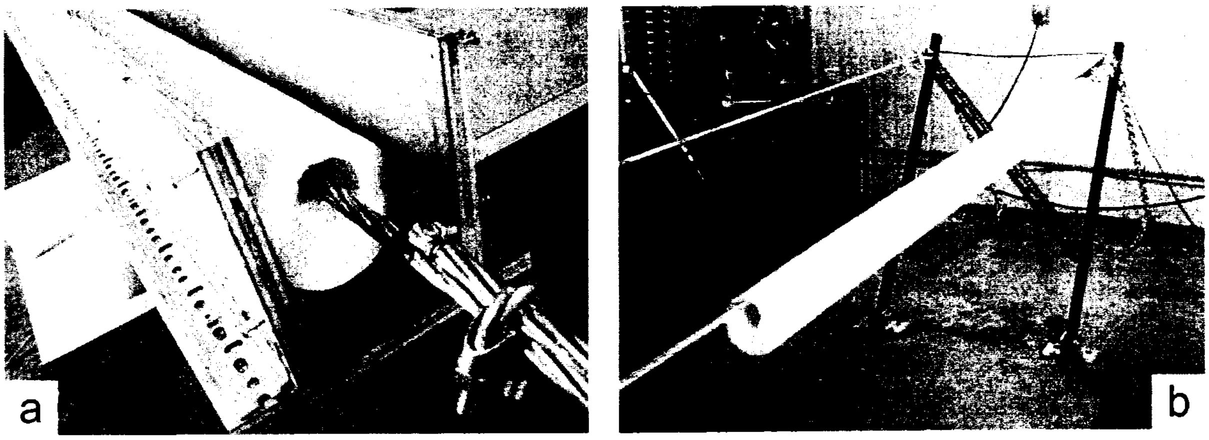

Fig.38 Hollow wet snow sleeve
a: Prior to removing the mold, b: Carefully de-molded

Once extracted, the plastic tube could not be removed from the setup and occupied half of the 5 m test span. Thus, hollow wet snow sleeves were limited to a maximum length of 2.5 m.

The first hollow sleeve had a low initial LWC (~15%) and a high density (0.53 g/cm³). Fig.39 shows the evolution of creep on the cross-sectional profile from 1hour after de-molding (Fig.39a) to 3 hours later (Fig.39b). Shedding was forced 4 hours after mold removal by pushing down slowly on the cable and releasing it suddenly.

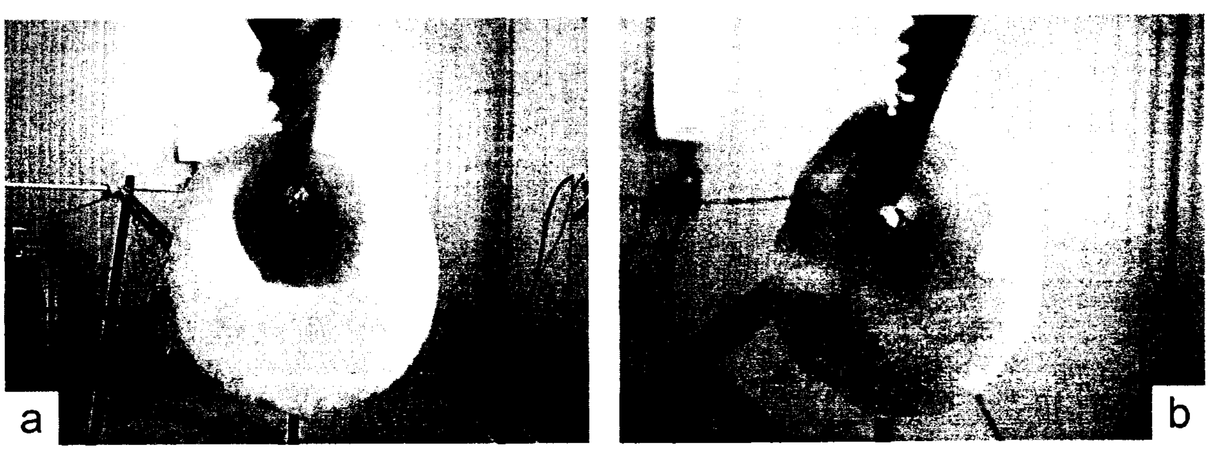

Fig.39 Evolution of the hollow sleeve profile: creep under self-weight
a: +1 hour, b: +4 hours

The second sleeve had a higher initial LWC (~22%) and a lower density (0.41 g/cm³). A fracture appeared on top of the sleeve after the first half hour, and became more apparent with time (Fig.40).

Natural shedding over the entire length of the sleeve was observed 1h15min after de-molding. Shedding occurred before there could be any sign of melting (i.e. before the appearance of water droplets), and progressed from one end in an "unzipping" manner. The speed of propagation of shedding was estimated from the video footage at 13.6 m/s (see snapshots of the propagating shedding phenomenon in the first column of Appendix B).

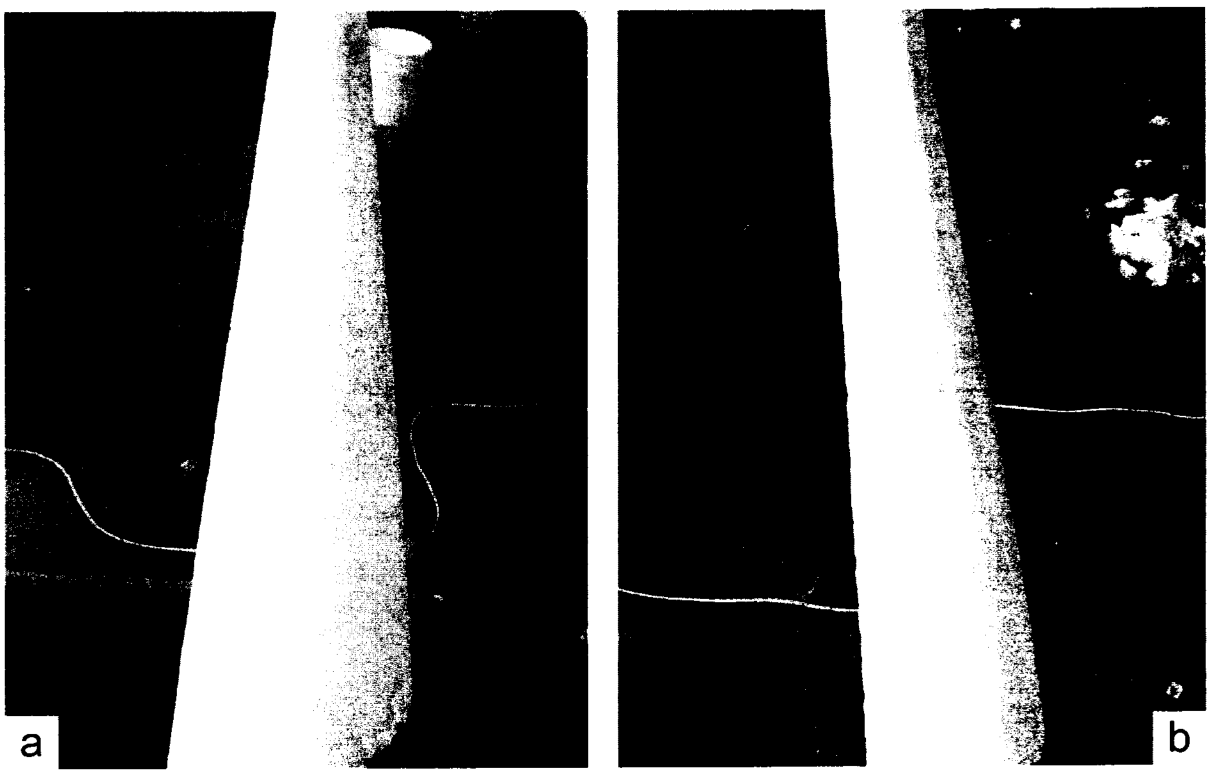

Fig.40 Fracture on top of a hollow sleeve
a: After mold removal, b: +1 hour

Table 4: Summary of measurements for the hollow sleeve tests

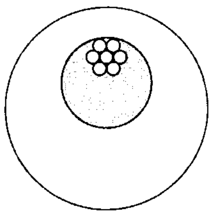

time	0h	+4h forced shedding
density	0.53 g/cm^3	0.55 ~ 0.7 g/cm^3
LWC	14.8%	21.1% (top)
		41.8% (bottom)

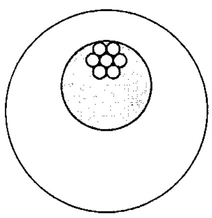

time	0h	+1h15 natural shedding
density	0.41 g/cm^3	0.45 ~ 0.6 g/cm^3
LWC	21.9%	n.a.
Speed		Shedding at 13.6m/s

7.7 Observations for snow sleeves under radiation input

Two tests were conducted under simulated radiation heating. One test was performed on an eccentric wet snow sleeve, and one test on a hollow sleeve (Fig. 41).

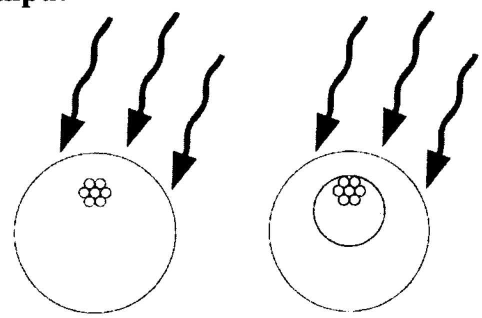

Fig.41 Snow sleeves under radiation heating

The objective of these tests was to see if adding a realistic radiation heating effect on an accretion would change its shedding behavior. Solar radiation was simulated by using 450W halogen work lamps installed 1.8 m above the cables (Fig.42).

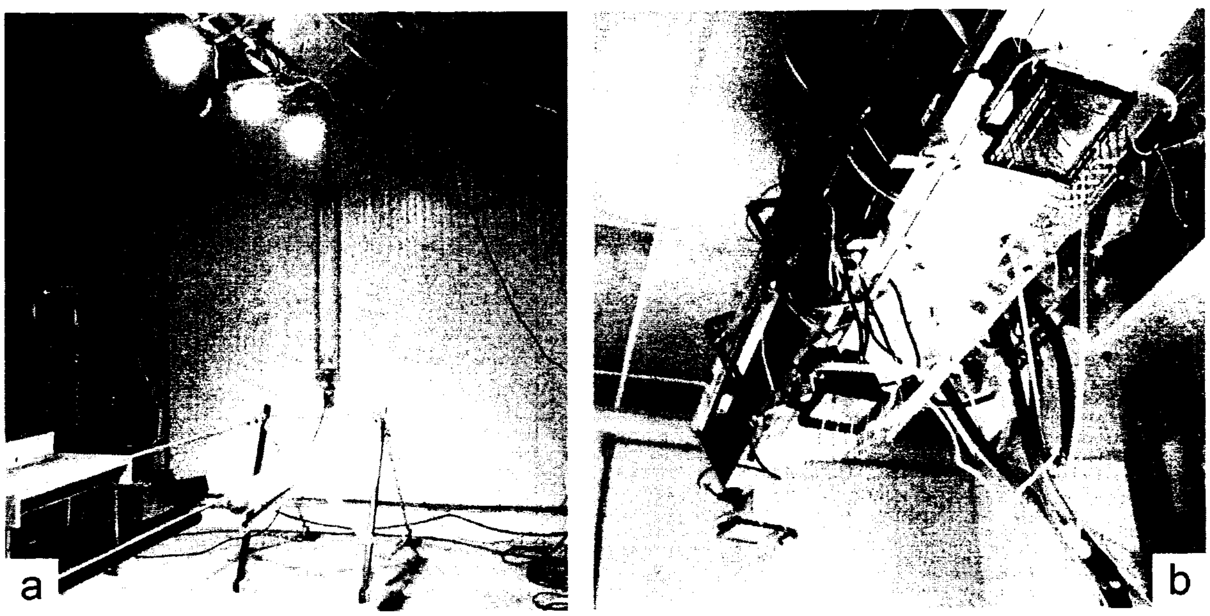

Fig.42 Solar radiation simulator installed above the experimental setup

At a distance of 1.8 m above the ground a single lamp projects its light on a 3.5 m^2 area. By overlapping the projections as in Fig.43 the test section was subjected to the equivalent of two full light beams on a single square of 3.5 m^2 (2 x 450 W / 3.5 m^2 = 257.1 W/m^2).

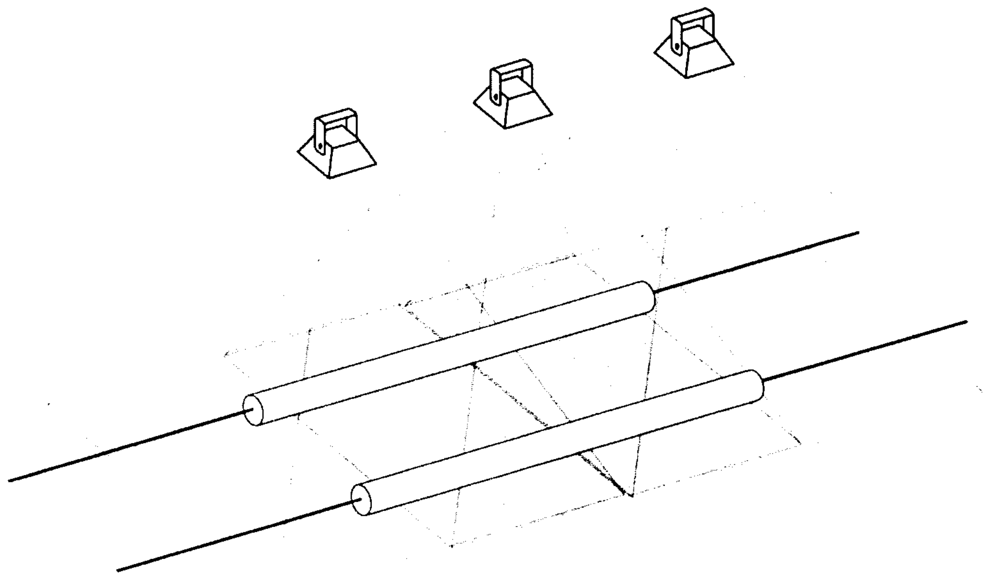

Fig.43 Projection overlaps on the test section

Without a light meter it is difficult to determine the actual radiation intensity on the test section. The maximum incident radiation on the test section was estimated close to 260 W/m^2. However, it is likely that this is an overestimate and that the light distribution was not uniform over the projected areas. Some of the lamps' radiations were also lost as heat through the casings and as diffuse light outside of the projection footprints but it is impossible to quantify these amounts. A rough approximation would be that the test section was subjected to 200 W/m^2 ~ 250 W/m^2.

Solar radiation data for a Northern latitude corresponding to the French Southern Alps is given in Table 5a and 5b. Radiation intensity values were interpreted from data obtained from the National Renewable Energy Laboratory (NREL) affiliated to the U.S. Department of Energy (National Renewable Energy Laboratory web reference, solar radiation data).

Weather condition	December 21st (9:30am to 2:30pm)	March 21st (8am to 4pm)
Very cloudy	80-100 W/m²	200-250 W/m²
Cloudy	100-150 W/m²	250-400 W/m²
Sunny	300-400 W/m²	600-700 W/m²

Table 5a: Incident Solar Radiation on a horizontal surface for a 43.6° N latitude (Toronto, Canada; Portland, MA, USA; Provence and Southern Alps, France)

Weather condition	December 21st (9:30am to 2:30pm), March 21st (8am to 4pm), June 21st (7am to 5pm)
Very cloudy	250-300 W/m²
Cloudy	300-500 W/m²
Sunny	800-900 W/m²

Table 5b: Direct normal radiation for a 43.6° N latitude (Toronto, Canada; Portland, MA, USA; Provence and Southern Alps, France)

Because of their exposed location, shape and surface texture natural cylindrical sleeves are better at collecting solar radiation than horizontal surfaces, independently of the time of day or year. However, they are not perfect collectors and they are not subjected to the same amount of radiation as a direct normal surface would be. A good approximation of the actual amount of radiation to be expected in the field would lie between the values given for a horizontal surface and a normal surface.

When compared to the values in Tables 5a and 5b the simulated radiation of 200 W/m² ~ 250 W/m² is found to correspond to realistic natural conditions under cloudy skies.

Table 6: Summary of observations under simulated solar radiation

Observations for a hollow sleeve

- The accretion shed <u>totally</u> and in an unzipping mode.
- The speed of propagation of shedding was estimated at 12.5 m/s from the video footage (see the second column of Appendix B).
- The accretion shed 45 minutes after mold removal.
- The overall LWC of the accretion reached 37% at the time of shedding.

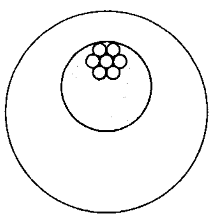

time	0h	+0h45 natural shedding
density	0.40 g/cm³	0.4 ~ 0.6 g/cm³
LWC	17.6%	36.6%
Speed		Shedding at 12.5 m/s

Observations for an eccentric sleeve

- The accretion shed <u>partially</u> and in an unzipping mode.
- Shedding was not initiated at one of the ends: it started at the middle of the sleeve after a <u>visible amount of creep.</u>
- The speed of propagation of shedding was estimated at 12.1 m/s from the video footage (see the third column of Appendix B).
- The accretion shed 2 hours after mold removal.

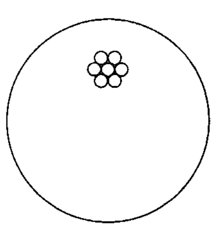

time	0h	+2h natural shedding
density	0.37 g/cm³	0.4 ~ 0.7 g/cm³
LWC	11.6%	n.a.
Speed		Shedding at 12.1 m/s

7.8 Forced shedding experiments

Pull-down experiments were performed to evaluate the amount of vertical force necessary to rip snow sleeves from the cable. A 40 cm sleeve segment was cut and isolated on the cable; the apparatus grabbed the accretion from its sides, leaving the cable free to punch through the top of the sleeve. The apparatus was filled slowly with steel ballast and water, until rupture (Fig.44).

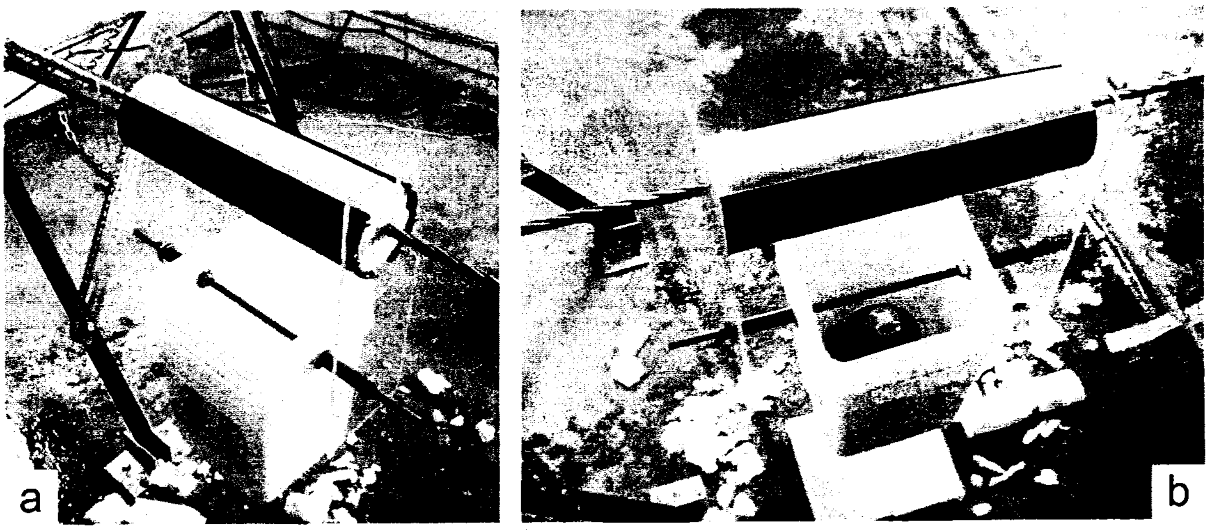

Fig.44 Pull-down test apparatus
a: Attached to a sample section, empty
b: Before rupture, fully loaded (~570 N/m)

The force and the equivalent vertical acceleration necessary to cause shedding of the wet snow accretion can be calculated from the total mass of the apparatus at rupture:

$M =$ total mass of apparatus (loaded)

$m =$ [mass of cable + snow sleeve] per meter of cable

$g =$ gravitational constant (9.81 m/s^2)

$F = M \times g =$ applied force (down)

$a = \frac{F}{m} = \frac{M \times g}{m} =$ equivalent vertical acceleration

Two series of experiments were carried out successfully on centered sleeves (without simulated radiation input). The results given in Table 7 confirm that the holding strength of a snow sleeve decreases as melting progresses.

	Test 1		Test 2	
Time from de-molding	+30 minutes	+10 hours	+30 minutes	+4 hours
Density (g/cm³)	0.44	0.66	0.37	0.57
LWC	16.9%	27.9% (top) 48.4% (bottom)	8.3%	16.5% (top) 31.8% (bottom)
M: Total mass (kg)	22.2	8.3	23.5	16.0
F: Force to shed accretion (N/m)	544	204	576	391
A: Equivalent vertical acceleration	14g	6g	17g	10g

Table 7: Summary of results for the pull-down tests

7.9 Discussion of the experimental study

The objective of these experiments was to reproduce wet snow sleeves of different shapes and to observe how they shed naturally when the ambient temperature is controlled and held constant.

At the beginning of this study, a target range for the density of wet snow was established between 0.2 g/cm^3 and 0.6 g/cm^3. This range covers all of the density values observed in France during the 1980's observation program. The upper and lower bounds of the range are used by Électricité de France as static design criteria. The techniques described in section 7.2 for the making of wet snow sleeves generally produce accretions of medium density (0.4 g/cm³) with good uniformity, both in density and LWC. Using fresh dry snow with large snowflakes, however, it is difficult to achieve densities higher than 0.5 g/cm³ and to obtain good sleeve uniformity. Higher densities may be achieved successfully by using mechanically transformed dry snow (e.g. finer grain snow found in dunes formed by blowing snow).

The snow sleeves of sections 7.4 and 7.5 (centered and eccentric, without simulated radiation) did not exhibit the expected behavior of random partial shedding or sudden unzipping as described by observers in chapter 5. Instead, shedding progressed very slowly from the bare cable ends, even if the climate room was set to a higher temperature (e.g.10°C to 15°C).

The amount of time taken for sections to droop and shed was longer for eccentric sleeves than for centered sleeves. In fact, the time interval between shedding events was almost doubled. This may sound counter-intuitive since the snow thickness between the cable and the warmer air was reduced by a half. However, snow is a very good insulator and most of the heat that caused accretion segments to droop and shed actually flowed from the warm air, through the cable, to the snow grains touching the cable. By offsetting the center of the accretion the ground wire was in a "dryer" location that conducted less heat than if it were surrounded by a mix of snow grains and liquid water. The slower heat flow reflected itself in the increased time interval.

It should be noted that, once the LWC of the bottom of a snow sleeve exceeds 35%, it is really easy to dislodge it by tapping on the cable. Bottoms in excess of 35% ~ 40% LWC are maintained on the sleeve by tensile capillary forces that are rather weak in comparison to the cohesive forces in the top half (LWC < 28%). The picture in Fig.45 was taken after tapping gently on the cable until the bottom of the eccentric accretion shed. The sleeve portion that remained on the cable showed good cohesion and most of the snow grains touching the cable were actually frozen onto the metal strands. Once exposed to warm air, the cable melted those bonds and a thin water film formed between the remaining accretion and the cable, causing it to slowly twist to the bottom in a corkscrewing manner (following the lay angle of the strands), and shed. The entire process took more than an hour.

Fig.45 Persistent accretion following bottom shedding

The hollow sleeve profile of section 7.6 was made to mimic a specific type of accretion shape subjected to creep, as observed in the field. Its relevance is questionable, but it did demonstrate an interesting "unzipping" type of shedding. The speed of propagation of shedding was measured at 13.6 m/s.

Experiments reported in sections 7.4 to 7.6 did not include a heating effect. The only heat provided to the accretion was in the form of weak natural convection (warm still air). Natural wet snow sleeves are created by the effect of the wind. The amount of heat supplied by forced convection is not negligible and other heating sources such as solar radiation and Joule effect also contribute to increase the LWC of the accretion.

Without a direct heat supply, the rate of production of liquid water in the snow sleeve is slow with respect to the rate at which the melt water migrates through the accretion and escapes (water droplets). As a consequence, the LWC of the top of the accretion never reaches its critical value and the sleeve remains on the cable and melts slowly. This was observed in sections 7.4 to 7.5, as the LWC of the top of the accretions did not rise above 28%, thus preventing creep of the snow sleeve. Adding a realistic heating effect caused the accretion to creep and changed the shedding behavior.

Two trends have been observed under a similar heating effect:

- Wet snow with a higher initial LWC sheds faster. This is obvious since the accretion requires less heat to reach its critical LWC value.
- Wet snow with a higher initial density takes longer to shed than with a lower density. Although the accretion is heavier, it has a higher cohesive strength and it contains a larger mass of ice. With the same heat flux, denser snow takes more time to achieve a LWC sufficiently high to cause its shedding.

No snow sleeve was observed to shed spontaneously along its entire length. All shedding observations were initiated at one point along the cable segment, and progressed at a measurable speed. Under simulated radiation, the speed of propagation of snow shedding along the cable was measured at 12.5 m/s and 12.1 m/s. These speeds are relatively close to one another, even if one was obtained from a hollow snow profile and the other from a full sleeve. Further investigation could demonstrate whether this self-shedding speed is constant or if it depends on the cable diameter and the density of the accretion. Considering the speed of 13.6 m/s obtained in section 7.6, it would appear that natural self-shedding speeds of propagation are possible at speeds up to 14 m/s.

This speed of propagation can be used in finite element analysis to evaluate the effects of wet snow shedding from a suspended cable. A numerical modeling technique has been developed for this study to evaluate the response of an overhead ground wire subjected to different snow-shedding scenarios and it is the subject of chapter 8.

The pull-down tests performed demonstrated the strong cohesion of freshly accreted wet snow sleeves. Fresh accretions were able to sustain static loads in excess of 500 N/m. From a simple calculation it has been estimated that it would take a vertical acceleration greater than 14g's to rip the accretions from the ground wire. As it was pointed out in chapter 6, dry snow and low LWC wet snow are expected to behave in the same way. The type of failure (ductile, brittle) and the strength of dry snow depend largely on the rate at which the loading is applied. Dry snow is brittle and weaker at high loading rates: this suggests that the actual acceleration needed to break a fresh wet snow sleeve could be much less than the calculated value.

Pull down tests were only performed on full sleeves. Performing these tests on a hollow sleeve proved to be impractical because the manipulations carried during the installation of the test apparatus often caused the accretion to break off the cable.

In future works it would be interesting to investigate different heating effects in more details. More sophisticated equipment would be required, such as a more accurate and more uniform radiation simulator, a transverse wind generator (Fig.46), and an energized conductor span (3 m to 4 m long). Those are all feasible and would be great additions to the CIGELE climate rooms.

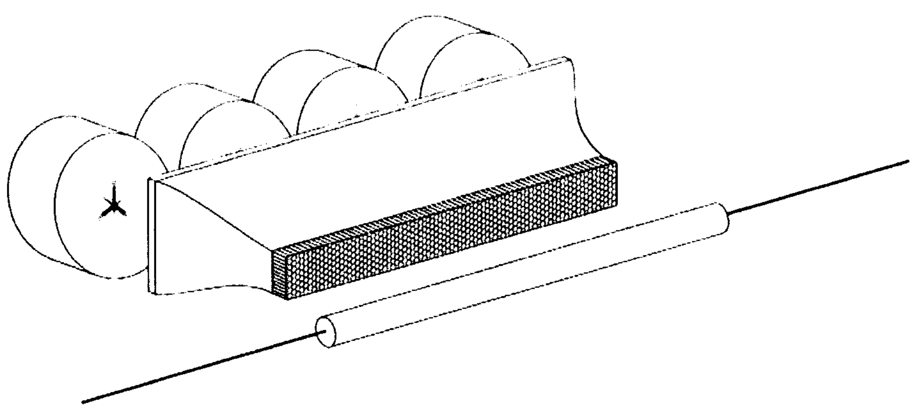

Fig.46 Forced convection apparatus

It is likely that simulated radiation would be the most effective at causing creep and shedding since it acts directly on the top half of the accretion; forced convection brings more heat to one side of the accretion, and Joule heating affects the snow mass in a more uniform way from its center.

The CIGELE facilities are equipped with a materials testing machine located in a small climate room. This machine could be used in the future to test the mechanical resistance of wet snow sleeves of varying densities and LWC values. Bending and axial traction tests could be performed at different loading rates in order to map the mechanical failure envelope of wet snow sleeves. Such a study may test the hypothesis that wet snow does not rupture and shed from a cable following bending or axial traction unless the loading rate and the total deformation are very large. Tests could also be performed to evaluate the creep performance of snow under sustained loading. Wet snow mechanics is practically inexistent as a field of research and the data that could be generated from this study would have a significant scientific value.

8. Numerical Modeling Study

8.1 Previous ice-shedding models

Overhead cable dynamics have been the subject of a number of numerical studies initiated by McClure at McGill University. A particular branch of this research field emerged in the early 1990's when researchers attempted to model the response of a cable following ice shedding (Jamaleddine 1993, 1994) (Roshan Fekr 1995, Roshan Fekr and McClure 1998).

Jamaleddine and Roshan Fekr explored many ice-shedding scenarios on single and multiple spans of overhead cables. Variable parameters included ice thickness, span length, partial ice shedding and difference in support elevation. These models were 2-dimensional simplifications of actual overhead lines and did not consider the flexibility of the support towers. They consisted of cables pinned at the ends, and hinged suspension strings. The general modeling approach has been summarized in McClure and Lapointe (2003) with emphasis on transient response following a cable rupture and it is readily applicable to the shedding of ice or snow. It is important to note that the modeling work of Jamaleddine was validated experimentally (Jamaleddine 1993, 1994).

The work of Kálmán, Ph.D. student at CIGELE, is an advanced application to ice shedding induced by a mechanical shock on the cable (Kálmán *et al.* 2005). Ice deposits are modeled as beam finite elements connected in parallel to cable elements. Ice beam elements are assigned a failure criterion based on axial and bending stresses. Ice elements that exceed this failure criterion are removed from the model (element death upon failure) during the direct time step integration of the equations of motion. This model serves as a powerful tool to estimate the amount of ice that can be shed following the application of a shock load.

The commercial finite element package ADINA has been used extensively and successfully to study different nonlinear cable dynamics and lattice structure models (McClure and Lapointe 2003). All of the finite element models mentioned above were built using ADINA.

8.2 Numerical modeling approach

Based on a modified version of the previous ice-shedding models, a snow-shedding modeling technique has been developed for this study using ADINA. The material properties and the span of the cable used to illustrate the modeling technique match those of a real overhead ground wire commonly used in Southern France, in regions often subjected to severe wet snow events.

8.2.1 Cable model

A single cable spanning 470 meters is modeled as a chain of two-dimensional, two-node isoparametric truss elements. It is pinned at the ends and the flexibility of the towers and foundations is not included in the model. To allow for cable slackening, the stiffness of each cable element is prescribed in tension only. The initial static position of each node is calculated using the theoretical inextensible catenary equation (see example in Appendix C). The initial equilibrium state is determined by static analysis under the cable self-weight and initial strains.

The overhead ground wire characteristics (Almelec-Steel 94.1) are as follows:

Diameter $D = 12.60$ mm
Cross-sectional area $A = 94.1$ mm^2
Mass per cable length $\mu = 0.481$ kg/m → Weight $F = 4.72$ N/m
Density $\rho = 5\ 111$ kg/m^3
Modulus of elasticity $E_T = 112$ GPa
Tension, ultimate $T_{ult} = 80\ 350$ N
Tension, initial (bare cable) $T_i = 11\ 000$ N

In the dynamic analysis the cable elements undergo large displacements with small strains and the mass of each element is assumed to be lumped at the nodes. The material nonlinearity (tension-only) and the large displacements expected when the cable is subjected to a snow-shedding scenario make this a nonlinear model. The response of the cable is obtained by direct time integration of the incremental form of the equations of motion using the Newmark-β trapezoidal rule.

8.2.2 Damping

Aerodynamic damping is neglected. For modeling the transient response of an overhead cable following ice-shedding and snow-shedding scenarios it is believed that most of the structural damping comes from friction between the individual strands.

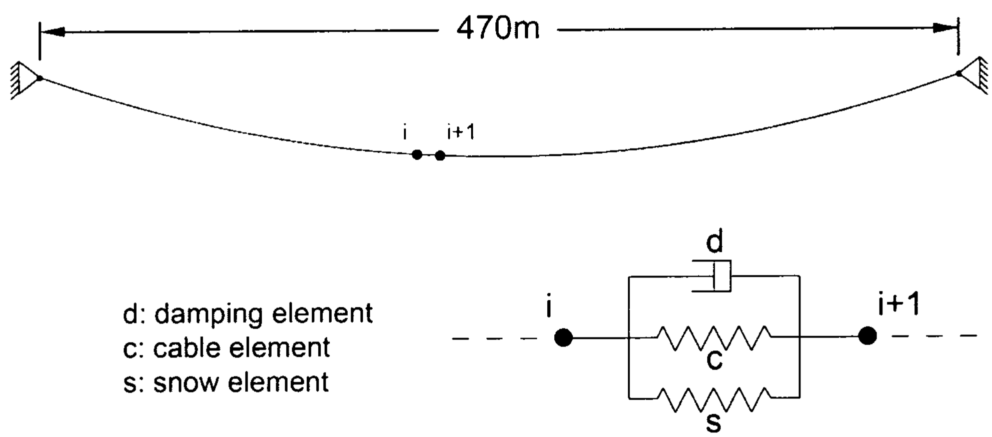

Fig.47 Lumped parameter model of a snow-covered ground wire

Physical damping is usually introduced in cable models by including a viscous dashpot in parallel to each truss (cable) element (Fig.47). In ADINA these damping elements are modeled using non-linear spring elements (generic lumped parameter elements) without mass or stiffness. Damping is prescribed by a viscous damping constant C associated to each nonlinear spring. C is calculated using the following equation:

$$C = 2\,\xi\, m\omega = 2\,\xi\sqrt{AE\mu} \qquad (8.1)$$

where ξ is the damping ratio, AE is the axial rigidity of the cable and μ is the mass of the cable per unit length. Different damping ratios between 1% and 2% have been used for a bare cable in the most recent modeling studies (McClure and Lapointe 2003, Kálmán *et al.* 2005). Unfortunately, modeling damping by using parallel elements did not appear to work properly with the version of ADINA used for this study (900 nodes edition v8.2.2). As shown later in section 8.3.2, damping did not appear in the response: this requires further investigation.

Damping has little effect on the maximum transient response since it usually occurs during the first or second peak. However, including damping in the numerical model is necessary to filter out spurious modes of vibration introduced by the finite element discretization of the cable. Artificial numerical damping has been used successfully in ice-shedding and other transient dynamics models. A modification of the parameters of the integration technique (Newmark-β with $\delta > 0.5$, $\alpha > 0.25$) provides useful algorithmic damping that filters out higher frequencies. Also, the modified technique provides some amplitude decay that resembles viscous damping, and a small amount of period elongation. The parameters of the Newmark-β integration technique were set to $\delta = 0.7$ and $\alpha = 0.4$ for all the analyses reported in chapter 8.

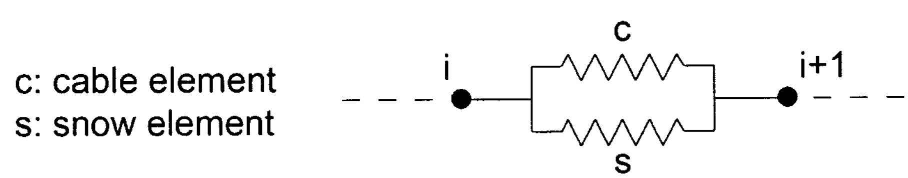

Fig.48 Modified cable model

A modified cable model that incorporates Rayleigh damping (Fig.48) was used instead of the parallel dashpot model. Rayleigh damping is defined as a linear combination of the mass and stiffness matrices:

$$C = aM + bK \tag{8.2}$$

where C is the damping matrix, M is the mass matrix, K is the stiffness matrix. The Rayleigh parameters a and b can be obtained from the following relationship:

$$a + b\omega_i^2 = 2\omega_i\xi_i \tag{8.3}$$

a and b are determined by prescribing the amount of damping needed at two different frequencies of oscillation.

For example, using 3.0% damping on the first mode and 4.1% on the 80^{th} mode of vibration for the ground wire model containing 80 elements:

$$\omega_1 = 2.009\,\text{rad/s}\,, \qquad \xi_1 = 0.030$$

$$\omega_{80} = 51.440\,\text{rad/s}\,, \qquad \xi_{80} = 0.041$$

Substituting in equation (8.3) and solving for a and b:

$\boldsymbol{a = 0.02374}$ $\qquad$ $\boldsymbol{b = 0.00155}$

As will be seen later in section 8.3.2, using these Rayleigh constants produced an acceptable amount of damping when the cable was subjected to a loading equivalent to a sudden snow-shedding scenario.

8.2.3 Snow model

Snow is modeled using non-linear spring elements (generic lumped parameter elements) with zero stiffness and damping properties. Snow elements only have an assigned mass, and their weight is modeled as vertical loads acting on the nodes. The snow load of each element is governed by a time function and its mass varies according to the same time input: this enables the virtual removal of any snow element from the cable, at the time prescribed by the user. The propagation of snow shedding is modeled by removing the mass and weight of neighboring elements at time intervals corresponding to the desired speed of shedding.

For this study, the range of snow density values has been set between 0.20 and 0.60 g/cm³ and the highest design overload used by EDF is a 4.2cm radial snow accretion.

→ The worst scenario for this ground wire model (**4.2cm radial, 0.60 g/cm³**) corresponds to an overload of **4.19 kg/m**, or **41.1 N/m**. This overload is used in the next sections whenever the cable is said to be "snow-covered".

8.2.4 Analysis procedure for a snow-shedding model

1. The inextensible catenary profile of the cable under its own weight is evaluated using an Excel spreadsheet (see Appendix C). This profile defines the initial geometry and strains to be used in ADINA as input for static analysis.

2. A static analysis of 10 time steps is used to obtain the equilibrium position of the nodes under a uniform load simulating the weight of the cable and taking into account the cable elasticity.
3. The analysis is restarted in *static* mode for another 10 time steps to add the weight of the snow elements onto the cable. Steps 2 and 3 may be performed in a single static analysis of 20 time steps. Performing them in two separate analyses enables the user to confirm the validity of the initial static equilibrium under self weight.
4. The analysis is restarted (at time step 20) in *transient dynamic* mode to evaluate the response of the cable subjected to snow shedding. The duration of the calculated response is prescribed by specifying the number and size of time steps. Guidelines to determine a proper time step size are given in the next section.

8.2.5 Selection of an adequate time step size for the integration technique

Following the guidelines recommended by Bathe (1996) for an implicit unconditionally stable time integration method (e.g. Newmark-β with $\delta \geq 0.5$, $\alpha \geq \frac{1}{4}(\delta + 0.5)^2$), time steps should be small enough to capture the essential features of the wave propagation problem induced by snow shedding. The smallest half-wavelength that can be represented by a discretized cable corresponds to the distance between two nodes. For a model containing 40 elements (the coarsest model considered) the critical wavelength is 2 x 470m / 40 = 23.5 m. Using 10 time steps between each node to represent a wave traveling at a speed of 111m/s the recommended time step size is:

$$\left(\frac{23.5\text{m}}{10}\right) \times \frac{1}{111\text{m/s}} = 0.021 \text{ s.}$$

Time step size also varies according to the loading applied. A safe time step size should be about one tenth of the duration of an applied impulse or load increment. For example, the time step chosen to apply the load illustrated in Fig.52 should be 0.0005 s from time 2.000 to 2.005, then, a time step of 0.02 s would be adequate from time 2.005 until the end of the analysis (e.g. until time 42).

An important feature of ADINA is its ability to automatically reduce the size of the time step by a pre-defined factor if the solver has difficulties converging. A maximum step size should always be prescribed, especially if there is a transient loading being applied.

8.3 Preliminary models

Preliminary models were aimed at validating the mesh size of the cable model and verifying key aspects such as the effect of damping on the response and the speed of propagation of a shock wave along the cable.

8.3.1 Mesh validation

Three different mesh sizes have been selected to demonstrate the convergence of the dynamic response. The number of elements doubles from one mesh to the next: 40, 80 and 160 elements. The response of a bare, undamped ground wire subjected to a steep trapezoidal pulse load is evaluated by using each mesh size. The load is applied at the mid span point only, has a magnitude of 5 kN (up) and a duration of 0.2 seconds. The time functions governing the cable weight and pulse loads are illustrated in Fig.49.

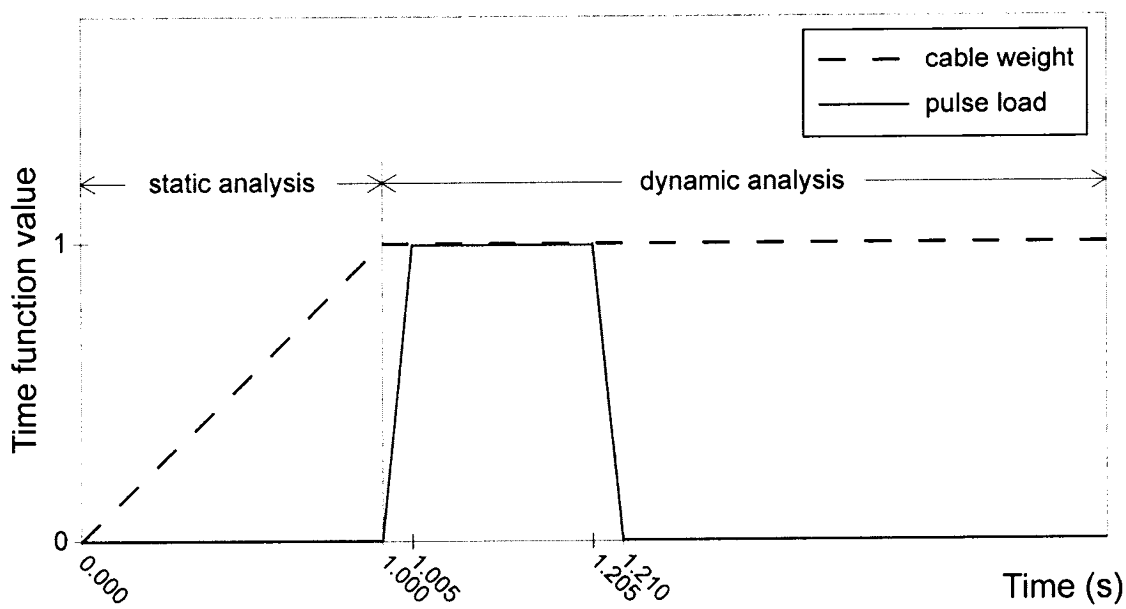

Fig.49 Time functions for a pulse load on a cable

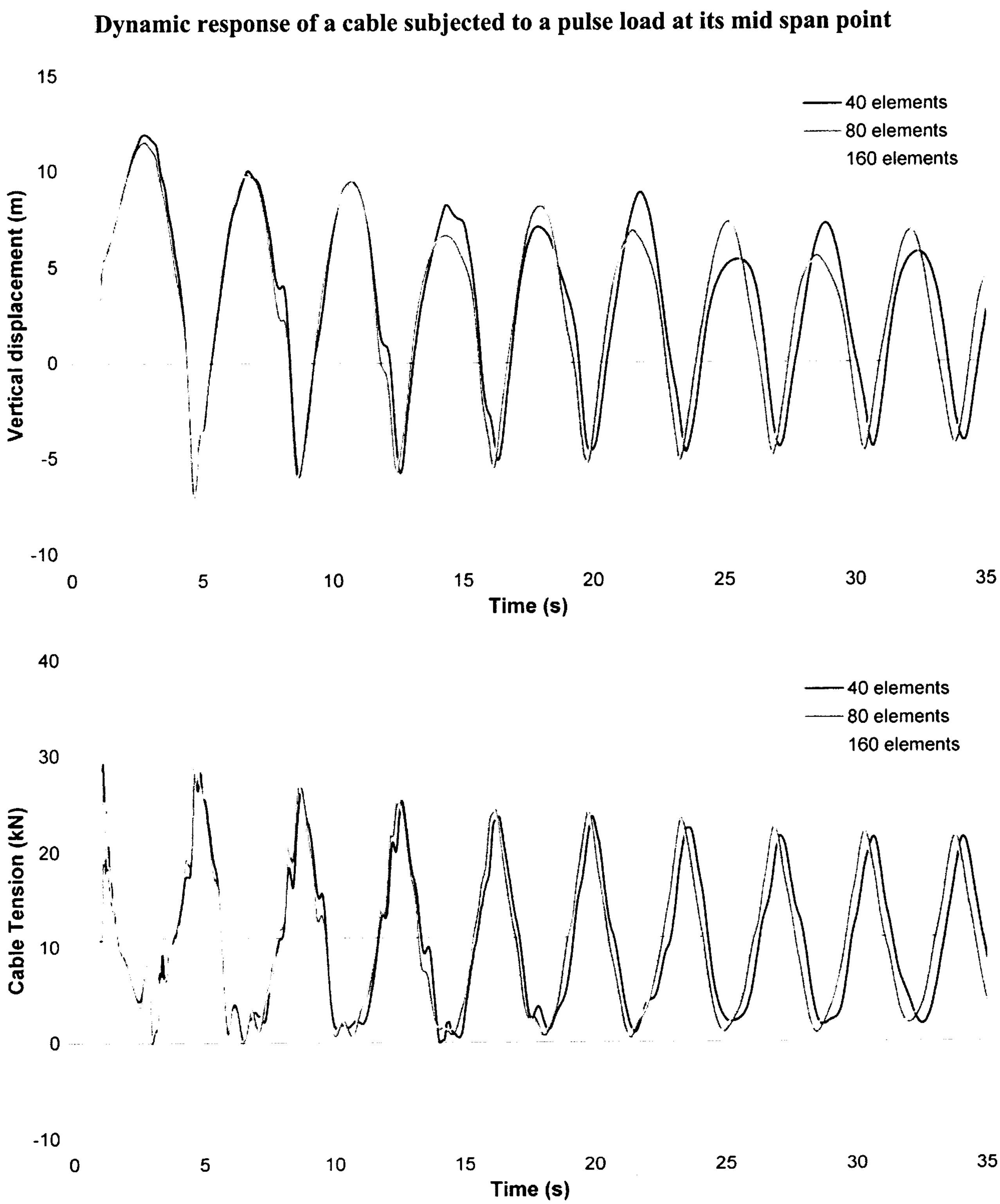

Fig.50 Mesh size validation
Top: Vertical displacement at the mid span point
Bottom: Cable tension at the end

The plots generated from the ADINA outputs (Fig.50) show that the dynamic response converges as the number of elements increases. The model containing 80 elements is found to be adequate for further modeling purposes: it is sufficiently refined to capture the dynamic response of the cable and it takes less than one minute of computer time to calculate the output of a 40-second simulation.

The maximum vertical jump approaches 12 m at the mid span and occurs during the first peak of the response. The maximum cable tension of 30 kN is reached during the second tension peak, which corresponds to the largest negative displacement at the mid span. On the tension plot, the dashed horizontal line at 11 kN indicates the static cable tension. This corresponds to the steady-state tension in the cable after the transient response and free cable oscillations damp out.

Some damping appears in the response of the cable. This is due to the modified Newmark-β integration technique (with $\delta = 0.7$, $\alpha = 0.4$) used to eliminate the effects of spurious modes of vibration.

8.3.2 Damping validation

The damped response of a bare cable subjected to the same pulse loading as in section 8.3.1 is shown in Fig.51. The responses obtained with Rayleigh damping and with the parallel dashpot method (with 10% axial damping) have been superimposed over the undamped response obtained in 8.3.1 for the 80-element mesh.

The damped and undamped responses differ slightly in their displacement amplitudes. Period elongation effects are apparent after 20 seconds. The maximum cable tension occurs at the second peak in all the models. As expected the amount of visible damping displayed by the Rayleigh-damped model is greater than for the undamped case. Surprisingly the model using parallel dashpots shows less damping than the undamped model. Another feature that makes this model less appealing is the fact that the mid span displacement reached at the fourth peak is 70% larger than predicted by the undamped model. The dashpot modeling technique does not appear to work as it should.

Dynamic response of a cable subjected to a pulse load at its mid span point

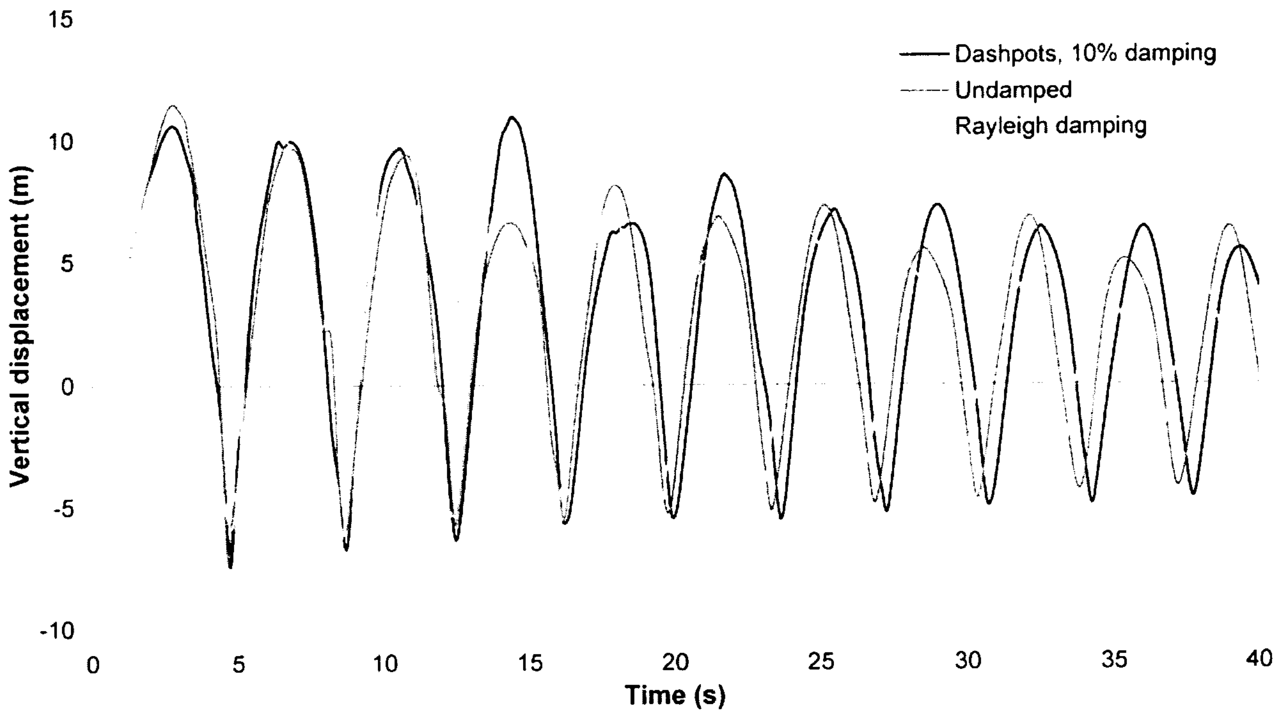

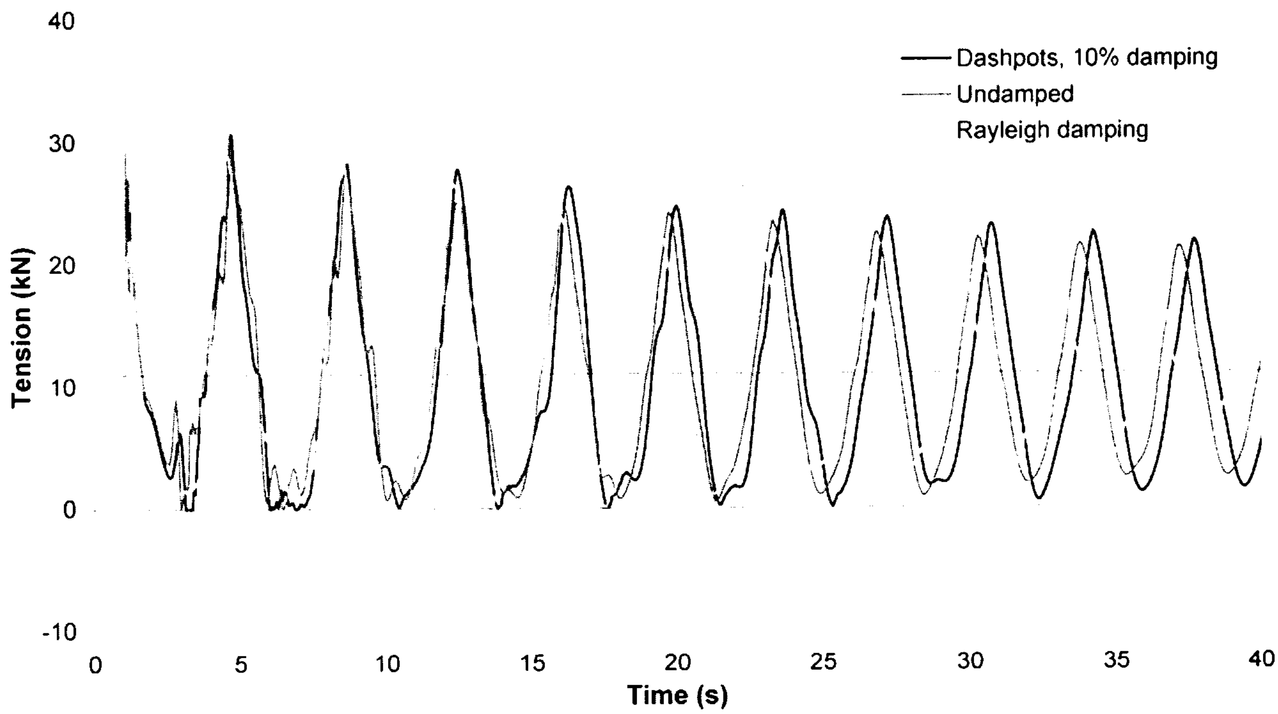

Fig.51 Damped and undamped response under a pulse loading
Top: Vertical displacement at the mid span point
Bottom: Cable tension at the tower

The damped response of a cable subjected to sudden snow shedding is shown in Fig.53. The cable, loaded initially with its self-weight and a tension of 11kN, is loaded with 41.1 N/m of snow in the static analysis and the entire snow load is removed during the first 5 milliseconds of the dynamic analysis (Fig.52).

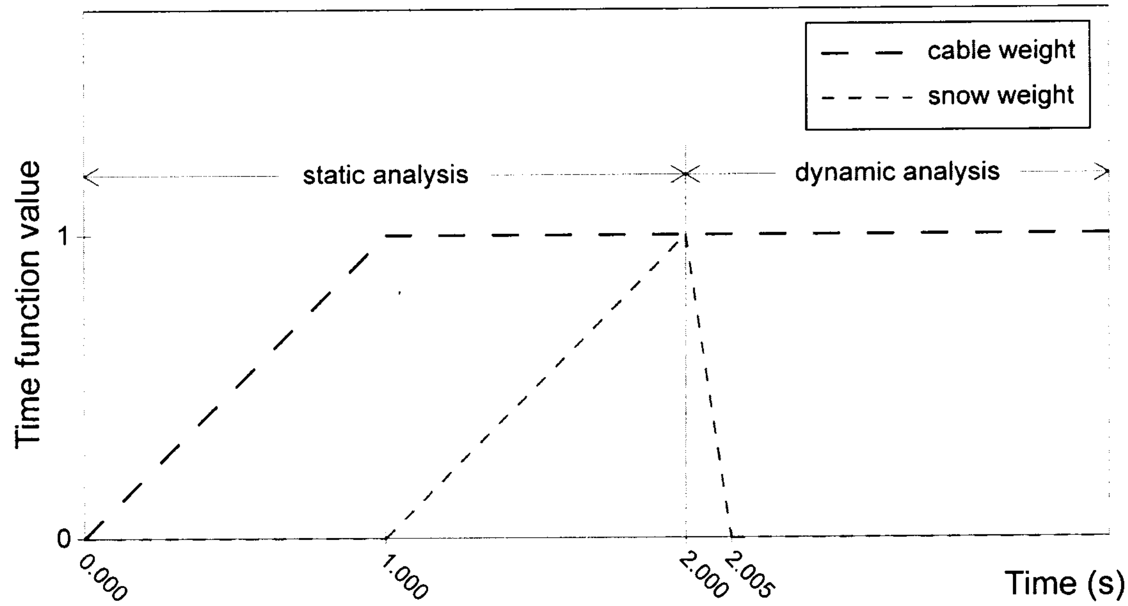

Fig.52 Time functions for a sudden shedding scenario

The tension plot shows that the cable became slack on a number of occasions. This can be observed on the graph whenever the response flattens out at the 0 kN level.

The damping ratio displayed by the response can be evaluated by using an approximation derived from the logarithmic decrement of a lightly damped system:

$$\xi = \frac{0.11}{N_{1/2}} \qquad (8.4)$$

where $N_{1/2}$ is the number of cycles to half amplitude.

From Fig.53, it takes 5 cycles for the displacement amplitude to reach approximately 50% of the first peak. Equation (8.4) yields a damping ratio of 2.2%.

Dynamic response of a cable subjected to sudden shedding on all nodes

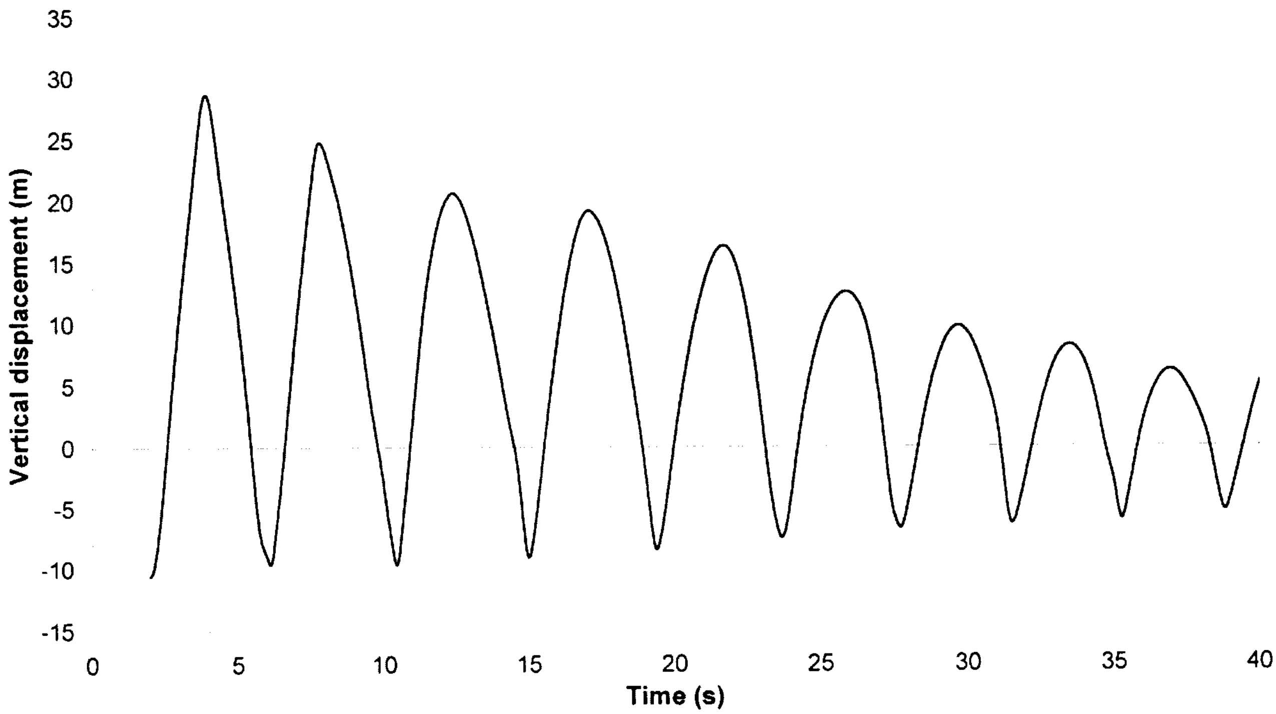

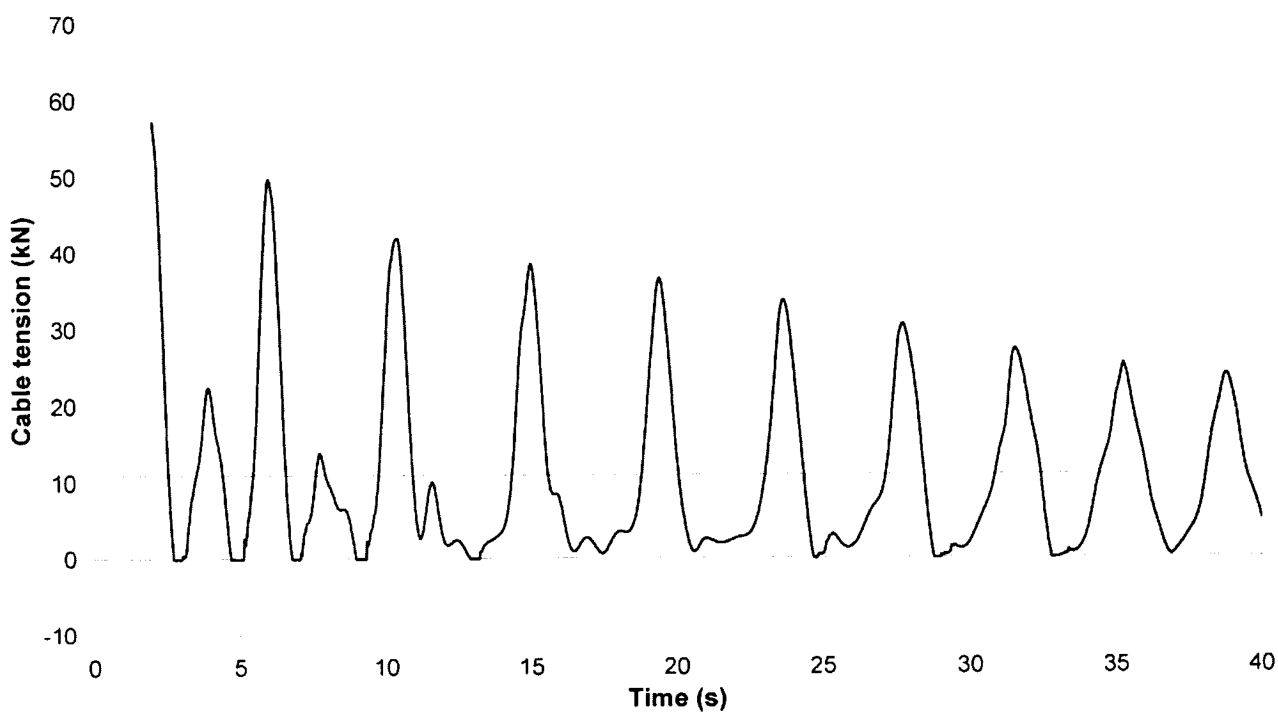

Fig.53 Damped cable response following sudden shedding
Top: Vertical displacement at the mid span point
Bottom: Cable tension at the end point

Although instantaneous accretion shedding on the total cable span is highly unlikely, it has been used in the past as a worst case scenario to simulate ice shedding in laboratories and on full-scale experimental lines (Dalle and Ratier 1983, Jamaleddine *et al.* 1993). To simulate ice shedding, sand bags attached to a cable were dropped simultaneously by triggering explosive devices.

The amount of overall damping displayed in Fig.53 is close to what was observed from full scale experiments in Dalle and Ratier (1983). Rayleigh damping is found to be adequate for further snow-shedding models. It has been included in all of the snow-shedding models of section 8.4.

8.3.3 Wave propagation verification

The speed at which a wave propagates along a snow-covered cable can be estimated visually from the response output of a cable subjected to a strong pulse load. The loading shown in Fig.54 was used to generate a 50 kN pulse at the mid span point of a snow-covered ground wire (41.1 kN/m snow load).

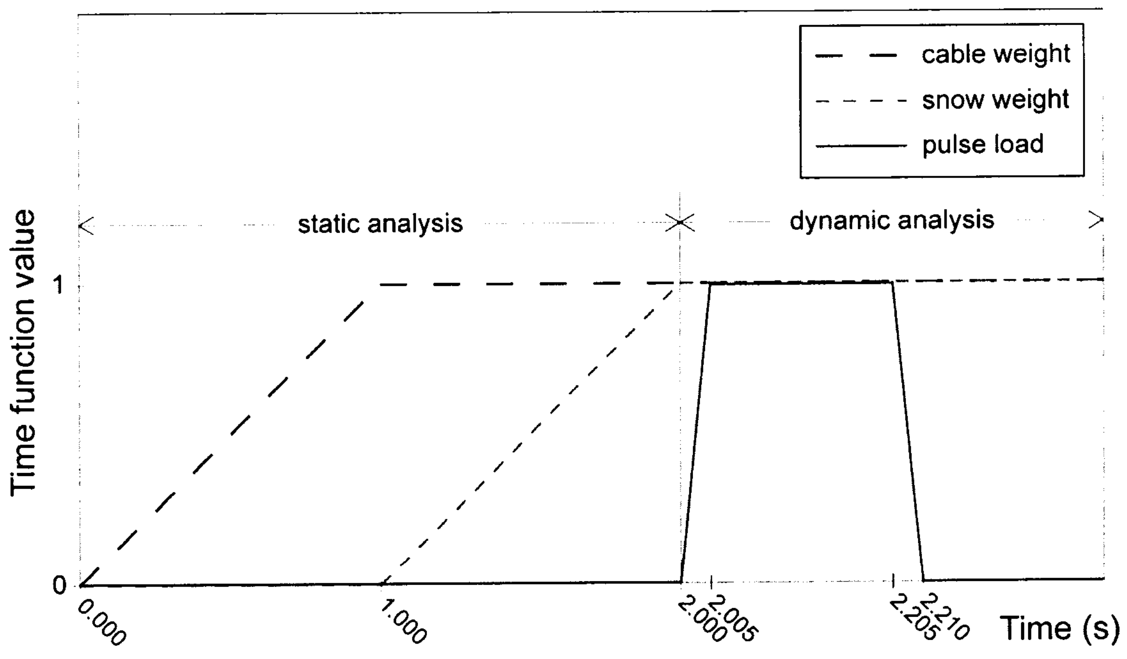

Fig.54 Time functions for a pulse load on a snow-loaded cable

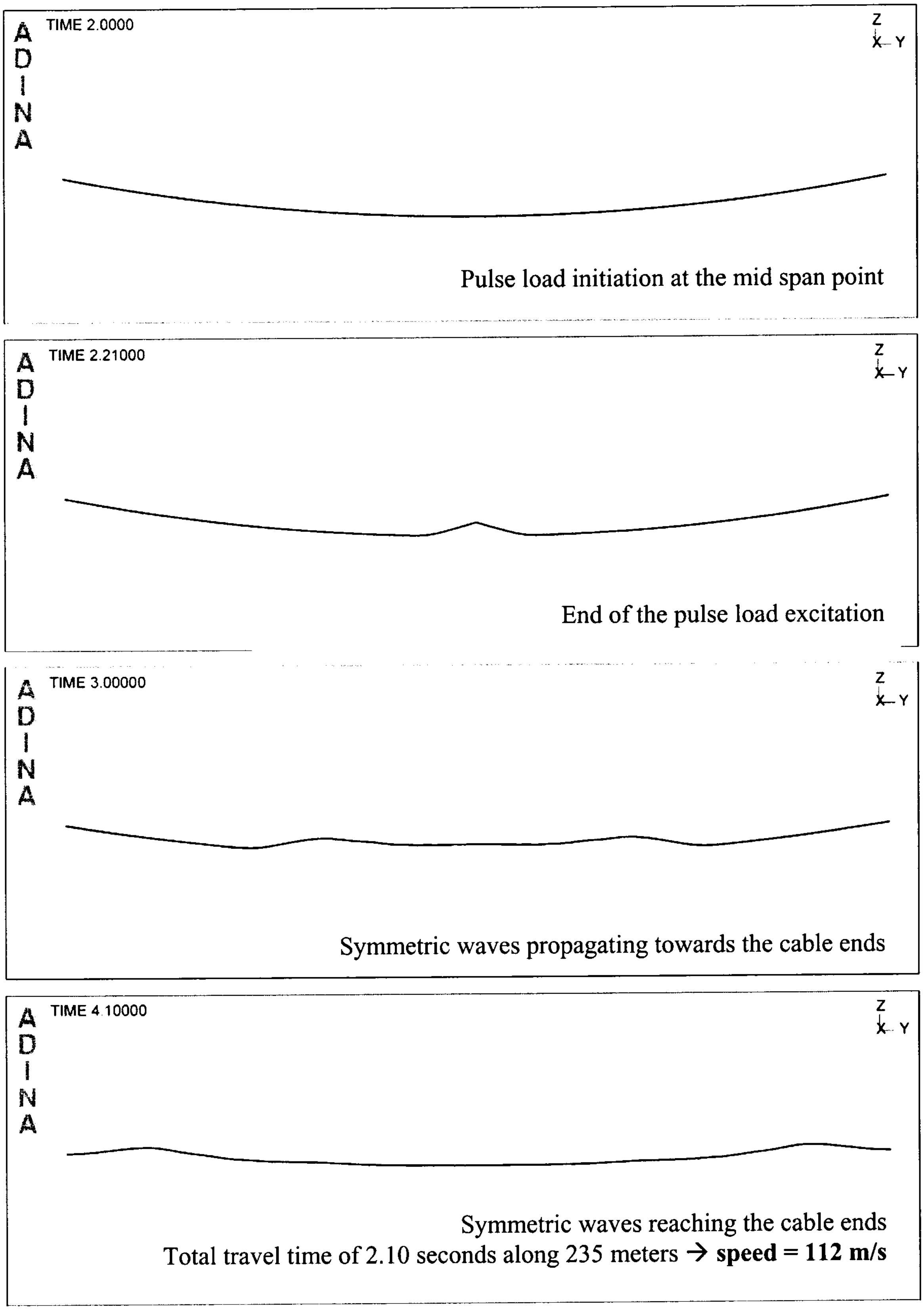

Fig.55 Wave propagation along a cable (Rayleigh-damped, snow-loaded)

The transverse wave produced by the pulse load took 2.1s to travel the 235 m distance from the mid span point to the end points (Fig.55). This corresponds to a speed of **112 m/s**, which is in agreement with the **111 m/s** speed estimated by equation (5.1) on p.27.

8.4 Wet snow shedding models

Based on observations reported in the field and during the experimental part of this study, it appears that snow does not shed in a sudden manner from an overhead cable. Instead, shedding progresses along a cable at various speeds.

Two speeds have been identified to evaluate the effects of snow shedding from the 470-m ground wire model:

→ **111 m/s** = speed at which **total unzipping** may progress

→ **14 m/s** = speed at which **partial natural shedding** was observed in a climate chamber (on a 2.5-m cable section)

8.4.1 Complete snow shedding by unzipping

The speed at which a tranverse wave travels along the 470-m snow-covered ground wire model is estimated at 111 m/s (from equation (5.1) on p.27). The response of the ground wire is evaluated in this section by assuming that a transverse wave may trigger shedding as it progresses along the entire span. At this time it is impossible to tell how pronounced the wave needs to be in order to remove the snow, therefore it is not included in the model. Snow-unzipping is simulated by removing the snow elements from the model at the rate of 111 m/s.

A separate time function is defined for each snow element. For example, Fig.56 represents the time functions governing the snow and cable elements between nodes 2 and 3. Each snow element takes 0.053 s to shed in the model (470-m cable meshed with 80 elements shedding at 111 m/s): the first element sheds from time 2.000 to 2.053, the second one sheds from time 2.053 to 2.106, etc. An illustration of the different loading and unloading steps can be found in Appendix E.

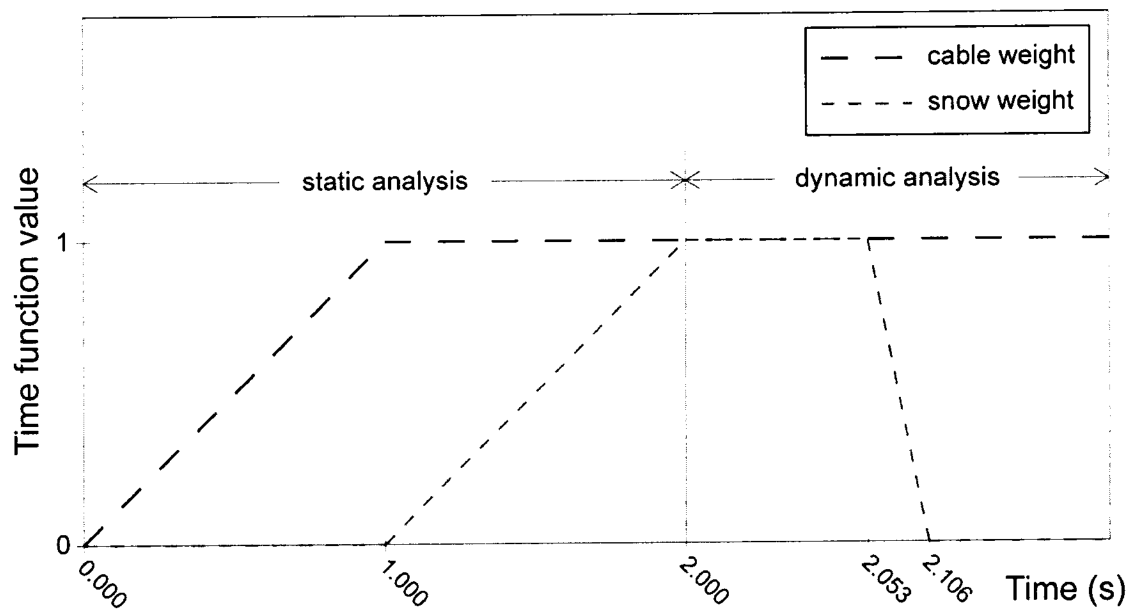

Fig.56 Time functions for snow-unzipping between two nodes
(80-element model, 111 m/s snow-unzipping, between nodes 2 & 3)

The response of the cable subjected to snow shedding at 111 m/s is shown in Fig.57A and Fig.57B. The zero value on the displacement plot represents the static position of the bare cable.

The maximum vertical cable jump at the mid span is 6.62 m and it occurs at the third peak. The maximum cable jump is 6.01 m at the quarter span (91% of the max mid span value) and it occurs at the fifth peak. These displacement values are more or less of the same order as those described by Guilbeault in his observations of wet snow unzipping (Guilbeault 2005).

The cable becomes slack during the first rebound. Once the cable is totally unloaded the tension oscillates between 4 kN and 20 kN (± 8 kN oscillation).

Dynamic response of a cable subjected to total snow unzipping at 111 m/s

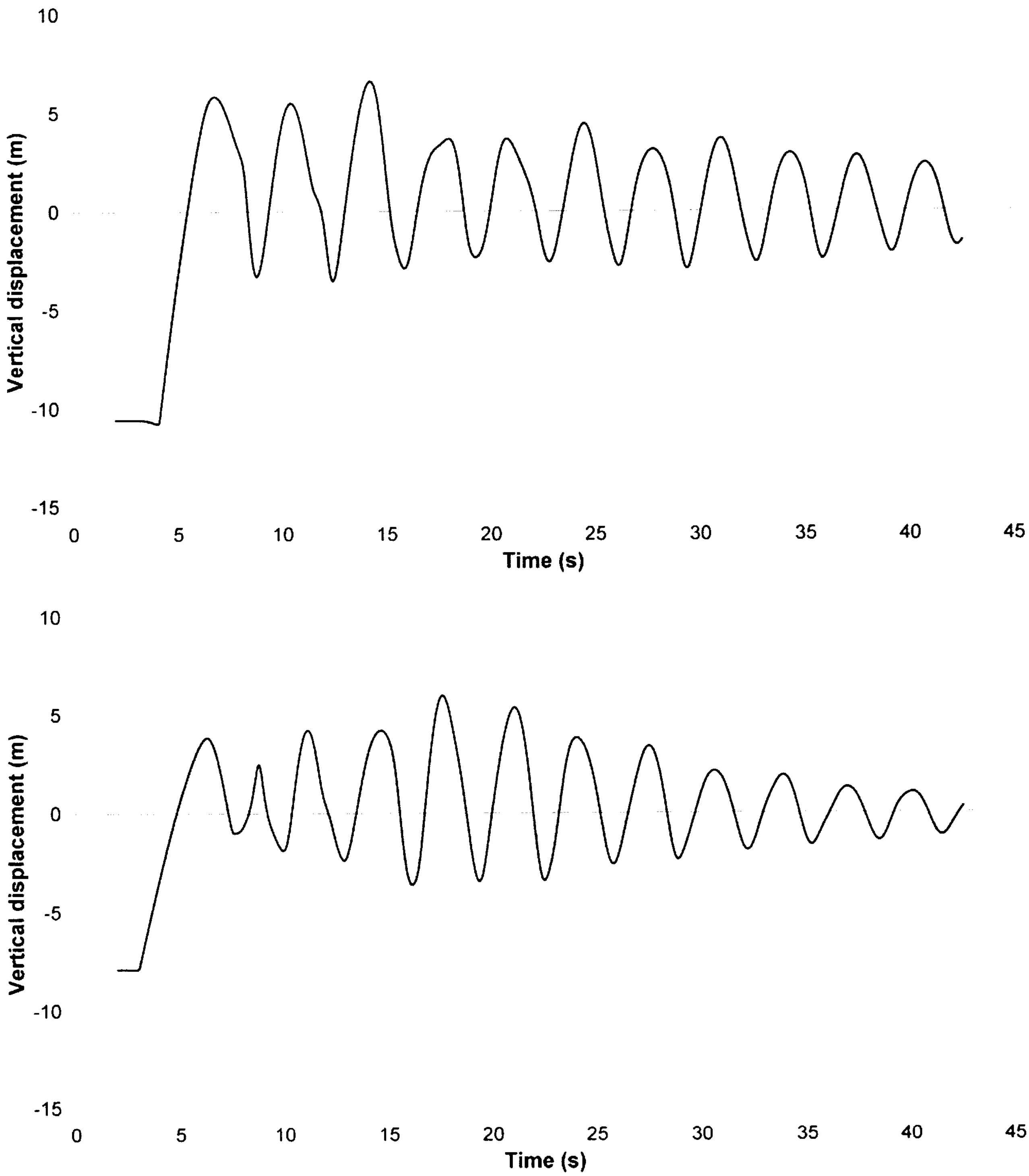

Fig.57A Cable response under total shedding - displacement
Top: Vertical displacement at the mid span point
Bottom: Vertical displacement at the first quarter span point

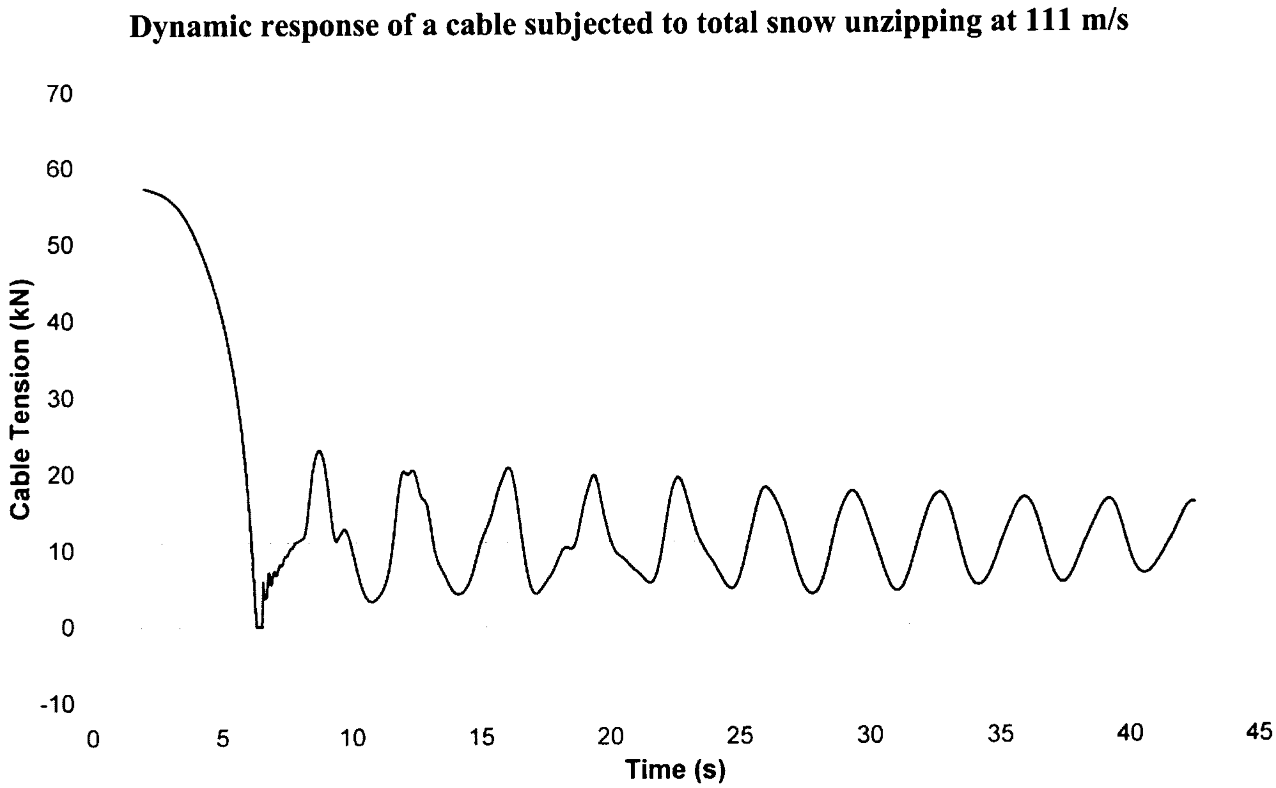

Fig.57B Cable response under total shedding - tension
Cable tension at the end point

8.4.2 Partial snow shedding

During the experimental study (Chapter 7) wet snow on a short cable segment was observed to shed naturally at speeds up to 14 m/s. This speed is used in this section to evaluate the response of three partial shedding scenarios.

Roshan Fekr and McClure (1998) confirmed that the effects of accretion shedding are greatest when it occurs at the center of the span. There are no field records for the length of partial snow-shedding segments; they have been described as ranging from a few meters to a few tens of meters in length (Admirat 2006).

To study the effect of partial snow shedding, segments of different lengths are removed symmetrically at a rate of 14 m/s, from the mid span point towards both cable ends.

Three different shedding lengths were chosen:

- 4 elements (5% of the total cable length, or 23.5 m)
- 6 elements (7.5% of the total cable length, or 35.25 m)
- 8 elements (10% of the total cable length, or 47.0 m)

The response of the ground wire model subjected to these partial shedding scenarios is shown in Figs.58A, B and C. The most obvious feature showing from the response plots is that cable oscillations following partial snow shedding are approximately proportional to the amount of snow removed. Displacement oscillations for the 10% scenario are twice as large as for the 5% scenario (at the mid span and at the quarter span).

Cable tension oscillations are also approximately proportional (Fig.58C). For the 10% shedding scenario the tension oscillates from 48 kN to 56 kN (± 4 kN oscillation).

Vertical acceleration plots were generated to get a better feel of their magnitude along the ground wire. The top plot in Fig.58B shows the vertical accelerations of the node adjacent to the last snow-shedding element. In other words, this corresponds to the acceleration of the snow-loaded node closest to the mid span point once the shedding process is over. Acceleration magnitudes are generally larger for a longer shedding length, but they are not proportional to the shedding length. For the 10% and 7.5% scenarios the largest upward acceleration reaches 2.25 m/s^2. For 5% shedding the maximum upward acceleration is 2.0 m/s^2.

The bottom plot in Fig.58B shows the vertical accelerations at the quarter span (more than 100 m away). Upward accelerations reach a maximum of 1.75 m/s^2 for 10% shedding and 1.5 m/s^2 for the 5% scenario. Maximum quarter span accelerations are approximately 75% of the accelerations of the node adjacent to the last snow-shedding element.

Dynamic response of a cable subjected to partial snow shedding at 14 m/s

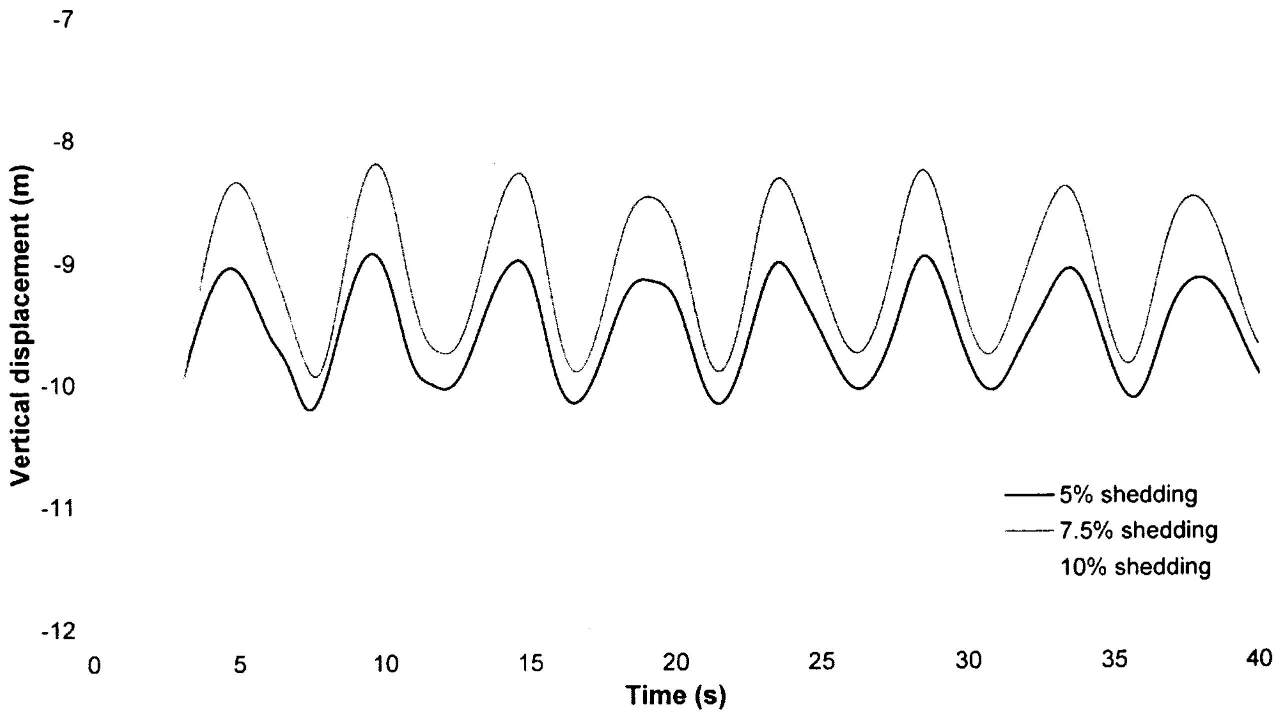

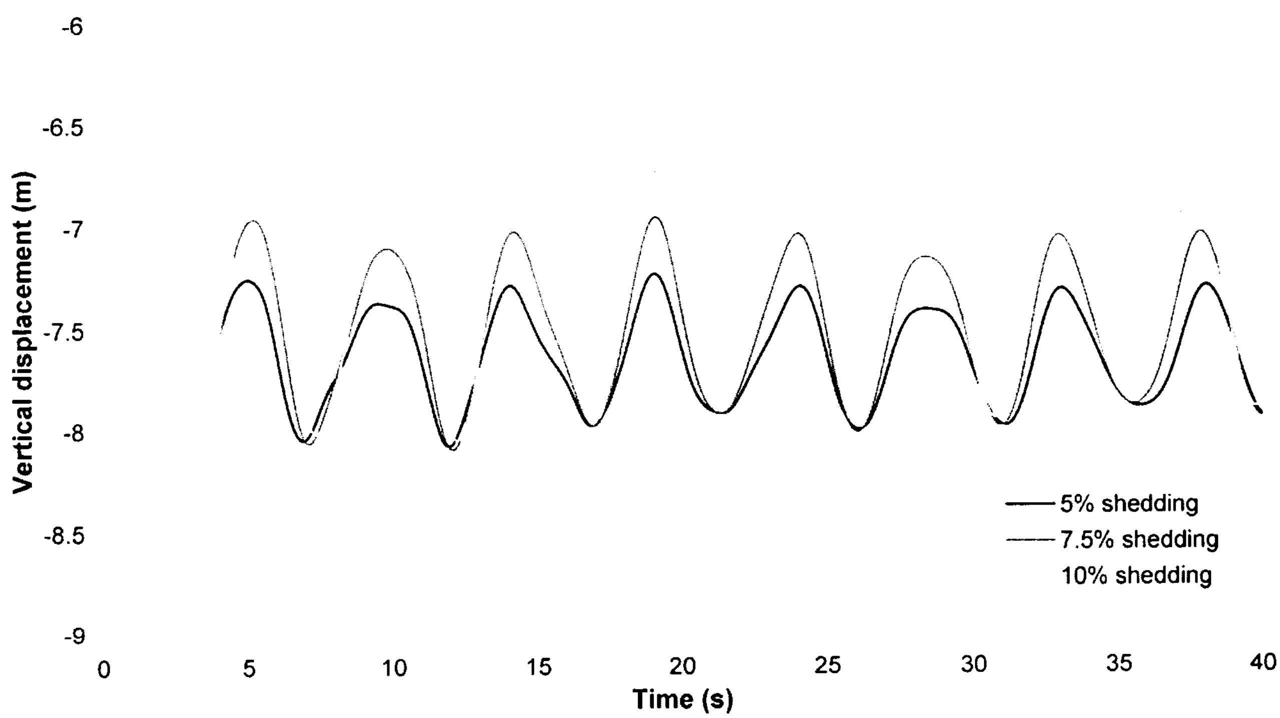

Fig.58A Cable response under partial shedding - displacement
Top: Vertical displacement at the mid span point
Bottom: Vertical displacement at the quarter span point

Dynamic response of a cable subjected to partial snow shedding at 14 m/s

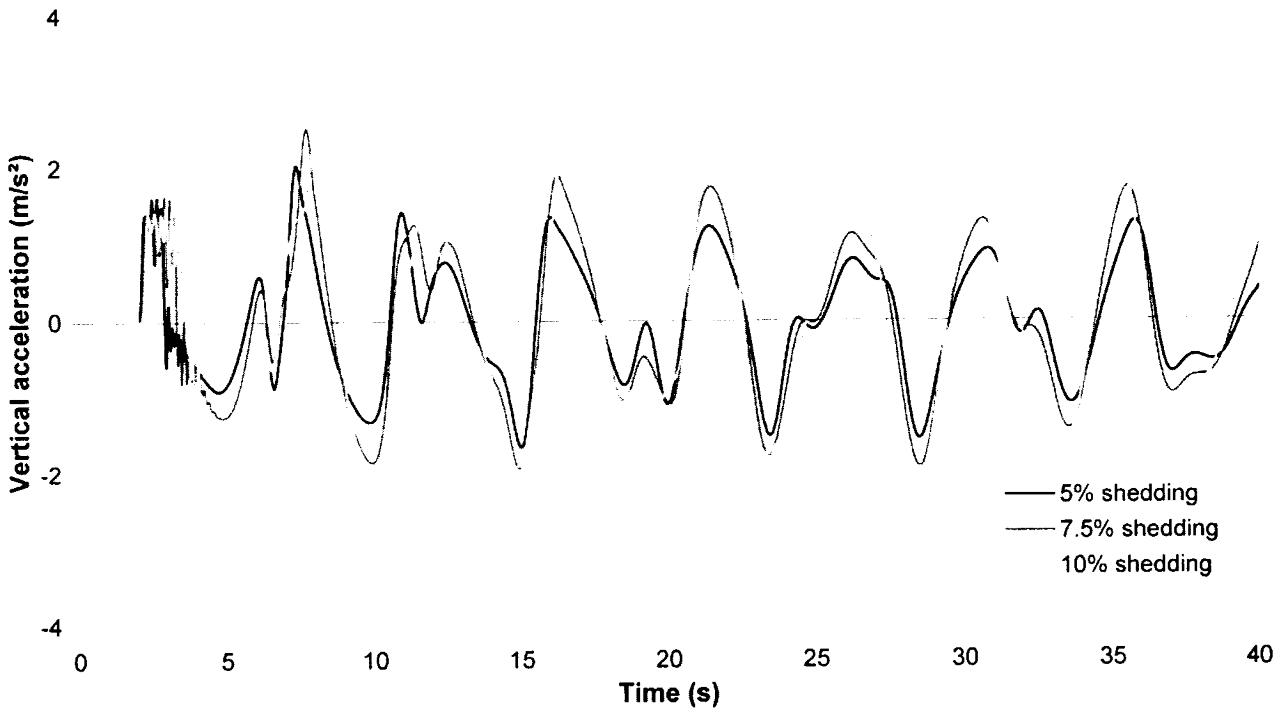

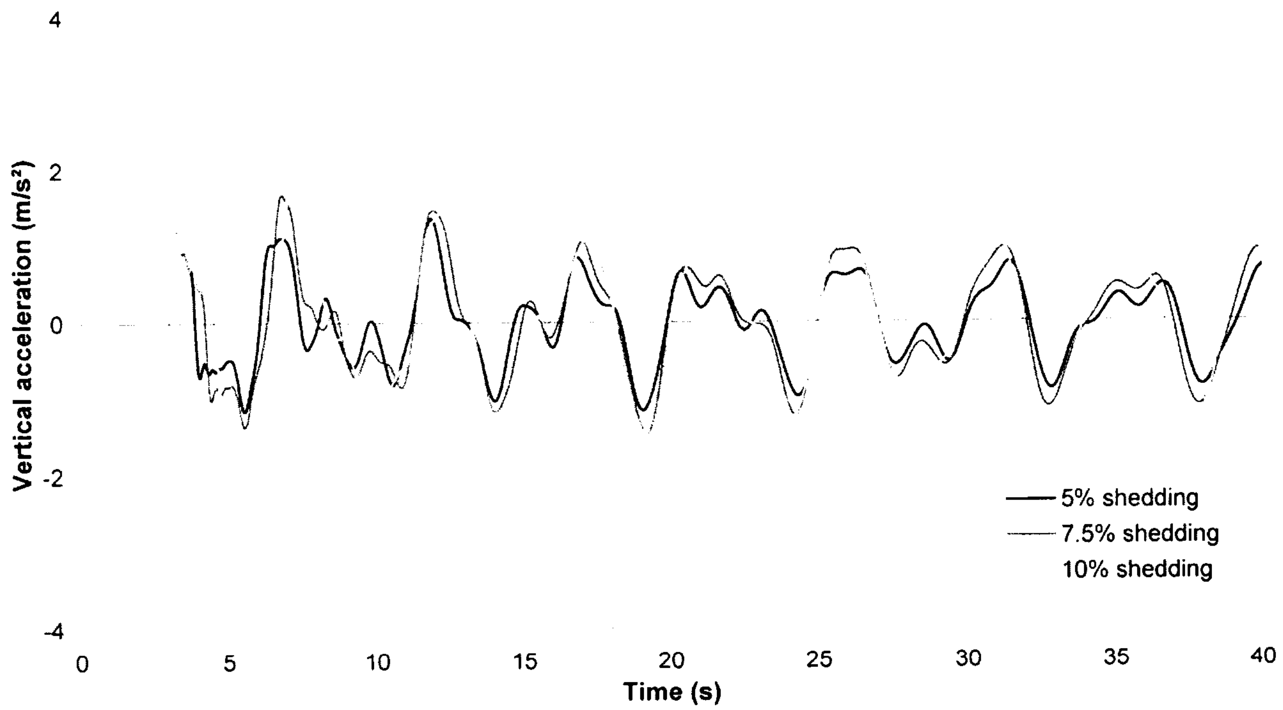

Fig.58B Cable response under partial shedding - acceleration

Top: Vertical acceleration of the node adjacent to the last snow-shedding element

Bottom: Vertical acceleration at the quarter span point

Dynamic response of a cable subjected to partial snow shedding at 14 m/s

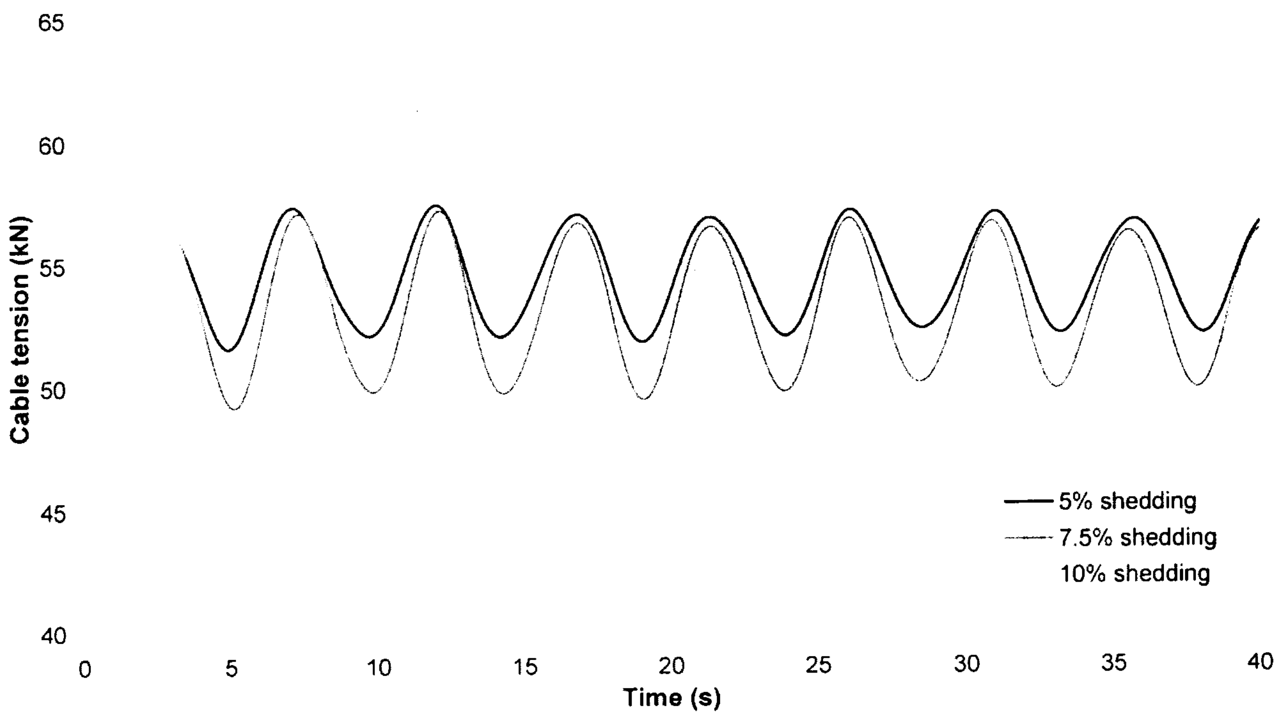

Fig.58C Cable response under partial shedding - tension
Cable tension at the end point

8.5 Discussion of the numerical modeling study

The first objective of this chapter on numerical modeling was to demonstrate the feasibility of evaluating the dynamic response of a ground wire subjected to snow shedding at a prescribed rate. Using some of the observations reported in the field and in the previous experimental chapter two speeds of shedding were identified and used for different shedding scenarios.

In many aspects, the snow-shedding model developed is similar to its ice-shedding predecessors. What really differentiates it from the previous models is that each cable and snow element is governed by a separate time function. This enables the user to prescribe the instant at which any snow element may appear or disappear from the model. This method allows for modeling any possible shedding scenario.

Rayleigh damping performed well for most models. The Rayleigh constants used in this study are specific to the snow-free ground wire model used. Damping was well displayed in the response of the ground wire subjected to a quasi-step load (sudden shedding, Fig.53). It also appeared in the snow-shedding scenarios unzipping at 111 m/s (Fig.57B), once the transient oscillations had faded ($t > 30$ s).

Very little damping showed up in the partial-shedding cases because the Rayleigh parameters were adjusted for the bare cable model only. The snow-covered cable had a large inertia and its natural frequencies of oscillation differed greatly from the bare cable. For the partial-shedding model a different set of Rayleigh constants should have been used to simulate damping in the cable and in the snow mass. It was not considered necessary to do so since the maximum response components are not really affected by damping.

An important result from this work is the demonstration that the effects of partial shedding are proportional to the amount of snow removed. For instance, mid span displacements and cable tension amplitudes were doubled when the snow-shedding percentage was doubled. It is uncertain whether this trend would continue if longer segments were removed from the cable span (e.g. 25%, 50%, etc...).

As the LWC of a snow sleeve increases and gets close to a critical value it becomes easy to trigger its shedding by subjecting it to a vertical acceleration. The magnitude of the acceleration required depends on the state of the snow sleeve and loading factors: without the presence of wind or vertical jumps the accretion will simply fall under its own weight. If the snow state and the environmental conditions are favorable it is likely that an upward acceleration of small magnitude (for example, less than 1g or 9.81 m/s^2) would be sufficient to cause the sleeve to shed. Such accelerations can be generated by a wave traveling along the cable or more simply by oscillations caused by partial shedding. It has been demonstrated in section 8.3.2 that upwards accelerations due to partial shedding can reach 2.25 m/s^2 on the remaining snow accretion.

It is the opinion of the author that on real snow sleeves this acceleration may not be sufficient to cause further shedding. Natural variability in snow sleeve uniformity (in size, density and LWC) on a span of a few hundreds of meters in length prevents the sleeve from reaching a critical LWC along its entire span at the same instant. It may be possible to trigger further shedding if the accretion is subjected to an upwards acceleration greater than 5 m/s^2. This requires further investigation and more field observations.

Snow shedding generates cable tension oscillations. On a real conductor these oscillations would have an effect on adjacent spans. The numerical modeling technique should be used to study the effect of total and partial shedding on multiple spans. An even more ambitious evolution of the model would be three-dimensional and would include ground wires, phase conductors and the flexibility of the support structures.

Another improvement to the model would be to add a failure criterion to the snow elements. Since wet snow sleeves usually shed when they loose their cohesion, the criterion does not need to be based on their mechanical properties. Individual snow elements could be assumed to shed when their vertical acceleration exceeds a pre-defined threshold (e.g. element death upon exceeding a 5 m/s^2 upward acceleration). This sort of user-supplied failure criterion is possible in ADINA.

9. Conclusions

For a better understanding of wet snow shedding, an exhaustive explanation was given in the first chapters about the nature of wet snow and the mechanism by which it can accumulate on overhead cables. Wet snow particles carried by the wind tend to adhere to an cable, so that the accreted mass grows out into the wind causing an eccentric load on the windward side of the cable. The wind is responsible for packing the accreting snow grains to a high density; it also plays a key role in the heat balance of the accretion which influences its liquid water content (LWC). Two modes of accretion have been observed along the span of an overhead cable: axial growth and cylindrical sleeve growth.

The physical properties of wet snow are extremely variable. Different ratios of ice, water and air produce microstructures with different densities and LWC. This leads to a wide range of adhesive properties and strength. The microstructure of wet snow is continuously evolving and it undergoes metamorphism with changes in LWC and heat flux. The mechanical properties of freshly accumulated wet snow are very different from those of shedding wet snow.

A limited amount of information exists on the subject of wet snow shedding from an overhead cable and only a fraction of it is found in the scientific literature. Field observations are sparse and rarely end up being published. Most of the field observations reported in this thesis were obtained by communicating directly with researchers who have actually witnessed the phenomenon of wet snow shedding. Combining the information available in the literature with relevant field observations led to a better understanding of the wet snow shedding mechanism.

Reproducing wet snow sleeves in a laboratory environment using simple and inexpensive tools is possible.

Some pertinent observations emerged from the laboratory experiments performed on simulated snow sleeves:

- An added heat flux needs to be supplied to the accretions to recreate the same conditions leading to natural shedding.
- When snow sleeves lose their cohesion and break off from a cable the rupture propagates along the accretion. The rate at which natural shedding propagates has been measured between 12 and 14 m/s for three successful experiments.
- The strength of low-LWC wet snow sleeves is large. Their holding strength was measured in excess of 500 N/m.

Based on the previous work of McClure *et al.* (Jamaleddine *et al.* 1993, Roshan Fekr and McClure 1995, McClure and Lapointe 2003) a numerical modeling technique using nonlinear finite element analysis was successfully developed to evaluate the response of an overhead cable subjected to any snow-shedding scenario. To demonstrate the capabilities of the technique the response of an overhead ground wire under different snow-shedding scenarios was evaluated. Some interesting observations were made about wet snow shedding for the particular case studied:

- Total unzipping of a wet snow sleeve progressing at the same speed as a transverse wave leads to displacement amplitudes of the order of a few meters.
- The amplitude of the cable tension and displacement oscillations produced by partial wet snow shedding are proportional to the amount of snow removed (for shedding in the range of 5% and 10% of the total span).
- Vertical accelerations generated by partial shedding could be sufficient to trigger more shedding on the same span. This requires further investigation.

Many future avenues of research were identified during this study. At present, there is no workable method to relate the properties of snow (i.e. snow type, grain size and shape, density, LWC, temperature) to its response when subjected to a given load. To the author's knowledge, mechanical properties have been determined experimentally for a few dry snow cases but there is no mention of any experiment ever performed on wet snow in the literature. Material testing is now possible at the CIGELE Pavillon de recherche sur le givrage and the facility is an ideal location to study snow.

Other experimental research needs lie in a more rigorous study of the heating effects that influence the LWC of wet snow sleeves. Such a study could be combined with a validation/revision of the thermodynamic models established by Grenier and Admirat during the 1980's and by Poots in 1990's.

Natural snow shedding observations are difficult to perform because of the rarity and transient nature of such events. It is doubtful that there will be any useful field observations in the future, unless a research group sets up an ambitious project similar to the 1980's line observation program in France.

This study has shown that wet snow sleeves can be recreated in a laboratory environment. In future works the microscopic aspect of these simulated sleeves should be studied and compared to those observed in the field. More rigorous quality control would be needed if reproduced snow sleeves are to be used for materials testing purposes. They could also be used to observe the influence of heating effects and snow properties on the speed at which a shedding fracture naturally propagates.

The finite element modeling technique developed for wet snow shedding should be applied to multiple spans of cable, and ideally to a full 3-dimensional model of an overhead line including the support structures. Considering the very low cohesive forces of wet snow sleeves at the instant prior to their natural shedding, a failure criterion should be added to the model based on a threshold upward acceleration, not on mechanical stresses.

References

Admirat P. and MacCagnan M. (1985) "Observations de neige collante sur les lignes électriques". EDF-DER HM/72-5287, 41 p.

Admirat P., Sakamoto Y., Lapeyre J.-L. and MacCagnan M. (1986) "Quantitative results and proposed mechanisms on wet snow accretion in the Ishiuchi wind-tunnel facilities". *Proceedings of the 3rd International Workshop on Atmospheric Icing – IWAIS'86*, pp. 155-160.

Admirat P. and Lapeyre J.-L. (1986) "Observations d'accumulation de neige collante à la station de Bagnères de Luchon les 6, 7 Avril 1986 – Effet préventif des contrepoids antitorsion". EDF-DER HM/72-5535, 26 p.

Admirat P. and Sakamoto Y. (1988) "Wet snow on overhead lines: state-of-art". *Proceedings of the 4th International Workshop on Atmospheric Icing – IWAIS'88*, pp. 7-13.

Admirat P., Lapeyre J.-L. and Dalle, B. (1990) "Synthesis of field observations and practical results of the 1983-1990 "Wet Snow" programme of Électricité de France". *Proceedings of the 5th International Workshop on Atmospheric Icing – IWAIS'90*, B6-2(1) – B6-2(5).

Admirat P. (2006) Communications related to the 1980's French wet-snow observation program, the France-Japan wet snow studies collaboration and his personal observations of wet snow accumulation and shedding on overhead lines.

Bader H., Haefeli R., Bucher E., Neher J., Eckel O., Thams C. and Niggli P. (1939) Der Schnee und seine Metamorphose. USA Snow, Ice and Permafrost Research Establishment, Translation 14 (1954).

Bathe K.-J. (1996) *Finite element procedures*. Prentice Hall, Upper Saddle River, NJ, USA, 1037 p.

Colbeck S. C. (1973) "Theory of metamorphism of wet snow". *United States Army Corps of Engineers, Cold Regions Research & Engineering Laboratory, Hanover, N.H., Research Report*, n 313, Dec 1973, 17 p.

Colbeck S. C. (1979) "Grain clusters in wet snow". *Journal of Colloid and Interface Science*, v 72, n 3, Dec. 1979, pp. 371-384.

Colbeck S. C. (1982) "Overview of seasonal snow metamorphism". *Reviews of Geophysics and Space Physics*, v 20, n 1, pp. 45-61.

Colbeck S. C. (1995) "Of wet snow, slush & snowballs". *The Avalanche Review*, v 13, n 5, Mar 1995.

Colbeck S. C. (1997) "A review of sintering in seasonal snowpack". *United States Army Corps of Engineers, Cold Regions Research & Engineering Laboratory, Hanover, N.H., CRREL Report* 97-10, Dec 1997, 11 p.

Colbeck S. C., Akitaya E., Armstrong R., Gubler H., Lafeuille J., Lied K., McClung D. and Morris E. (1990) "The international classification for seasonal snow on the ground". Issued by *The International Commission on Snow and Ice of the International Association of Scientific Hydrology*. 23 p.

Colbeck S. C. and Ackley S. F. (1982) "Mechanisms for ice bonding in wet snow accretions on power lines". *Proceedings of the 1st International Workshop on Atmospheric Icing – IWAIS'82*, pp. 25-30.

Dalle B. and Ratier M. (1983) "Étude du comportement dynamique d'une portée tendue de ligne munie ou non d'espaceur lors de la décharge d'un manchon de givre". EDF-DER HM/72-5075, 15 p.

Denoth A. (1980) "The pendular - funicular liquid transition in snow". *Journal of Glaciology*, v 25, n 91, pp. 93–97.

Denoth A. (1982) "The pendular - funicular liquid transition and snow metamorphism". *Journal of Glaciology,* v 28, n 99, pp. 357–364.

EDF (1986) "Studies on wet snow accretion on electric wires". EDF-DER HM/72-5532, 32 p.

Elíasson Á. J. and Thorsteins E. (1996) "Wet snow icing combined with strong wind". *Proceedings of the 7th International Workshop on Atmospheric Icing – IWAIS'96*, pp. 131-136.

Elíasson Á. J. and Thorsteins E. (2000) "Field measurements of wet snow icing accumulation". *Proceedings of the 9th International Workshop on Atmospheric Icing – IWAIS'00*, 8 p.

Elíasson Á. J., Thorsteins E. and Ólafsson H. (2000) "Study of wet snow events on the south coast of Iceland". *Proceedings of the 9th International Workshop on Atmospheric Icing – IWAIS'00*, 8 p.

Fukue M. (1977) "Mechanical performance of snow under loading". Ph.D. Thesis. Department of Civil Engineering and Applied Mechanics, McGill University, QC, Canada, 253 p.

Grenier J.-C., Admirat P. and MacCagnan M. (1986) "Theoretical study of the heat balance during the growth of wet snow sleeves on electrical conductors". *Proceedings of the 3rd International Workshop on Atmospheric Icing – IWAIS'86*, pp. 125-128.

Guilbeault P. (2005) Communications related to his personal observations of wet snow accumulation and shedding on overhead lines.

Huynh H. (2006) Communications related to his personal observations of wet snow accumulation and shedding on overhead lines.

Jamaleddine A., McClure G., Rousselet J. and Beauchemin R. (1993) "Simulation of ice-shedding on electrical transmission line using ADINA". *Computers and Structures*, Vol. 47, No. 4/5, pp. 523–536.

Jamaleddine A. (1994) "Effets statiques et dynamiques du délestage de la glace sur les lignes aériennes de transport d'énergie électrique". PhD Thesis. École Polytechnique, Université de Montréal, QC, Canada, 429 p.

Kálmán T., Farzaneh M., Kollár L.E., McClure G. and Leblond A. (2005) "Dynamic behavior of iced overhead cables subjected to mechanical shocks". *Proceedings of the 6th International Symposium on Cable Dynamics*, Charleston, USA, pp. 339-346.

Lapeyre J.-L. and Dalle B. (2006) Communications related to the 1980's French wet-snow observation program, the France-Japan wet snow research collaboration and personal observations of wet snow accumulation and shedding on overhead lines.

Langham E. J. (1981) Chapter on "Physics and properties of snowcover" found in the *Handbook of Snow: Principles, Processes, Management & Use*, edited by Gray, D.M. and Male, D.H. Pergamon Press Canada, Willowdale, ON, Canada, 776 p.

McClure G. and Lapointe M. (2003) "Modeling the structural dynamic response of overhead transmission lines". *Computers and Structures*, n.81, pp. 825–834.

Poots G. (1996) *Ice and snow accretion on structures*. Research Studies Press (England) and John Wiley and Sons Inc., New York, NY, USA, 330 p.

Roshan Fekr M. (1995) "Dynamic response of overhead transmission lines to ice-shedding". M. Eng. Thesis. Department of Civil Engineering and Applied Mechanics, McGill University, Montreal, QC, Canada, 116 p.

Roshan Fekr M. and McClure G. (1998) "Numerical modelling of the dynamic response of ice-shedding on electrical transmission lines". *Atmospheric Research*, vol.46, pp. 1-11.

Roshan Fekr M., McClure G. and Hartmann D. (1998) "Investigation of transmission line failure due to ice shedding effects using dynamic analysis". *Proceedings of the 8th International Workshop on Atmospheric Icing – IWAIS'98*, pp. 11-16.

Sakamoto Y. (2000) "Snow accretion on overhead wires". *Philosophical Transactions of the Royal Society*, v 358, n 1776, pp. 2941-2970.

Sakamoto Y. (2005) Communications related to his personal observations of wet snow accumulation and shedding on overhead lines and in wet snow wind tunnels.

Sakamoto Y., Tachizaki S. and Sudo N. (2005) "Snow accretion on overhead wires". *Proceedings of the 11th International Workshop on Atmospheric Icing – IWAIS'05*, pp. 3-9.

Shugo M., Okamoto M. and Oura H. (2002) "Experimental examination on snow accretion characteristics on transmission lines". *Proceedings of the 10th International Workshop on Atmospheric Icing – IWAIS'02*, P-1, pp. 1-4.

Skelton P. L. I. and Poots G. (1991) "Snow accretion on overhead line conductors of finite torsional stiffness". *Cold Regions Science and Technology*, 19, pp. 301-316.

St. Lawrence W. F. and Tang T. E. (1981) "A constitutive relation for the deformation of snow". *Cold Regions Science and Technology*, 4, pp. 3-14.

Strauss B. (1986) "Mapping of snow and ice accretion occurrences from synoptical meteorological measurements". *Proceedings of the 3rd International Workshop on Atmospheric Icing - IWAIS 86*, pp. 49-56.

Wakahama G., Kuroiwa D. and Gotō K. (1977) "Snow accretion on electric wires and its prevention". *Journal of Glaciology*, v 19, n 81, pp. 479-487.

Wakahama G. (1979) "Experimental studies of wet snow accretion on electrical lines developed in a strong wind". *Journal of Natural Disaster Science*, 1, pp. 21-33.

Yukino T., Hase Y., Matsuda M., Nishimura H. and Imaizumi M. (1998) "Experiment of Snow Accretion and Geometrical Analysis of the Shape". *Proceedings of the 8th International Workshop on Atmospheric Icing – IWAIS'98*, pp. 95-99.

Web References

Environment Canada's Climatic Database: Meteorological Records for Montreal, Quebec on March 22nd, 2001 and Halifax, Nova Scotia on November 13th and 14th, 2004. Retrieved September 1st, 2005 from http://www.climate.weatheroffice.ec.gc.ca

The Weather Network: 30 year statistics for Bagotville, QC, Canada. Retrieved May 1st, 2006 from http://www.theweathernetwork.com/weather/stats/pages/C02036.htm?CAQC0996

National Renewable Energy Laboratory, a national laboratory of the U.S. Department of Energy, Office of Energy Efficiency and Renewable Energy: Solar Radiation Data Manual for Buildings. Retrieved March 15th, 2006 from http://rredc.nrel.gov/solar/pubs/bluebook

Report Reference

Nova Scotia Utility and Review Board (2005) "*In the matter of The Public Utilities Act, R.S.N.S. 1989, c.380, as amended - and - In the matter of a Public Review of the Power Outages Resulting from the Storm of November 13 and 14, 2004*", filed on January 18th 2005, 114 p.

Appendix A

Sample calorimetric calculation table for a centered snow sleeve (including pull-down tests)

Calorimeter

Constants

Cwater : Specific heat of water	4.184	kJ/kg-C
Cice : Specific heat of ice	1.84	kJ/kg-C
L : Specific latent heat of fusion (ice)	333.51	kJ/kg

	March 17th - centered sleeve		
	15:00 5m sleeve	18:00 top	18:00 bottom
Warm water			
[m1]: mass (g)	456.42	458.06	478.98
[T1]: temperature (deg C)	51.5	54.0	53.8
Snow			
[m2]: mass (g)	60.093	54.731	90.043
[T2]: temperature (deg C)	0	0	0
Mix			
[m3]: mass (g)	516.513	512.791	569.023
[T3]: temperature (deg C)	37.3	41.4	37.0
LWC			
[m2L]: liquid water mass (g)	4.967	9.031	28.596
[m2S}: ice mass (g)	55.126	45.700	61.447
LWC (%mass)	8.26	16.50	31.76
Snow density			
outside diameter (mm)	101.6	88.9	
inside diameter (mm)	12.7	12.7	
sample length (mm)	66.0	78.7	
mass (g)	192.3	273.5	
Density (g/cm^3)	0.36	0.57	
Pull down test			
time	15:40	18:40	
total hung mass (kg)	23.50	15.95	
down force (N)	230.5	156.5	
Environment			
set temperature (deg C)	3	3	
actual temperature (deg C)	2.4	2.9	
relative humidity (%)	80-85	80-85	

Appendix B

Snapshots of wet snow shedding – fracture propagation

First column: shedding of a hollow sleeve at 13.6 m/s

Second column: shedding of a hollow sleeve at 12.5 m/s under simulated radiation

Third column: shedding of an eccentric sleeve at 12.1 m/s under simulated radiation

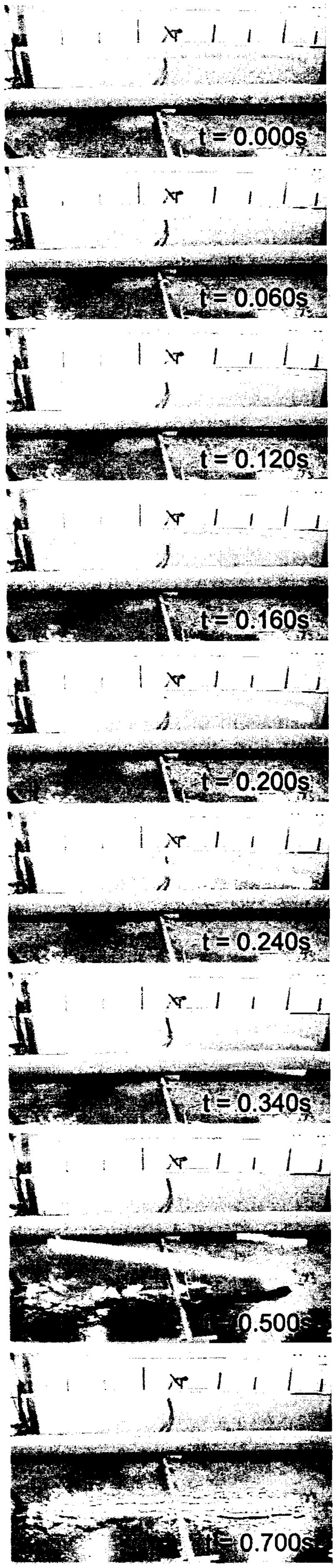
t = 0.000s
t = 0.060s
t = 0.120s
t = 0.160s
t = 0.200s
t = 0.240s
t = 0.340s
t = 0.500s
t = 0.700s

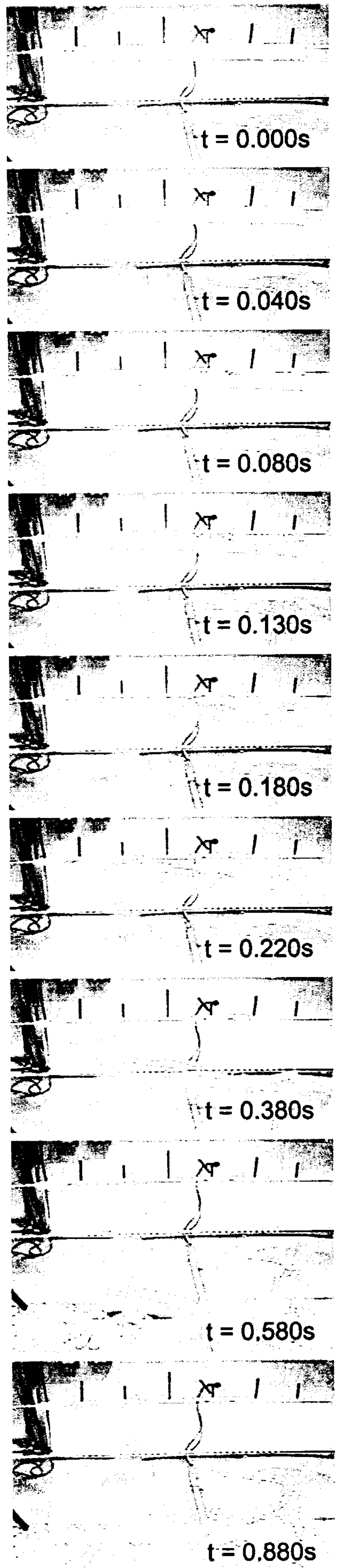
t = 0.000s
t = 0.040s
t = 0.080s
t = 0.130s
t = 0.180s
t = 0.220s
t = 0.380s
t = 0.580s
t = 0.880s

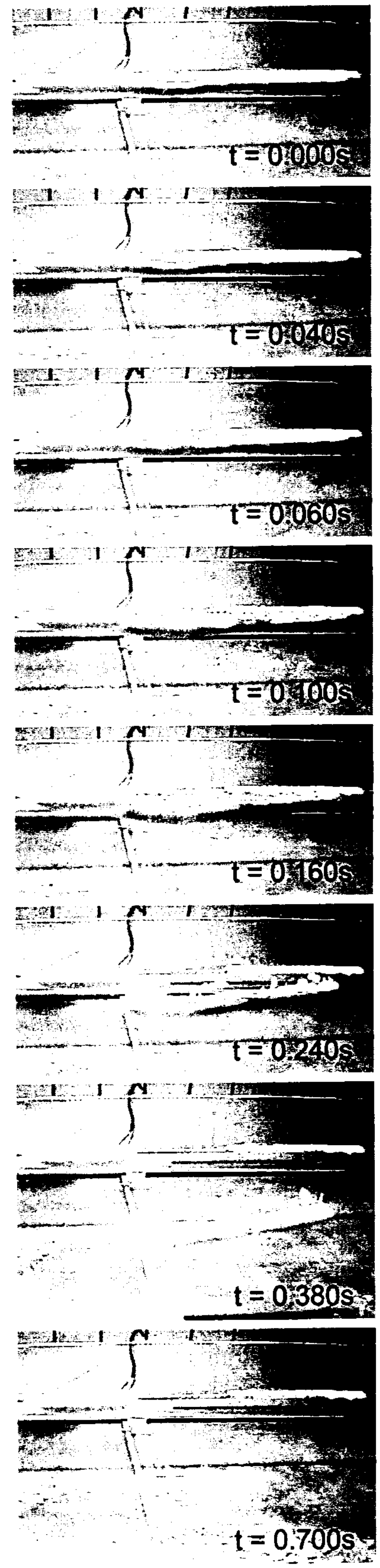
t = 0.000s
t = 0.040s
t = 0.060s
t = 0.100s
t = 0.160s
t = 0.240s
t = 0.380s
t = 0.700s

Appendix C

Theoretical catenary profile example

Calculation table used to obtain the initial position of individual nodes. Formulas based on the theoretical catenary equation:

$$Z = \frac{H}{w}\cosh\left(\frac{Y}{H/w}\right)$$

where H is the horizontal tension, w is the weight of the cable per unit length and Y and Z are absolute coordinates.

This particular example is for a 40 element ground wire model, 470m long, loaded only with its own weight (snow-free).

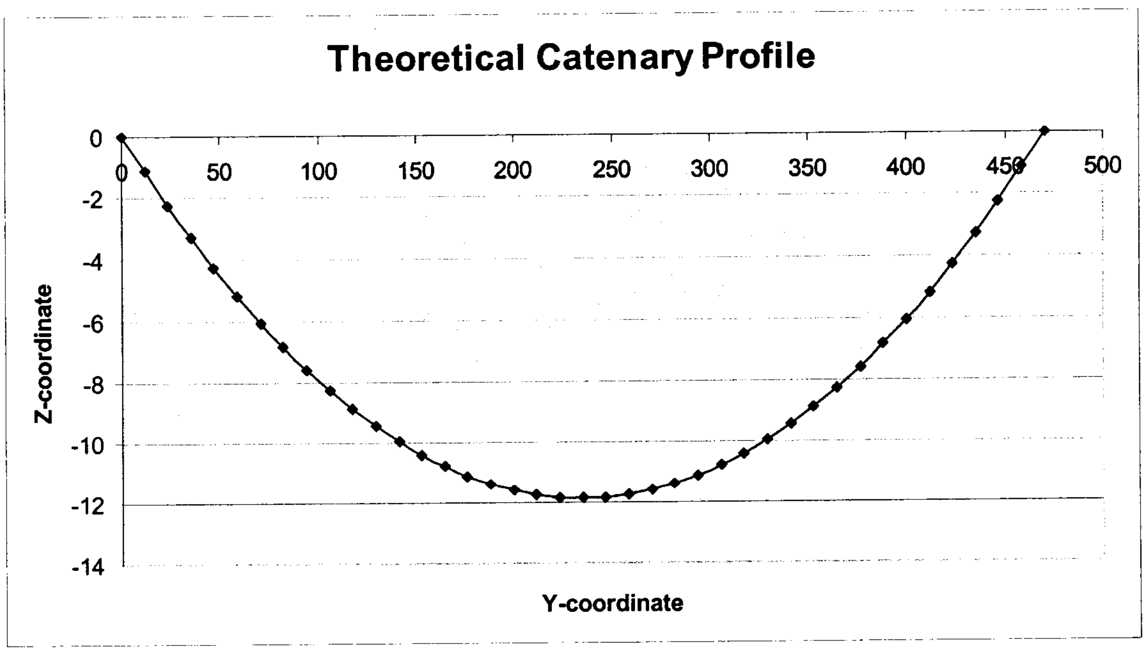

Cable weight per unit length	4.7186
Horizontal tension force	11000
Horizontal span of cable	470
Axial rigidity of cable	1.05E+07
Coordinates of origin	
x coordinate	0
y coordinate	0
z coordinate	0
Number of elements per cable	40
Number of nodes per element	**2**
Index of first node	1
Index of first element	1
Introduce h	0
Introduce horizontal angle deg	0

njoint	x0	y[j]	z[j]
1	0	0.00	0.0000
2	0	11.71	-1.1532
3	0	23.43	-2.2478
4	0	35.16	-3.2837
5	0	46.89	-4.2608
6	0	58.62	-5.1791
7	0	70.36	-6.0384
8	0	82.10	-6.8388
9	0	93.85	-7.5801
10	0	105.60	-8.2624
11	0	117.35	-8.8854
12	0	129.11	-9.4493
13	0	140.87	-9.9540
14	0	152.63	-10.3993
15	0	164.39	-10.7854
16	0	176.16	-11.1121
17	0	187.92	-11.3794
18	0	199.69	-11.5874
19	0	211.46	-11.7359
20	0	223.23	-11.8251
21	0	235.00	-11.8548
22	0	246.77	-11.8251
23	0	258.54	-11.7359
24	0	270.31	-11.5874
25	0	282.08	-11.3794
26	0	293.84	-11.1121
27	0	305.61	-10.7854
28	0	317.37	-10.3993
29	0	329.13	-9.9540
30	0	340.89	-9.4493
31	0	352.65	-8.8854
32	0	364.40	-8.2624
33	0	376.15	-7.5801
34	0	387.90	-6.8388
35	0	399.64	-6.0384
36	0	411.38	-5.1791
37	0	423.11	-4.2608
38	0	434.84	-3.2837
39	0	446.57	-2.2478
40	0	458.29	-1.1532
41	0	470.00	0.0000

elements	node1	node2	strain
1	1	2	0.00105
2	2	3	0.001049
3	3	4	0.001049
4	4	5	0.001048
5	5	6	0.001048
6	6	7	0.001047
7	7	8	0.001047
8	8	9	0.001047
9	9	10	0.001046
10	10	11	0.001046
11	11	12	0.001046
12	12	13	0.001046
13	13	14	0.001045
14	14	15	0.001045
15	15	16	0.001045
16	16	17	0.001045
17	17	18	0.001045
18	18	19	0.001045
19	19	20	0.001045
20	20	21	0.001045
21	21	22	0.001045
22	22	23	0.001045
23	23	24	0.001045
24	24	25	0.001045
25	25	26	0.001045
26	26	27	0.001045
27	27	28	0.001045
28	28	29	0.001045
29	29	30	0.001046
30	30	31	0.001046
31	31	32	0.001046
32	32	33	0.001046
33	33	34	0.001047
34	34	35	0.001047
35	35	36	0.001047
36	36	37	0.001048
37	37	38	0.001048
38	38	39	0.001049
39	39	40	0.001049
40	40	41	0.00105
		Average strain	**0.001046**

Appendix D

Frequencies of vibration for a bare ground wire model (snow-free)

(See tabulated values on the next page)

Observations:

- The first two resonant frequencies are very close to one another, but the mode shapes are quite different (half of a sine wave vs. a full sine wave).

- Frequencies increase from mode #1 to #80 but seem to level off and converge towards the 80th.

- Curious modes of vibration appear after the 80th mode: the mode shapes appear as loops in the cable. In reality these modes would not be possible because of the bending rigidity of the cable. These arise because the cable is modeled as a succession of axial elements (e.g. a chain model). Mode # 86 is shown on page 109 to illustrate the spurious "loop" mode.

- Frequencies increase from mode #80 to #158 and also seem to level off towards the highest.

Frequency #	Frequency (rad/s)	Frequency (Hz)	Period (s)
1	2.009	0.3198	3.12700
2	2.015	0.3207	3.11900
3	3.118	0.4962	2.01500
4	4.034	0.6420	1.55800
5	5.056	0.8047	1.24300
6	6.046	0.9622	1.03900
7	7.053	1.123	0.89080
8	8.047	1.281	0.78080
9	9.046	1.440	0.69460
10	10.04	1.597	0.62600
11	11.03	1.755	0.56980
12	12.01	1.911	0.52320
13	12.99	2.068	0.48370
14	13.96	2.223	0.44990
15	14.94	2.377	0.42070
16	15.90	2.530	0.39520
17	16.86	2.683	0.37270
18	17.81	2.834	0.35280
19	18.75	2.984	0.33510
20	19.69	3.134	0.31910
21	20.62	3.281	0.30470
22	21.54	3.428	0.29170
23	22.45	3.574	0.27980
24	23.36	3.717	0.26900
25	24.25	3.860	0.25910
26	25.14	4.001	0.24990
27	26.02	4.141	0.24150
28	26.88	4.278	0.23370
29	27.74	4.415	0.22650
30	28.58	4.549	0.21980
31	29.42	4.682	0.21360
32	30.24	4.813	0.20780
33	31.05	4.942	0.20230
34	31.30	4.981	0.20080
35	31.85	5.070	0.19730
36	32.64	5.195	0.19250
37	33.41	5.318	0.18800
38	34.18	5.439	0.18390
39	34.92	5.558	0.17990
40	35.66	5.675	0.17620
41	36.38	5.790	0.17270
42	37.09	5.903	0.16940
43	37.78	6.013	0.16630
44	38.46	6.121	0.16340
45	39.12	6.227	0.16060
46	39.77	6.330	0.15800
47	40.40	6.431	0.15550
48	41.02	6.529	0.15320
49	41.62	6.625	0.15100
50	42.21	6.718	0.14890
51	42.78	6.808	0.14690
52	43.33	6.896	0.14500
53	43.87	6.982	0.14320
54	44.39	7.064	0.14160
55	44.89	7.144	0.14000
56	45.37	7.222	0.13850
57	45.84	7.296	0.13710
58	46.29	7.368	0.13570
59	46.72	7.436	0.13450
60	47.14	7.502	0.13330
61	47.53	7.565	0.13220
62	47.91	7.625	0.13110
63	48.27	7.682	0.13020
64	48.61	7.737	0.12930
65	48.93	7.788	0.12840
66	49.23	7.836	0.12760
67	49.52	7.881	0.12690
68	49.78	7.923	0.12620
69	50.03	7.962	0.12560
70	50.25	7.998	0.12500
71	50.46	8.031	0.12450
72	50.65	8.061	0.12410
73	50.82	8.088	0.12360
74	50.96	8.111	0.12330
75	51.09	8.132	0.12300
76	51.20	8.149	0.12270
77	51.29	8.163	0.12250
78	51.36	8.174	0.12230
79	51.41	8.182	0.12220
80	51.44	8.187	0.12210
81	62.49	9.945	0.10060
82	93.67	14.91	0.06708
83	124.8	19.87	0.05033
84	155.9	24.82	0.04029
85	187.0	29.76	0.03360
86	218.0	34.69	0.02883
87	248.9	39.61	0.02525
88	279.7	44.51	0.02247
89	310.4	49.39	0.02025
90	340.9	54.26	0.01843
91	371.4	59.11	0.01692
92	401.7	63.93	0.01564
93	431.8	68.73	0.01455
94	461.8	73.50	0.01361
95	491.6	78.24	0.01278
96	521.2	82.95	0.01206
97	550.6	87.63	0.01141
98	579.8	92.28	0.01084
99	608.8	96.89	0.01032
100	637.5	101.50	0.00986
101	666.0	106.00	0.00943
102	694.2	110.50	0.00905
103	722.2	114.90	0.00870
104	749.9	119.40	0.00838
105	777.3	123.70	0.00808
106	804.4	128.00	0.00781
107	831.2	132.30	0.00756
108	857.7	136.50	0.00733
109	883.8	140.70	0.00711
110	909.6	144.80	0.00691
111	935.1	148.80	0.00672
112	960.1	152.80	0.00654
113	984.9	156.70	0.00638
114	1009	160.60	0.00623
115	1033	164.40	0.00608
116	1057	168.20	0.00595
117	1080	171.90	0.00582
118	1103	175.50	0.00570
119	1125	179.00	0.00559
120	1147	182.50	0.00548
121	1168	185.90	0.00538
122	1189	189.30	0.00528
123	1210	192.50	0.00519
124	1230	195.70	0.00511
125	1249	198.80	0.00503
126	1268	201.90	0.00495
127	1287	204.80	0.00488
128	1305	207.70	0.00481
129	1323	210.50	0.00475
130	1340	213.20	0.00469
131	1356	215.90	0.00463
132	1372	218.40	0.00458
133	1388	220.90	0.00453
134	1403	223.30	0.00448
135	1417	225.60	0.00443
136	1431	227.80	0.00439
137	1445	229.90	0.00435
138	1457	232.00	0.00431
139	1470	233.90	0.00428
140	1481	235.80	0.00424
141	1492	237.50	0.00421
142	1503	239.20	0.00418
143	1513	240.80	0.00415
144	1522	242.30	0.00413
145	1531	243.70	0.00410
146	1539	245.00	0.00408
147	1547	246.20	0.00406
148	1554	247.30	0.00404
149	1560	248.30	0.00403
150	1566	249.20	0.00401
151	1571	250.10	0.00400
152	1576	250.80	0.00399
153	1580	251.40	0.00398
154	1583	252.00	0.00397
155	1586	252.40	0.00396
156	1588	252.70	0.00396
157	1590	253.00	0.00395
158	1590	253.10	0.00395

Spurious loop mode #86

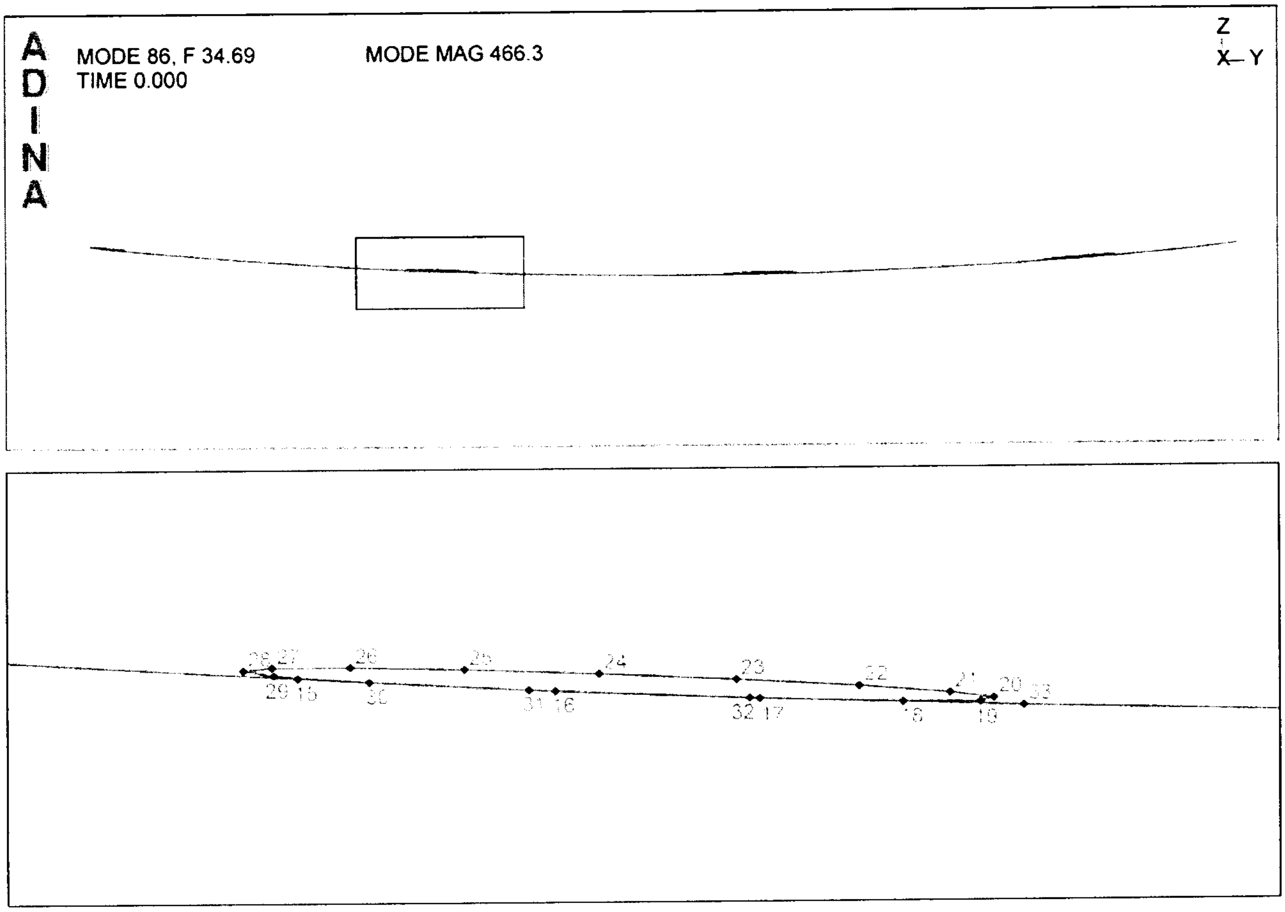

Appendix E

Load application and removal

- Cable weight application (static) from time 0.000 to time 1.000
- Snow weight application (static) from time 1.000 to time 2.000
- Snow element and weight removal (dynamic) from time 2.000 to time 6.234
- Dynamic analysis under cable weight only, from time 6.234

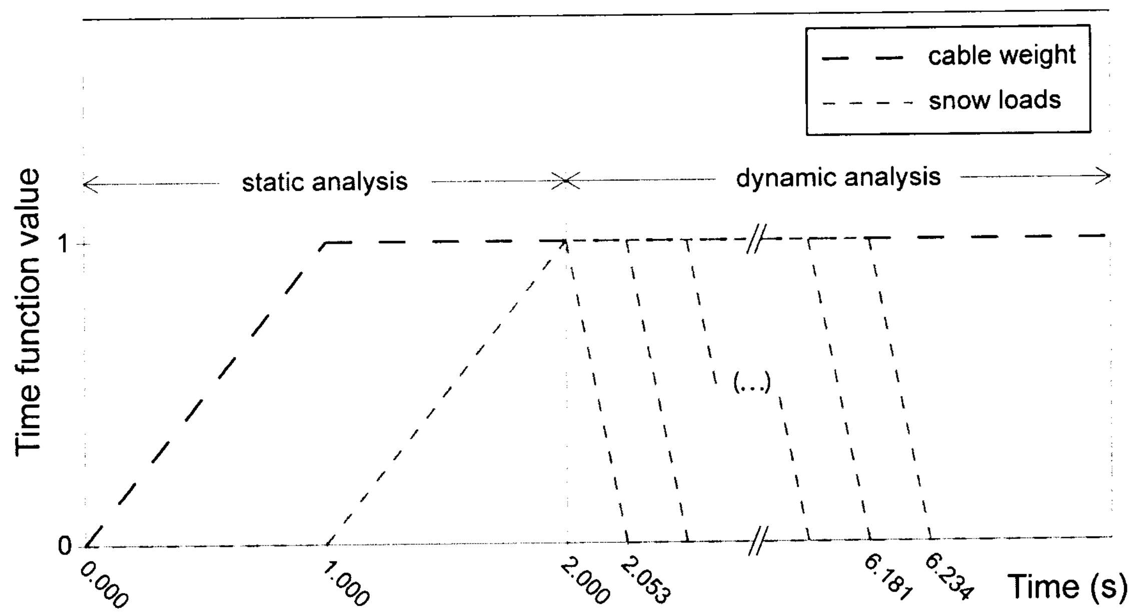

The next two pages show the loads applied to the cable model as they appear in the ADINA user interface. The gray bars are arrows representing loads applied on individual nodes.

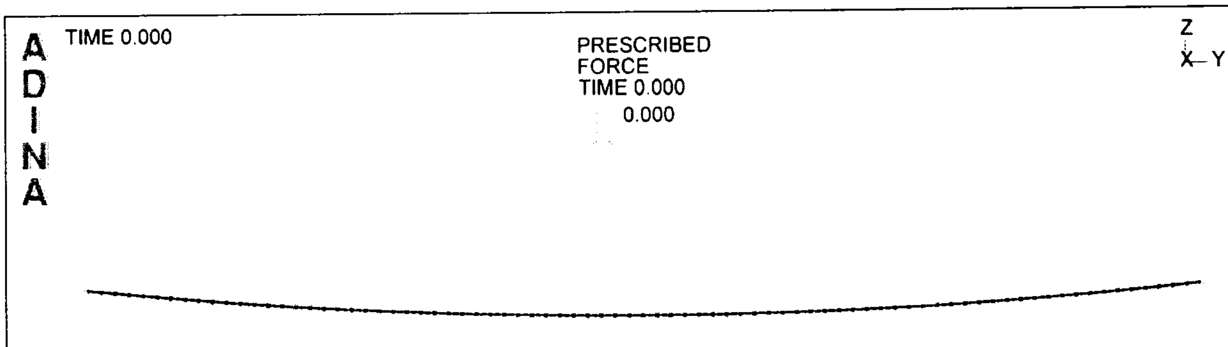

Meshed cable

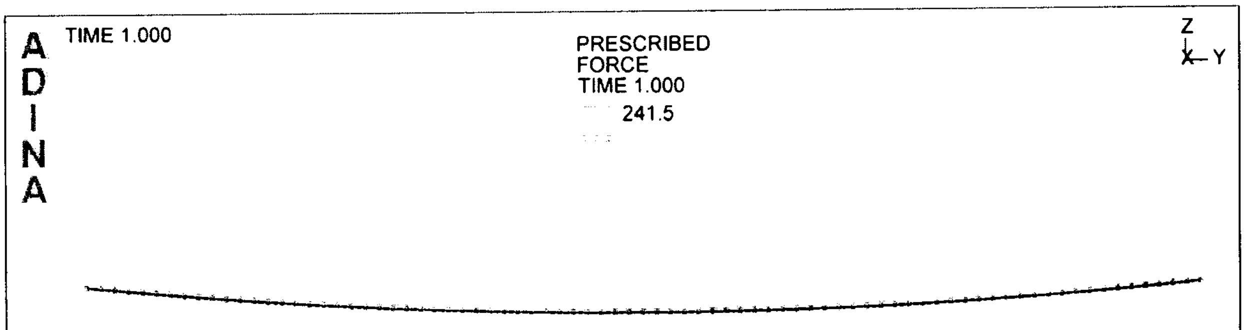

Cable self-weight static load seen as a thin line (uniform load)

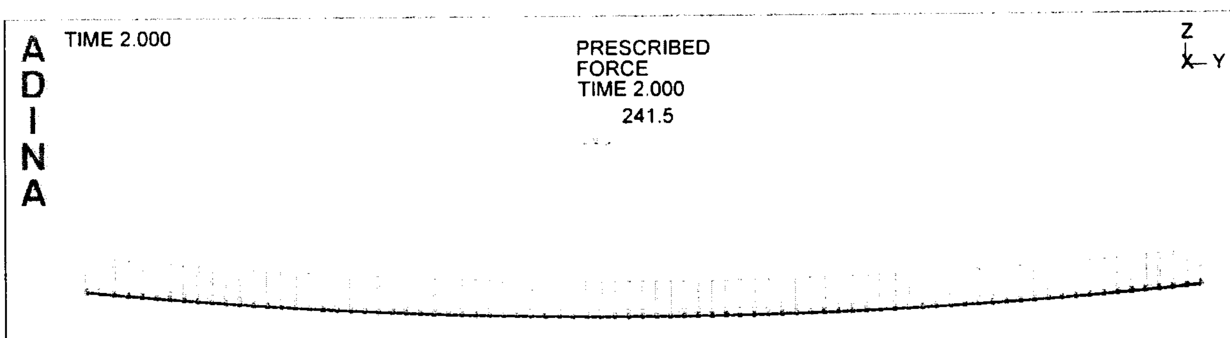

Snow overload of 41.1 N/m applied to individual nodes

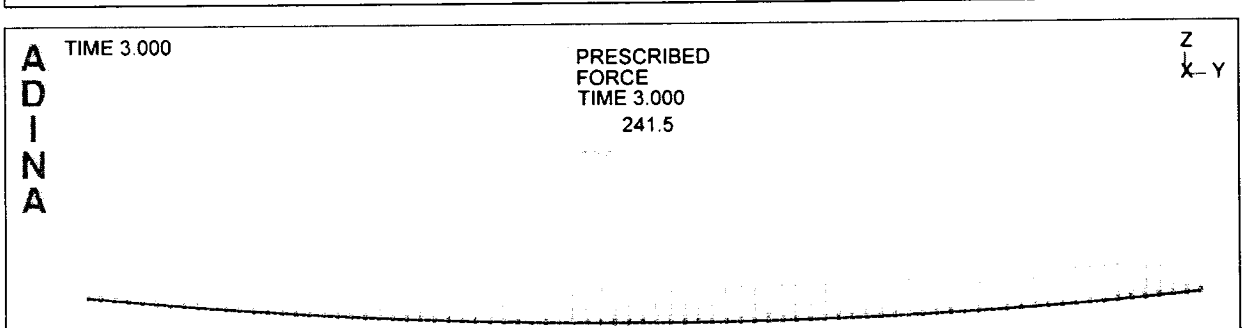

Snow overload being removed at the rate of 111 m/s (unzipping)

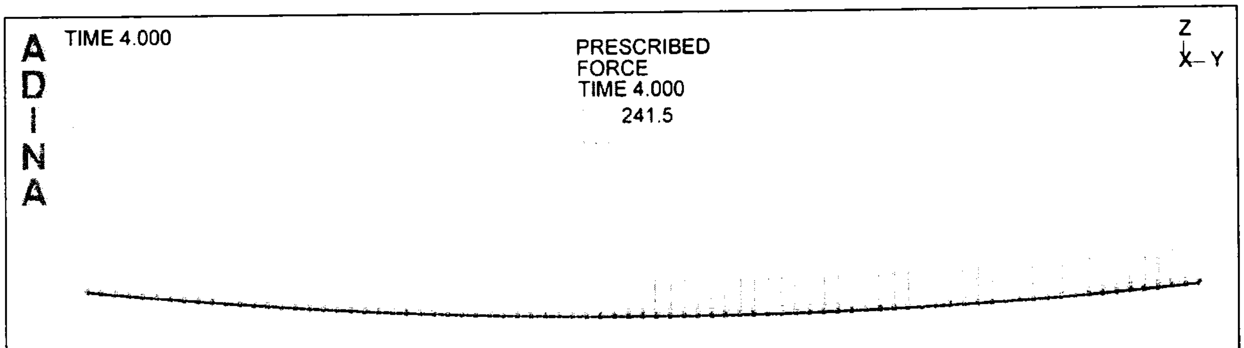

Snow overload being removed at the rate of 111 m/s (unzipping)

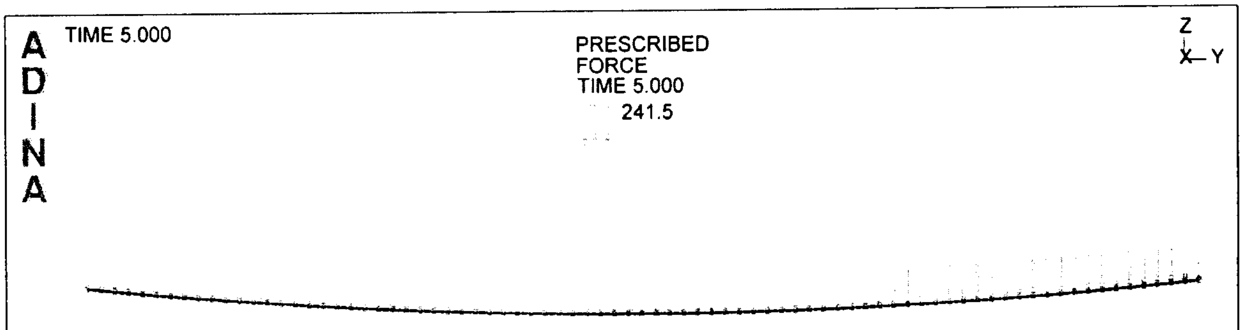

Snow overload being removed at the rate of 111 m/s (unzipping)

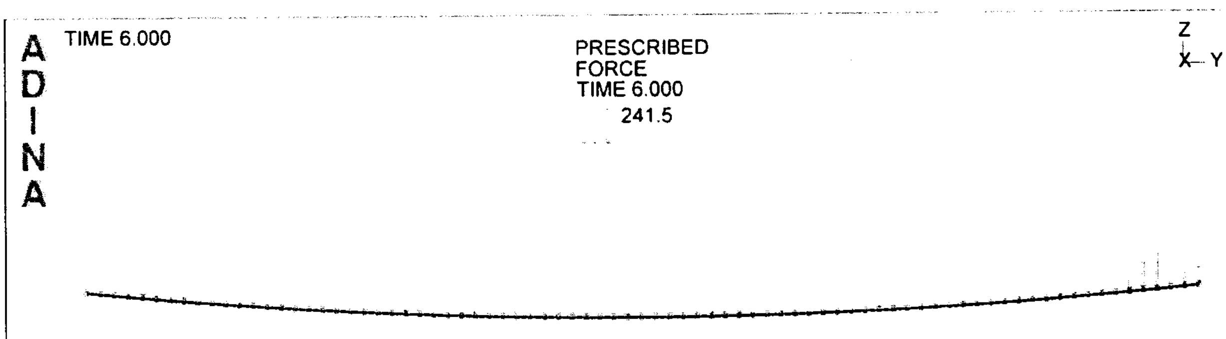

Snow overload being removed at the rate of 111 m/s (unzipping)

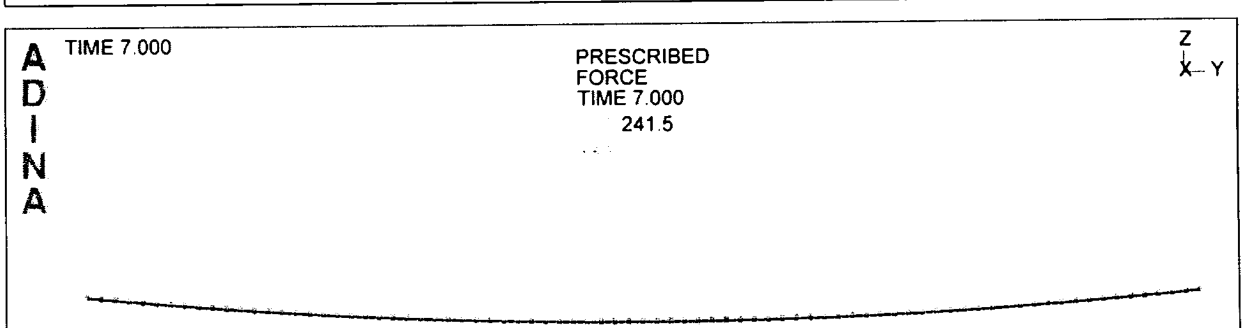

The dynamic analysis continues with the cable weight only